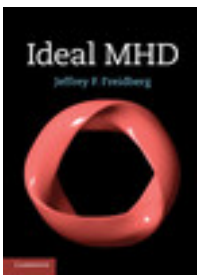

Ideal MHD

Jeffrey P. Freidberg

Book DOI: http://dx.doi.org/10.1017/CBO9780511795046

Online ISBN: 9780511795046

Hardback ISBN: 9781107006256

Chapter

7 - Equilibrium: three-dimensional configurations pp. 223-326

Chapter DOI: http://dx.doi.org/10.1017/CBO9780511795046.008

Cambridge University Press

7

Equilibrium: three-dimensional configurations

7.1 Introduction

Two-dimensional configurations with toroidal axisymmetry have been investigated in Chapter 6. Many fusion concepts fall into this class – tokamaks of all types, the reversed field pinch, the levitated dipole, the spheromak, and the field reversed configuration. One common feature in each of these concepts is the need for a toroidal current to provide toroidal force balance, either using a perfectly conducting shell or a vertical field.

The need for a toroidal current is of particular importance to the tokamak and RFP, the most advanced of the axisymmetric configurations. The reason is that it is not possible to drive a DC toroidal current indefinitely with a transformer, the method now used in pulsed versions of these configurations. This conflicts with the general consensus that a magnetic fusion reactor must operate as a steady state device for engineering reasons to avoid cyclical thermal and mechanical stresses inherent in a pulsed device. In other words, some form of non-inductive current drive is required. This is an active area of research and while a scientifically sound and technologically viable technique may be possible theoretically, success still depends on current and future experimental development. Overall, non-inductive current drive represents a difficult challenge for the tokamak and RFP concepts.

The difficulty of non-inductive current drive is one of the primary motivations for investigating 3-D MHD concepts. Three-dimensional systems, although obviously more complicated geometrically, offer the potential of providing radial pressure balance and toroidal force balance without the need of a non-inductive current drive system.

Over the years a number of 3-D toroidal concepts have been proposed as possible fusion reactors. The only one that has survived the rigorous challenges of plasma physics is the stellarator. Consequently, Chapter 7 is focused on the MHD equilibrium of stellarators.

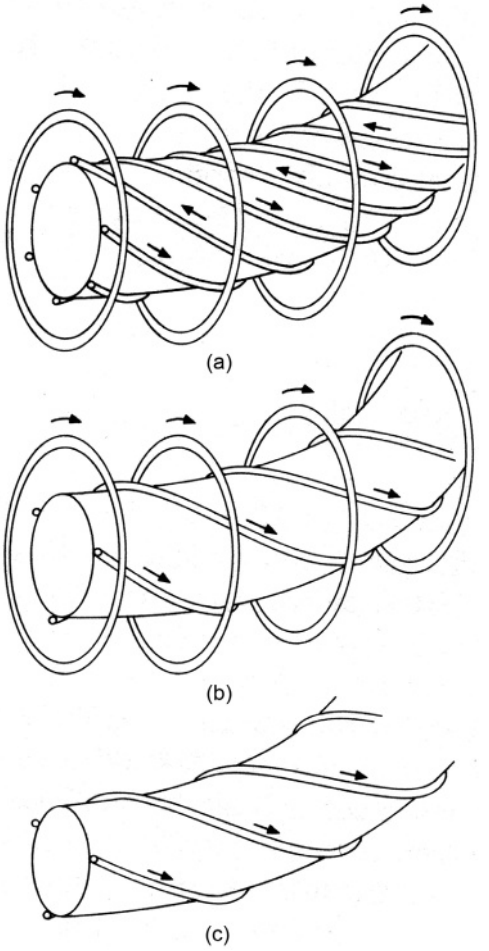

Figure 7.1 Schematic diagram of several types of stellarator windings: (a) original stellarator, (b) heliotron, and (c) torsatron.

Conceptually, a stellarator can be viewed as a straight helix bent into a torus. It is fundamentally a 3-D configuration. For purposes of intuition, several types of stellarator windings are illustrated schematically in Fig. 7.1. The plasma physics advantages of a stellarator can be summarized as follows. First, since stellarators can be held in equilibrium without a net current, or more accurately with only the naturally occurring bootstrap current, there is no need for an external non-inductive current drive system, a major advantage indeed. The stellarator is inherently a steady state device. Second, with zero, or at most a relatively small net bootstrap current, the threat of current-driven major disruptions is greatly if not completely alleviated. Third, even without plasma a vacuum stellarator magnetic field has well-defined closed nested flux surfaces with finite rotational transform and a unique magnetic

axis located in the center of the vacuum chamber. The magnetic field acts like a cage surrounding and confining the plasma. No cooperation from the plasma in the form of a large toroidal current is required for toroidal force balance.

These are considerable advantages. There are two counterbalancing disadvantages, one involving plasma physics and the other, engineering. The plasma physics problem is concerned with single-particle confinement and neoclassical transport. Since a stellarator is a three-dimensional configuration there are no exact conserved constants of the motion governing the trajectory of a particle except for the total energy. As shown in Section 7.7 this absence of conserved constants can lead to a rapid loss of particles through helical "loss cones." The resulting neoclassical losses can even exceed anomalous transport and are potentially a very serious problem. The resolution of this problem lies with the invention of two ideas, the quasi-symmetric stellarator and the quasi-isodynamic stellarator, which are special examples of the more general quasi-omnigenous stellarator. These are also explained in Section 7.7. An important geometric feature of these configurations is the necessity of a helical (rather than a circular toroidally symmetric planar) magnetic axis. Whether these new ideas will increase the energy confinement time in a stellarator so that it is equal to or better than that of a tokamak is an area of current interest with the results not yet in.

The second disadvantage involves the coil design. As might be expected the magnet system needed to produce a 3-D stellarator magnetic field is substantially more complicated than that of a 2-D toroidally symmetric configuration. This leads to increased costs and perhaps even to a lower limit on the maximum achievable magnetic field in the plasma because of the need to limit the magnetic stresses in the tight curvature sections of the 3-D coils. Examples of modern stellarator magnet systems are presented in Section 7.8 which describes two of the major stellarators in the world fusion program, the Large Helical Device (LHD) in Japan and Wendelstein 7-X (W7-X) in Germany.

In the end these disadvantages must be weighed against the advantages associated with not requiring an external non-inductive current drive system and the possibility of disruption-free operation. With respect to the overall "competition" between stellarators and tokamaks, it is fair to say that at the time this book is being written, similar size devices perform comparably well, but with the tokamak having an overall edge, primarily because of better energy transport.

Turning to specifics it is perhaps not surprising that a great deal of analysis is required to understand the stellarator concept. To accomplish this task the material in Chapter 7 is organized as follows. The discussion begins with the derivation of a recently developed asymptotic model applicable to modern stellarators. Qualitatively the new model describes a high $\beta \sim \varepsilon$, large aspect ratio stellarator with a loosely wound helical field. The model is analytically solved for a single helicity

stellarator including the cases of a low $\beta_t \ll \varepsilon$ system with arbitrary profiles and a high $\beta_t \sim \varepsilon$ system with the Solov'ev profiles. The goal here is to learn the answers to such basic questions as

- If a stellarator has no, or very small, net current how is a force induced to balance the tire tube and $1/R$ outward forces along R?
- If a stellarator has zero, or very small, net current how can changing the vertical field move the plasma inward or outward along R, as is observed experimentally?
- Does a stellarator have an analogous β_t/ε equilibrium limit similar to the one that occurs in a high beta tokamak?

The stellarator model is also solved numerically for a multiple helicity magnetic field for $\beta_t = 0$ and $\beta_t \sim \varepsilon$. It is shown how such systems, even with only two helicities, lead to very complicated sets of flux surfaces.

Lastly, to understand the problem of single-particle confinement in a 3-D geometry, the basic principles of neoclassical transport theory are described. This discussion provides the motivation for the concept of quasi-omnigenity and the corresponding inventions of quasi-symmetric and quasi-isodynamic stellarators. These ideas are then applied to the world's two largest stellarators, LHD and W7-X.

7.2 The high β stellarator expansion

7.2.1 Introduction

To put the present model in context we note that early in the fusion program, before the advent of large high-speed computers, much of MHD stellarator research was carried out using various approximate models, often based on a large aspect ratio or magnetic axis expansion (Greene and Johnson, 1961). These models provided valuable physical insight but, with respect to present day stellarators, are neither accurate enough for precision experimental design nor flexible enough to take into account neoclassical transport requirements. In fact the neoclassical transport requirements had not yet been elucidated during the period when these early theories were developed.

Since then, stellarator research has made great advances with the development of large high-speed computers. Sophisticated 3-D MHD codes have been developed that provide accurate information for experimental design and data analysis including neoclassical constraints resulting in configurations that are quasi-omnigenous, quasi-symmetric, or quasi-isodynamic (see for instance Boozer, 2004, and Helander *et al.*, 2012). However, with such a strong reliance on numerics, some of the physical insight and intuition obtained from simple analytic models has been substantially reduced if not lost. Bridging the gap

between the modern 3-D MHD numerical codes and the simpler earlier analytic theories is the focus of the present model.

The basic goal is the development of a relatively simple analytic model that describes the MHD equilibria of present day stellarators. It is important that, despite its simplicity, the model should allow for a non-planar helical magnetic axis, one the basic constraints imposed by favorable neoclassical transport.

The present work meets this challenge by means of a new high β, large aspect ratio expansion. The end result is a simplified model with the following properties:

- The model treats $\beta \sim \varepsilon$, which is the interesting regime of reactor interest.
- The model allows a finite $l = 1$ non-planar helical magnetic axis.
- The model allows a finite $l = 0$ mirror field modulation (such as in W7-X).
- The model allows finite flux surface modulations due to all $l \geq 2$ helical field components.
- The model treats $\iota/2\pi \sim 1$, which is the interesting regime of reactor interest.

In spite of the "simplicity" of the final model substantial analysis is still required because of the complexities associated with a general 3-D geometry. For ease of presentation the derivation is first carried out for the special case where there is no $l = 0$ mirror field. At the end of the analysis it is shown how the calculation can be generalized to include an $l = 0$ field. The derivation of the stellarator expansion follows below.

7.2.2 The basic equations

The stellarator equilibria of interest are described by the usual ideal MHD equations

$$\begin{aligned} \mathbf{J} \times \mathbf{B} &= \nabla p \\ \nabla \times \mathbf{B} &= \mu_0 \mathbf{J} \\ \nabla \cdot \mathbf{B} &= 0 \end{aligned} \tag{7.1}$$

The goal is to investigate stellarator equilibria by means of a large aspect ratio expansion. To exploit the large aspect ratio assumption it is convenient to rewrite the MHD equations in an equivalent but alternate form. Also, to help follow the analysis the new equations are listed in the order in which they are to be solved. The alternate form can be written as

$$\begin{aligned} \nabla \cdot \mathbf{B} &= 0 \\ \nabla \times \mathbf{B} &= \mu_0 \mathbf{J} \\ \mathbf{J}_\perp &= (\mathbf{B} \times \nabla p)/B^2 \\ \mathbf{B} \cdot \nabla p &= 0 \\ \nabla \cdot \mathbf{J} &= 0 \end{aligned} \tag{7.2}$$

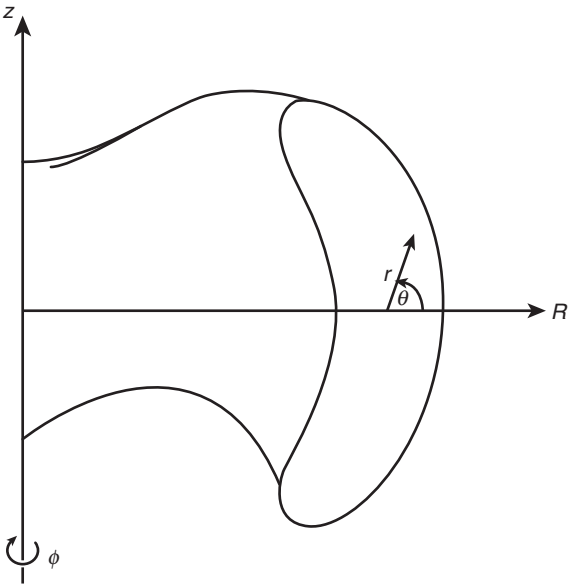

Figure 7.2 Geometry for the stellarator analysis.

7.2.3 The high β stellarator expansion

A stellarator equilibrium consists of a large toroidal magnetic field, small helical and axisymmetric poloidal magnetic fields, and a small pressure.[1] In carrying out the derivation one shall see that five independent dimensionless parameters appear in the analysis:

Inverse aspect ratio	$\varepsilon = a/R_0$
Normalized helical field amplitude	$\delta = \lvert\mathbf{B}_p\rvert/B_\phi$
Normalized plasma pressure	$\beta = 2\mu_0 p/B_\phi^2$
Poloidal periodicity mode number	l
Toroidal periodicity mode number	N

(7.3)

Here, B_ϕ and $\mathbf{B}_p$ are the toroidal and poloidal magnetic fields respectively. Note also that $\mathbf{B}_p$ contains a sum of helical and axisymmetric harmonics each of which depends on the minor radius, poloidal angle, and toroidal angle as follows:

$$\mathbf{B}_p(\mathbf{r}) = \sum_{l,N} \mathbf{B}_p^{(N,l)}(r, l\theta + N\hat{\phi}) \tag{7.4}$$

See Fig. 7.2 for the geometry. The axisymmetric component of $\mathbf{B}_p$ (e.g., the vertical field) corresponds to $N = 0$.

[1] A "small" pressure corresponds to $\beta_t \sim \varepsilon$ which for historical reasons is referred to as "high beta" because it is much larger than a "low beta" system corresponding to $\beta_t \sim \varepsilon^2$.

Table 7.1 *The high β stellarator expansion.*

Quantity	High β stellarator expansion
δ	ε
β	ε
N	1
l	1

The high β stellarator expansion is summarized in Table 7.1. The inverse aspect ratio $\varepsilon \ll 1$ is used as the basic expansion parameter and all other quantities are ordered with respect to ε.

A primary motivation for the expansion is that the ordering for the rotational transform (except for $l = 1$) must be chosen such that $\iota/2\pi \sim 1$. The ordering requirements to achieve this property can be ascertained by recalling that the rotational transform for a loosely wound, $l \geq 2$, small amplitude single helicity stellarator, derived in Section 6.7.4, is, in the present notation, given by

$$\frac{\iota}{2\pi} \approx \frac{(l-1)\delta^2}{N\varepsilon^2}\left(\frac{r}{a}\right)^{2(l-2)} \tag{7.5}$$

where r is the local plasma radius, a is the average radius of the plasma surface and $N = hR_0$ with $2\pi/h$ the helical wavelength.

Now, analysis shows that in order to produce a stellarator with a non-planar magnetic axis it is essential to assume $N \sim 1$ and indeed this is the ordering used in the expansion presented here. Physically, the implication of $N \sim 1$ is that there are a finite number of helical periods around the torus. Then, Eq. (7.5) implies that in order to make the rotational transform finite ($\iota/2\pi \sim 1$) one must order $\delta \sim \varepsilon$. Lastly, the value of beta is chosen to scale as $\beta \sim \varepsilon$ which is similar to the high beta tokamak ordering described in Section 6.5.

In order to carry out the expansion it is also necessary to distinguish the ordering of the poloidal vs. toroidal coordinates. Based on the orderings given in Table 7.1 one introduces the usual toroidal coordinates leading to

$$\begin{aligned} R &= R_0 + r\,\cos\theta & \nabla &= \nabla_\perp + \nabla_\parallel \\ Z &= r\,\sin\theta & a\nabla_\perp &= a\left(\mathbf{e}_r\frac{\partial}{\partial r} + \mathbf{e}_\theta\frac{1}{r}\frac{\partial}{\partial\theta}\right) \sim 1 \\ \hat{\phi} &= -\phi/N & a\nabla_\parallel &= \mathbf{e}_\phi\frac{aN}{R}\left(\frac{\partial}{\partial\phi}\right) = \mathbf{e}_\phi\frac{aN}{R_0 + r\,\cos\theta}\left(\frac{\partial}{\partial\phi}\right) \sim \varepsilon \end{aligned} \tag{7.6}$$

where R_0 is the toroidally averaged major radius of the magnetic axis, a is the toroidally averaged minor radius of the plasma, and R, $\hat{\phi}$, Z refer to the actual

laboratory coordinate system. Note that normalizing ϕ by N implies that one helical period corresponds to $0 \leq \phi \leq 2\pi$ so that the toroidal angle ϕ is related to the straight stellarator coordinates by $\phi = hz$. Also, $\mathbf{e}_R = \mathbf{e}_r \cos\theta - \mathrm{e}_\theta \sin\theta$, $\mathbf{e}_Z = \mathbf{e}_r \sin\theta + \mathbf{e}_\theta \cos\theta$, and $\mathbf{e}_{\hat{\phi}} = -\mathbf{e}_\phi$. With these definitions it follows that R, $\hat{\phi}$, Z and r, θ, ϕ are right-handed coordinate systems.

Here and below note that the characteristic length and magnetic field used to scale the variables appearing in the formulation are the minor radius a and the vacuum toroidal field at the midplane B_0 respectively.

Next, for consistency with the high β stellarator ordering, the expansions for the magnetic field, current density, and pressure must be chosen as

$$\begin{aligned} \mathbf{B} &= \left(B_{\phi 0}\frac{R_0}{R} + B_{\phi 1}\right)\mathbf{e}_\phi + \mathbf{B}_{p1} \approx \left(B_{\phi 0} - B_{\phi 0}\frac{r}{R_0}\cos\theta + B_{\phi 1}\right)\mathbf{e}_\phi + \mathbf{B}_{p1} \\ \mathbf{J} &= J_{\phi 1}\mathbf{e}_\phi + \mathbf{J}_{p1} \\ p &\approx p_1 \end{aligned} \tag{7.7}$$

where the numerical subscripts refer to the order in ε and the terms listed represent the minimum number required to obtain a closed set of equations. Also, the $(r/R_0)\cos\theta$ term is the large aspect ratio expansion of the vacuum toroidal field.

7.2.4 Reduction of the equations

The $\nabla \cdot \boldsymbol{B} = 0$ equation

The analysis begins with the application of the expansion to the $\nabla\cdot\mathbf{B} = 0$ equation. It is shown that the poloidal magnetic field $\mathbf{B}_{p1}$ can be written in terms of a scalar stream function A_1 equivalent to the toroidal component of vector potential. The analysis proceeds by first noting that to leading order the toroidal field is a vacuum field, a consequence of the assumption that the current density is a first-order quantity. Therefore the leading-order toroidal field is written as

$$B_{\phi 0}(r,\theta,\phi) = B_0 = \text{ constant} \tag{7.8}$$

It is here that the $l = 0$ mirror field has been set to zero. If such a field existed then one would have to replace B_0 with $B_0 M(\phi)$ where $M(\phi) = 1 + \Delta_0 \cos\phi$ with the Δ_0 representing the $l = 0$ mirror modulation. As stated however, the derivation below sets $M = 1$. At the end of the section it is shown how to add in the effects of a finite $\Delta_0 \sim 1$ mirror field.

Consider now the $\nabla \cdot \mathbf{B} = 0$ equation. The first non-vanishing contribution expressed in normalized coordinates reduces to

$$\nabla\cdot\mathbf{B} \approx \nabla_\perp \cdot \mathbf{B}_{p1} = 0 \tag{7.9}$$

The solution is easily obtained by exploiting the fact that $\nabla_\perp$ is a two-dimensional operator. This allows the introduction of a stream function $A_1(r,\theta,\phi)$ for the poloidal magnetic field as follows

$$\mathbf{B}_{p1} = \nabla_\perp A_1 \times \mathbf{e}_\phi \tag{7.10}$$

In this equation ϕ appears only as a parameter.

The $\nabla\cdot\mathbf{B} = 0$ equation yields no information about $B_{\phi 1}$. The first non-vanishing appearance of $B_{\phi 1}$ in the $\nabla \cdot \mathbf{B} = 0$ equation scales as $\nabla_\parallel \cdot (B_{\phi 1}\mathbf{e}_\phi) \sim \varepsilon^2$ and is therefore not required for the analysis. To summarize, the total magnetic field used in the analysis has the form

$$\mathbf{B} = B_0\left(1 - \frac{r}{R_0}\ \cos\theta + \frac{B_{\phi 1}}{B_0}\right)\mathbf{e}_\phi + \nabla_\perp A_1 \times \mathbf{e}_\phi \tag{7.11}$$

where $A_1(r,\theta,\phi)$ and $B_{\phi 1}(r,\theta,\phi)$ are unknowns.

The $\mu_0\boldsymbol{J} = \nabla \times \boldsymbol{B}$ equation

Ampere's law is given by $\mu_0\mathbf{J} = \nabla \times \mathbf{B}$. A simple calculation leads to the following expression for the first-order current density used in the analysis:

$$\mu_0\mathbf{J}_1 = -\mathbf{e}_\phi\nabla_\perp^2 A_1 - \mathbf{e}_\phi \times \nabla_\perp B_{\phi 1} \tag{7.12}$$

The $\boldsymbol{J}_\perp = (\boldsymbol{B} \times \nabla \mathrm{p})/\mathrm{B}^2$ equation

Perpendicular pressure balance yields an alternate form for $\mathbf{J}_\perp$ which ultimately leads to a relation between $B_{\phi 1}$ and p_1. A simple calculation shows that $\mathbf{J}_\perp \approx \mathbf{J}_{p1}$ where, from perpendicular pressure balance

$$\mathbf{J}_{p1} = \frac{1}{B_0}\mathbf{e}_\phi \times \nabla_\perp p_1 \tag{7.13}$$

Now, Eq. (7.13) is equated with the poloidal component of Eq. (7.12) leading to

$$\mathbf{e}_\phi \times \nabla_\perp\left(p_1 + \frac{B_0 B_{\phi 1}}{\mu_0}\right) = 0 \tag{7.14}$$

The solution consistent with the boundary condition that the pressure vanish at the edge of the plasma is

$$p_1 + \frac{B_0 B_{\phi 1}}{\mu_0} = 0 \tag{7.15}$$

This is just the usual θ-pinch radial pressure balance relation locally valid at every value of ϕ.

Summary of the fields

At this point it is convenient to summarize the expressions for the magnetic field and current density which can be written in terms of two scalar quantities A_1 and p_1:

$$\begin{aligned} \mathbf{B} &= B_0\left(1-\frac{r}{R_0}\cos\theta-\frac{\mu_0 p_1}{B_0^2}\right)\mathbf{e}_\phi+\nabla_\perp A_1\times\mathbf{e}_\phi \\ \mu_0\mathbf{J}_1 &= -\mathbf{e}_\phi\nabla_\perp^2 A_1-\nabla_\perp\left(\frac{\mu_0 p_1}{B_0}\right)\times\mathbf{e}_\phi \end{aligned} \tag{7.16}$$

What remains now is to derive the basic equations that determine A_1 and p_1.

The $\boldsymbol{B}\cdot\nabla\mathrm{p}=0$ equation

The first non-vanishing contribution to parallel pressure balance occurs in second order and is given by

$$\mathbf{B}\cdot\nabla p_1=0 \tag{7.17}$$

where

$$\mathbf{B}\cdot\nabla=\frac{B_0 N}{R_0}\frac{\partial}{\partial\phi}+\mathbf{B}_{p1}\cdot\nabla_\perp=\frac{B_0 N}{R_0}\frac{\partial}{\partial\phi}-\mathbf{e}_\phi\times\nabla_\perp A_1\cdot\nabla_\perp \tag{7.18}$$

This is the first equation relating A_1 and p_1.

The $\nabla\cdot\boldsymbol{J}=0$ equation

The final equation that closes the system is $\nabla\cdot\mathbf{J}=0$. This equation can be written as

$$\mathbf{B}\cdot\nabla\frac{J_\parallel}{B}+\nabla\cdot\mathbf{J}_\perp=0 \tag{7.19}$$

The first non-vanishing contribution also occurs in second order. The $J_\parallel$ term simplifies by noting that $J_\parallel\approx J_{\phi 1}$ and then substituting from Eq. (7.16).

$$\mathbf{B}\cdot\nabla\frac{J_\parallel}{B}=-\mathbf{B}\cdot\nabla\left(\frac{\nabla_\perp^2 A_1}{\mu_0 B_0}\right) \tag{7.20}$$

The $\mathbf{J}_\perp$ term in Eq. (7.19) simplifies by using perpendicular pressure balance

$$\begin{aligned} \nabla\cdot\mathbf{J}_\perp &= \nabla\cdot\left(\frac{\mathbf{B}\times\nabla p}{B^2}\right) \\ &= \frac{1}{B^4}\nabla_\perp p\times\mathbf{B}\cdot\nabla_\perp B^2 \\ &= \frac{2}{B^2}\nabla_\perp p\times\mathbf{B}\cdot\boldsymbol{\kappa} \end{aligned} \tag{7.21}$$

where $\boldsymbol{\kappa} = \mathbf{b} \cdot \nabla \mathbf{b}$ is the curvature vector, $\mathbf{b} = \mathbf{B}/B$, and use has been made of the relation $\mathbf{J} \cdot \nabla p = 0$. The first non-vanishing contribution to the curvature vector is due to toroidicity; that is if one writes $\mathbf{b} \approx \mathbf{e}_\phi + \mathbf{B}_{p1}/B_0$ then

$$\boldsymbol{\kappa} \approx \mathbf{e}_\phi \cdot \nabla \mathbf{e}_\phi \approx -\frac{\mathbf{e}_R}{R_0} = -\frac{1}{R_0}(\mathbf{e}_r \cos\theta - \mathbf{e}_\theta \sin\theta) \tag{7.22}$$

This expression is substituted into Eq. (7.21) yielding

$$\nabla \cdot \mathbf{J}_\perp = -\frac{2}{R_0 B_0} \nabla_\perp p_1 \cdot \mathbf{e}_Z \tag{7.23}$$

The two contributions to $\nabla \cdot \mathbf{J} = 0$ can now be combined leading to

$$\mathbf{B} \cdot \nabla(\nabla_\perp^2 A_1) = -\frac{2\mu_0}{R_0} \nabla_\perp p_1 \cdot \mathbf{e}_Z \tag{7.24}$$

where $\mathbf{B} \cdot \nabla$ is again given by Eq. (7.18). This slightly more complicated equation describes the second relation between A_1 and p_1.

Equations (7.17) and (7.24) describe the basic high β stellarator expansion in the absence of an $l = 0$ mirror field.

Including a finite $l = 0$ *mirror field*

The inclusion of a finite $l = 0$ mirror field requires a generalization of the form for the background toroidal field and the introduction of a set of simple flux coordinates. Specifically, the equilibrium toroidal field is replaced by $B_{\phi 0} = B_0 \rightarrow B_0 M(\phi)$ where[2]

$$M(\phi) = 1 + \Delta_0 \cos\phi \tag{7.25}$$

Here the ordering for the modulation amplitude is $\Delta_0 \sim 1$. Note that for M to represent a vacuum field (i.e., $\nabla \times \mathbf{B}_{\phi 0} = 0$) consistent with the high β stellarator expansion one requires that $M(r,\theta,\phi) \rightarrow M(\phi)$.

The derivation including an $l = 0$ field closely parallels the one just presented without such a field. The details are as follows. The $\nabla \cdot \mathbf{B} = 0$ equation reduces to

$$\nabla \cdot \mathbf{B} \approx \nabla_\perp \cdot \mathbf{B}_{p1} + \frac{B_0 N}{R_0} \dot{M} = 0 \tag{7.26}$$

with an over dot denoting $d/d\phi$. For the case above $\dot{M} = dM/d\phi = -\Delta_0 \sin\phi$. The solution is easily found and is given by

[2] The derivation described here can be further generalized to include multiple toroidal harmonics in ϕ (e.g. terms proportional to cos 2ϕ, cos 3ϕ, etc.). However, this generalization is not needed for present purposes.

$$\mathbf{B} = B_{\phi 0}\left(1 - \frac{r}{R_0}\cos\theta + \frac{B_{\phi 1}}{B_{\phi 0}}\right)\mathbf{e}_\phi + \nabla_\perp A_1 \times \mathbf{e}_\phi - \frac{N}{2R_0}\dot{B}_{\phi 0} r\,\mathbf{e}_r \tag{7.27}$$

Next, Amperes Law ($\nabla \times \mathbf{B} = \mu_0 \mathbf{J}$) and perpendicular pressure balance ($\mathbf{J}_\perp = \mathbf{B} \times \nabla_p / B^2$) lead to a simple generalization of the θ-pinch radial pressure balance relation,

$$p_1 + \frac{B_{\phi 0} B_{\phi 1}}{\mu_0} = 0 \tag{7.28}$$

These results are substituted into the parallel pressure balance relation ($\mathbf{B} \cdot \nabla p = 0$) and the parallel current relation ($\mathbf{B} \cdot \nabla (J_\parallel / B) = -\nabla \cdot \mathbf{J}_\perp$) leading to two equations for the basic unknowns $p_1(r,\theta,\phi)$ and $A_1(r,\theta,\phi)$,

$$\begin{aligned} \mathbf{B} \cdot \nabla p_1 &= 0 \\ \mathbf{B} \cdot \nabla \left(\frac{\nabla_\perp^2 A_1}{B_{\phi 0}}\right) &= -\frac{2\mu_0}{R_0 B_{\phi 0}} \nabla_\perp p_1 \cdot \mathbf{e}_Z \\ \mathbf{B} \cdot \nabla &= \left(\frac{N}{R_0} B_{\phi 0} \frac{\partial}{\partial \phi} - \frac{N}{2R_0}\dot{B}_{\phi 0} r \frac{\partial}{\partial r} - \mathbf{e}_\phi \times \nabla_\perp A_1 \cdot \nabla_\perp\right) \end{aligned} \tag{7.29}$$

The final step in the formulation is to define a set of flux coordinates which further simplifies the equations. The coordinates are given by

$$\begin{aligned} u &= [M(\phi)]^{1/2}\, r \\ \theta &= \theta \\ \phi &= \phi \end{aligned} \tag{7.30}$$

In the new coordinates

$$\begin{aligned} \frac{\partial}{\partial r} &\to M^{1/2} \frac{\partial}{\partial u} \\ \frac{\partial}{\partial \theta} &\to \frac{\partial}{\partial \theta} \\ \frac{\partial}{\partial \phi} &\to \frac{\partial}{\partial \phi} + \frac{\dot{M}}{2M} u \frac{\partial}{\partial u} \\ \nabla_\perp &\to M^{1/2} \nabla_\perp = M^{1/2}\left(\mathbf{e}_r \frac{\partial}{\partial u} + \frac{\mathbf{e}_\theta}{u}\frac{\partial}{\partial \theta}\right) \\ \nabla_\perp^2 &\to M\,\nabla_\perp^2 = M\left(\frac{\partial^2}{\partial u^2} + \frac{1}{u}\frac{\partial}{\partial u} + \frac{1}{u^2}\frac{\partial^2}{\partial \theta^2}\right) \\ \mathbf{B} \cdot \nabla &\to M \mathbf{B} \cdot \nabla = M\left(\frac{B_0 N}{R_0}\frac{\partial}{\partial \phi} - \mathbf{e}_\phi \times \nabla_\perp A_1 \cdot \nabla_\perp\right) \end{aligned} \tag{7.31}$$

Here and below $\nabla_\perp$ becomes the standard cylindrical operator applied to the poloidal coordinates u, θ (rather than r, θ) in Eq. (7.31).

Observe that u^2 is proportional to the local (in ϕ) vacuum toroidal flux: $u^2 \propto B_{\phi 0}(\phi) r^2$. However, unlike the usual transformation to flux coordinates, in the present analysis the flux (i.e., u) is not an unknown quantity but is explicitly known because $B_{\phi 0}(\phi) = M(\phi) B_0$ is assumed to have been specified.

The transformation given by Eq. (7.30) is substituted into Eq. (7.29) leading to a simplified form of the new stellarator model:

$$\begin{aligned} \left(\frac{B_0 N}{R_0}\frac{\partial}{\partial\phi} - \mathbf{e}_\phi \times \nabla_\perp A_1 \cdot \nabla_\perp\right) p_1 &= 0 \\ \left(\frac{B_0 N}{R_0}\frac{\partial}{\partial\phi} - \mathbf{e}_\phi \times \nabla_\perp A_1 \cdot \nabla_\perp\right) \nabla_\perp^2 A_1 &= -\frac{2\mu_0}{R_0 M^{3/2}} \nabla_\perp p_1 \cdot \mathbf{e}_Z \end{aligned} \tag{7.32}$$

With flux coordinates the only difference between including and not including an $l = 0$ field is the appearance of $M^{-3/2}$ in the right-hand side of the second equation. However, the corresponding magnetic field and current density including an $l = 0$ field are more complicated. Expressed in the new coordinates, these quantities are given by

$$\begin{aligned} \mathbf{B} &= B_0 M \left[1 - \frac{u}{R_0 M^{1/2}} \cos\theta - \frac{\mu_0 p_1}{B_0^2 M^2}\right] \mathbf{e}_\phi + M^{1/2} \nabla_\perp A_1 \times \mathbf{e}_\phi - \frac{B_0 N}{2R_0}\frac{\dot{M}}{M^{1/2}} u\, \mathbf{e}_r \\ \mu_0 \mathbf{J}_1 &= -\mathbf{e}_\phi M \nabla_\perp^2 A_1 - \frac{\mu_0}{B_0 M^{1/2}} \nabla_\perp p_1 \times \mathbf{e}_\phi \end{aligned} \tag{7.33}$$

Equations (7.32) and (7.33) describe the desired high β stellarator model in terms of un-normalized variables. One final simplifying step is to introduce normalized variables as follows:

$$\begin{aligned} u &= a\rho \\ A_1 &= -(\varepsilon N a B_0) A \\ p_1 &= (\varepsilon N^2 B_0^2 / 2\mu_0)\beta \end{aligned} \tag{7.34}$$

with $A \sim \beta \sim 1$ and as before $ha = \varepsilon N$. The high β stellarator model reduces to

$$\begin{aligned} \left(\frac{\partial}{\partial\phi} + \mathbf{e}_\phi \times \nabla_\perp A \cdot \nabla_\perp\right) \beta &= 0 \\ \left(\frac{\partial}{\partial\phi} + \mathbf{e}_\phi \times \nabla_\perp A \cdot \nabla_\perp\right) \nabla_\perp^2 A &= \frac{1}{M^{3/2}} \nabla_\perp \beta \cdot \mathbf{e}_Z \end{aligned} \tag{7.35}$$

where $A(\rho, \theta, \phi)$ and $\beta(\rho, \theta, \phi)$ are the primary unknowns and

$$\nabla_\perp = \mathbf{e}_r \frac{\partial}{\partial \rho} + \frac{\mathbf{e}_\theta}{\rho} \frac{\partial}{\partial \theta} \tag{7.36}$$

is the standard cylindrical gradient operator written in ρ, θ (rather than u, θ) coordinates. The corresponding fields and current densities are given by

$$\begin{aligned} \frac{\mathbf{B}}{B_0} &= \left[M \left(1 - \frac{\varepsilon}{M^{1/2}} \rho \cos\theta \right) - \frac{\varepsilon N^2}{2M} \beta \right] \mathbf{e}_\phi - \varepsilon N \left(M^{1/2} \nabla_\perp A \times \mathbf{e}_\phi + \frac{\dot{M}}{2M^{1/2}} \rho \, \mathbf{e}_r \right) \\ \frac{\mu_0 a \, \mathbf{J}_1}{B_0} &= (\varepsilon N M \nabla_\perp^2 A) \, \mathbf{e}_\phi - \frac{\varepsilon N^2}{2M^{1/2}} \nabla_\perp \beta \times \mathbf{e}_\phi \end{aligned} \tag{7.37}$$

The examples discussed in the remainder of Chapter 7 are all based on Eq. (7.35) or its equivalent un-normalized form given by Eq. (7.32).

Islands

Before closing the discussion it is worth mentioning magnetic islands. Such islands can form near a separatrix or near rational flux surfaces within the plasma in multiple helicity systems. The basic high β stellarator model includes the effect of islands, which can be important in determining plasma transport. However, for reasons of mathematical simplicity these islands are always ignored (actually averaged out) whenever they arise in the examples that follow. In principle, one can assume that in a well-designed stellarator, the islands are very narrow in width and therefore would not have too large an effect on transport. Even so one must calculate the island width to verify this assumption, a task which only a few numerical codes can carry out. The point is that readers should be aware of the possibly important impact of islands even though they are ignored in the rest of the chapter.

7.3 Relation of the high β stellarator expansion to other models

At first glance, the high β stellarator model given by Eq. (7.32) is sufficiently different in appearance that it has no obvious connection or overlap with the previously derived two-dimensional models. In this section it is shown that such connections do indeed exist. Specifically, the high β stellarator model is shown to overlap with both the high β tokamak model and the straight stellarator model.

7.3.1 The high β tokamak

The high β tokamak is a special case of the high β stellarator obtained by utilizing the assumption of toroidal axisymmetry. For reference the basic high β tokamak equation (i.e., Eq. (6.96)) derived in Chapter 6 is repeated here:

$$\nabla^2\psi_0 = -R_0^2B_0^2\left[\frac{1}{B_0}\frac{d\tilde{B}}{d\psi_0} + \frac{2\mu_0}{B_0^2}\frac{dp}{d\psi_0}\left(\frac{r}{R_0}\right)\cos\theta\right] \tag{7.38}$$

The goal now is to show that the high β stellarator equations reduce to Eq. (7.38) in the appropriate limit.

To demonstrate this one sets $\partial/\partial\phi = 0$ in Eq. (7.32). Similarly all helical field amplitudes including $l = 0$ must be set to zero ($M = 1$) implying that $u = r$. The stellarator equations reduce to

$$\begin{aligned} \mathbf{e}_\phi \times \nabla_\perp A_1 \cdot \nabla_\perp p_1 &= 0 \\ \mathbf{e}_\phi \times \nabla_\perp A_1 \cdot \nabla_\perp(\nabla_\perp^2 A_1) &= \frac{2\mu_0}{R_0}\nabla_\perp p_1 \cdot \mathbf{e}_Z \end{aligned} \tag{7.39}$$

Next, note that A_1 is related to the poloidal flux ψ_0 appearing in the high β tokamak equations by $\psi_0 = R_0A_\phi = R_0A_1$. Substituting into Eq. (7.39) yields

$$\begin{aligned} \mathbf{e}_\phi \times \nabla_\perp \psi_0 \cdot \nabla_\perp p_1 &= 0 \\ \mathbf{e}_\phi \times \nabla_\perp \psi_0 \cdot \nabla_\perp(\nabla_\perp^2 \psi_0) &= 2\mu_0 R_0 \nabla_\perp p_1 \cdot \mathbf{e}_\phi \times \nabla(r\cos\theta) \end{aligned} \tag{7.40}$$

The solution to the first equation is, as expected, $p_1 = p_1(\psi_0)$. When inserted into the second equation this leads to

$$\mathbf{e}_\phi \times \nabla_\perp \psi_0 \cdot \nabla_\perp\left(\nabla_\perp^2\psi_0 + 2\mu_0 R_0 \frac{dp_1}{d\psi_0} r\cos\theta\right) = 0 \tag{7.41}$$

The solution to this equation is

$$\nabla_\perp^2\psi_0 = -2\mu_0 R_0 \frac{dp}{d\psi_0} r\cos\theta + G(\psi_0) \tag{7.42}$$

which, with a different but equivalent definition of $G(\psi)$, is identical to the high β tokamak equation given by Eq. (7.38).

7.3.2 The straight stellarator

The second comparison of interest involves the straight stellarator. Two steps are required to show that the high β and straight stellarator models coincide in the region of physics overlap. In the straight stellarator it is necessary to take

the limit of a low β loosely wound helix. In the high β stellarator one must consider a single helicity system in the limit of very large aspect ratio. In these limits the physics overlaps and each model should reduce to the same basic equation.

Consider first the straight stellarator whose behavior is governed by Eq. (6.173), repeated here for convenience:

$$\Delta^* \psi = -\mu_0 \frac{dp}{d\psi} - \frac{F}{l_0^2}\frac{dF}{d\psi} + \frac{2hl}{l_0^4}F \tag{7.43}$$

The loosely wound assumption corresponds to approximating $l_0^2 = l^2 + h^2 r^2 \approx l^2$ where h is the pitch number of the helix. In this limit

$$\Delta^* \psi \equiv \frac{1}{r}\frac{\partial}{\partial r}\left(\frac{r}{l_0^2}\frac{\partial \psi}{\partial r}\right) + \frac{1}{r^2}\frac{\partial^2 \psi}{\partial \alpha^2} \approx \frac{1}{l^2}\left[\frac{1}{r}\frac{\partial}{\partial r}\left(r\frac{\partial \psi}{\partial r}\right) + \frac{l^2}{r^2}\frac{\partial^2 \psi}{\partial \alpha^2}\right] = \frac{1}{l^2}\nabla^2 \psi \tag{7.44}$$

and Eq. (7.43) reduces to

$$\nabla^2 \psi = -\frac{d}{d\psi}\left(l^2 \mu_0 p + \frac{F^2}{2}\right) + \frac{2h}{l}F \tag{7.45}$$

The next step is to utilize the low β assumption. If one introduces δ as a small mathematical expansion parameter then the low β limit corresponds to the following ordering: $\beta \sim ha \sim B_p/B_0 \sim \delta \ll 1$. Then, in analogy with the derivation of the high β tokamak equations, the free function $F(\psi)$ is written as

$$F^2(\psi) = l^2 B_0^2 \left[1 - \frac{2\mu_0 p(\psi)}{B_0^2} + 2G_2(\psi)\right] \tag{7.46}$$

Here, $F(\psi)$ is replaced by $G_2(\psi)$, a new dimensionless free function that scales as $G_2 \sim \delta^2$. This form for $F(\psi)$ guarantees that radial pressure balance is identical to that in a θ-pinch which is the assumption made in the high β stellarator expansion. Substituting into Eq. (7.45) leads to the desired form of the straight stellarator equations in the overlap region,

$$\nabla^2 \psi = -l^2 B_0^2 \frac{dG_2}{d\psi} + 2hB_0 \tag{7.47}$$

The next task is to take the large aspect ratio, single helicity limit of the high β stellarator equations and see if they reduce to the same form as Eq. (7.47). One begins by setting $\phi = hz$, $M = 1$, and $u = r$. The proper way to take the limit is to assume that a is finite, ha is small but finite, and $R_0 \to \infty$. Now, the only

appearance of R_0 in Eq. (7.32) is in the denominator of the right-hand side of the second equation. In the overlap region this "toroidal" effect can be neglected and Eq. (7.32) reduces to

$$\begin{gathered}\left(B_0\frac{\partial}{\partial z}-\mathbf{e}_\phi\times\nabla_\perp A_1\cdot\nabla_\perp\right)p_1=0\\ \left(B_0\frac{\partial}{\partial z}-\mathbf{e}_\phi\times\nabla_\perp A_1\cdot\nabla_\perp\right)\nabla_\perp^2 A_1=0\end{gathered}\tag{7.48}$$

The last simplification is to apply the single helicity requirement. This requirement is a consequence of the fact that a straight stellarator has, by definition, helical symmetry; that is all quantities are functions only of r and $\alpha = l\theta + hz$, corresponding to a single helicity system. In addition, p_1 is written as $p_1(\psi)$ with ψ now serving as the flux surface label. The first of the high β stellarator equations reduces to

$$\left(hB_0r-l\frac{\partial A_1}{\partial r}\right)\frac{\partial\psi}{\partial\alpha}+l\frac{\partial A_1}{\partial\alpha}\frac{\partial\psi}{\partial r}=0\tag{7.49}$$

The solution is

$$hB_0r^2-2lA_1=H(\psi)\tag{7.50}$$

The free function $H(\psi)$ is determined by identifying ψ with the helical flux in the straight stellarator and then equating the magnetic fields from each model. A short calculation yields

$$\psi=\frac{1}{2}(hB_0r^2-2lA_1)\tag{7.51}$$

The second high β stellarator equation simplifies to

$$\left(\frac{\partial\psi}{\partial r}\frac{\partial}{\partial\alpha}-\frac{\partial\psi}{\partial\alpha}\frac{\partial}{\partial r}\right)\nabla^2A_1=0\tag{7.52}$$

The solution is $\nabla^2A_1=\hat{G}(\psi)$ which after eliminating A_1 by means of Eq. (7.51) reduces to

$$\nabla^2\psi=G(\psi)+2hB_0\tag{7.53}$$

where $G(\psi)=-l\hat{G}(\psi)$. Observe that Eq. (7.53), with a different but equivalent definition of $G(\psi)$, is identical in form to Eq. (7.47) thereby demonstrating that both models do indeed overlap.

The discussion above has shown that the high β stellarator model reduces to known models in the appropriate regions of physics overlap. These models include the high β tokamak and the straight stellarator. The conclusion is that the high β stellarator model is based on a sound physical foundation and describes a wide range of multidimensional fusion concepts.

7.4 The Greene–Johnson limit

The purpose of this section is to show the relationship between the high β and Greene–Johnson stellarator models. The Greene–Johnson (GJ) model is an early and elegant expansion describing the MHD behavior of stellarators including radial pressure balance and toroidal force balance in a multi-helicity system (Greene and Johnson, 1961). In the context of modern stellarators the only important physics excluded from the model is the existence of a finite helical magnetic axis, which is a requirement to suppress neoclassical particle losses. The nature of the GJ expansion is such that the magnetic axis is forced to be circular with only small helical modulations. In fairness to Greene and Johnson it should be emphasized that at the time of their analysis neoclassical theory had not yet been developed and therefore there was no strong motivation to allow for a finite helical magnetic axis.

A substantial amount of analysis is required to (1) derive the GJ model and (2) reduce the high β stellarator (HBS) model to the GJ model in the overlap region. The critical steps are outlined here and the HBS details can be found in Appendix E.

7.4.1 Comparison of expansions

The discussion begins with a comparison of the different ordering assumptions used in both models. The inverse aspect ratio $\varepsilon \ll 1$ is again used as the basic expansion parameter and all other parameters are ordered with respect to ε. The ordering comparison is shown in the middle two columns in Table 7.2.

Table 7.2 *Comparison of stellarator expansions.*

Quantity	High β stellarator	Greene–Johnson	Overlap model
δ	ε	$\varepsilon^{1/2}$	$\varepsilon^{3/4}$
β	ε	ε	ε
N	1	$1/\varepsilon$	$1/\varepsilon^{1/2}$
l	1	1	1

A primary feature motivating both expansions is that the rotational transform (except for $l = 1$) must be of order unity: $\iota/2\pi \sim 1$. This property can be verified explicitly by recalling that the rotational transform for a loosely wound, $l \geq 2$, single helicity stellarator is given by

$$\frac{\iota}{2\pi} \approx \frac{(l-1)\delta^2}{N\varepsilon^2}\left(\frac{r}{a}\right)^{2(l-2)} \tag{7.54}$$

where r is the local plasma radius and a is the average radius of the plasma surface.

Recall that in order to produce a stellarator with a helical magnetic axis it is necessary to assume $N \sim 1$, which is the ordering used in the HBS expansion. This is in contrast to the GJ ordering, which assumes that $N \sim 1/\varepsilon$ is large. Even so, the GJ equilibrium equations (in the limit of a loosely wound helical field) can be obtained from the HBS model (in the limit of a tightly wound helical field) by the introduction of a subsidiary expansion where N is assumed to be large but not too large.

Physically, the implication of $N \sim 1$ in an HBS is that there are a finite number of helical periods around the torus as compared to a large number in the GJ expansion. Equally important, the assumption $\delta \sim \varepsilon$ in the HBS analysis is required in order to make the rotational transform finite: $\iota/2\pi \sim 1$ as implied by Eq. (7.54). In comparison, the GJ expansion requires $\delta \sim \varepsilon^{1/2}$ for $\iota/2\pi \sim 1$. Lastly, the value of beta for both expansions scales as $\beta \sim \varepsilon$, which is similar to the high β tokamak ordering.

At first glance reducing N from order $1/\varepsilon$ to order 1 might seem to be more restrictive and lead to a simpler analysis. Just the opposite is true. The HBS analysis is far more complicated and much less restrictive. It allows for a finite helical magnetic axis, finite helical modulations of the flux surfaces, and brings toroidal effects into the calculation earlier, in the same order as helical effects.

7.4.2 The Greene–Johnson limit of the HBS model

This subsection outlines the reduction of the HBS model to the GJ model in the appropriate region of overlap. To carry out this task it is necessary to introduce a common subsidiary expansion into each model so that the physics does indeed overlap. An intuitive way to view the physics is as follows. The HBS model will now allow N to become large (i.e., there are many helical periods around the torus) but not too large, subject to the constraints of $\iota/2\pi \sim 1$ and $\beta \sim \varepsilon$. In contrast, the GJ model will now allow N to become small (i.e., there are fewer helical periods around the torus) but not too small, also subject to the constraints of $\iota/2\pi \sim 1$ and $\beta \sim \varepsilon$. This corresponds to the region of overlap. Specifically, it is assumed that

$1 \ll N \ll 1/\varepsilon$ which is satisfied if $N \sim 1/\varepsilon^{1/2} \gg 1$. The complete ordering for the overlap model, consistent with the constraints is shown in the last column of Table 7.2.

The analysis starts with the un-normalized version of the HBS model given by Eq. (7.32). New normalized variables are introduced that are consistent with the overlap ordering. The new definitions are

$$\begin{aligned} \rho &= \frac{r}{a} \sim 1 \\ A &= -\frac{A_1}{aB_0 N^{1/2}\varepsilon} \sim 1 \\ \beta &= \frac{2\mu_0 p_1}{\varepsilon B_0^2} \sim 1 \end{aligned} \tag{7.55}$$

Since the physics overlap is closely tied to the ordering for the number of helical periods the definitions in Eq. (7.55) have been chosen so that $1/N$ rather than ε appears as the expansion parameter in the normalized equations which are given by[3]

$$\begin{aligned} \frac{\partial \beta}{\partial \phi} &= -\frac{1}{N^{1/2}} \mathbf{e}_\phi \times \nabla_\perp A \cdot \nabla_\perp \beta \\ \frac{\partial (\nabla_\perp^2 A)}{\partial \phi} &= -\frac{1}{N^{1/2}} \mathbf{e}_\phi \times \nabla_\perp A \cdot \nabla_\perp (\nabla_\perp^2 A) + \frac{1}{N^{3/2}} \mathbf{e}_Z \cdot \nabla_\perp \beta \end{aligned} \tag{7.56}$$

where $\nabla_\perp$ is the gradient in ρ, θ coordinates.

The subsidiary expansion can now be applied. One sees that in both equations the right-hand side is small when $N \sim 1/\varepsilon^{1/2}$ is large, suggesting a solution by a straightforward expansion technique. The details of the expansion are lengthy and are presented in Appendix E. The end result is that the overlap limit of the HBS model has the form of a single Grad–Shafranov-like partial differential equation for the normalized poloidal flux $\psi(\rho, \theta)$. This equation has two free functions of ψ: the pressure $p(\psi) \propto \beta(\psi)$ and the average toroidal current density $\langle J_\phi \rangle \propto J(\psi)$. There is also a contribution from the vacuum helical field. The final Grad–Shafranov-like equation is given by

$$\nabla_\perp^2 \psi = -J - \frac{d\beta}{d\psi}(x - \langle x \rangle) + \nabla_\perp^2 \left(\sum_1^\infty \frac{i}{n} \mathbf{e}_\phi \cdot \nabla_\perp A_n^* \times \nabla_\perp A_n \right) \tag{7.57}$$

[3] Note that it can easily be shown that the GJ ordering implies that $M = 1 + O(\delta)$. This is the reason why M does not explicitly appear in Eq. (7.56).

Here, $x = \rho \cos\theta$ and

$$\begin{aligned}
\psi(\rho,\theta) &= \frac{1}{2\pi a^2 B_0}\psi_p && \text{Normalized poloidal flux } \psi_p \\
\beta(\psi) &= \frac{2\mu_0}{\varepsilon B_0^2}p && \text{Normalized plasma pressure } p \\
J(\psi) &= -\frac{\mu_0 R_0}{B_0}\langle J_\phi\rangle && \text{Normalized toroidal current density } J_\phi
\end{aligned} \tag{7.58}$$

and $\langle\ \rangle$ denotes the average over poloidal angle (written in terms of poloidal arc length $l_p = l_p(\theta)$)

$$\langle Q\rangle = \frac{\oint Q(r,\theta)\dfrac{dl_p}{|\nabla_\perp\psi|}}{\oint \dfrac{dl_p}{|\nabla_\perp\psi|}} \tag{7.59}$$

Lastly, the vector potential is written as $A(\rho,\theta,\phi) = \overline{A}(\rho,\theta) + \tilde{A}(\rho,\theta,\phi)$. The functions $A_n(r,\ \theta)$ in Eq. (7.57) are the amplitudes of the vector potential $\tilde{A}$ corresponding to the vacuum helical fields,

$$\begin{aligned}
\tilde{A}(\rho,\theta,\phi) &= \sum_{n\neq 0} A_n(\rho,\theta)\, e^{in\phi} \\
A_n(\rho,\theta) &= \sum_{l\neq 0} \frac{\delta_{nl}}{2lN^{1/2}\varepsilon}\rho^{|l|}e^{il\theta}
\end{aligned} \tag{7.60}$$

with $\delta_{nl}^2 = (B_{\rho,nl}^2 + B_{\theta,nl}^2)_{\rho=1}/B_0^2$. The quantity $\overline{A}(\rho,\theta)$ is the toroidally averaged component of the vector potential and is related to the poloidal flux function by

$$\overline{A}(\rho,\theta) = \psi - \sum_1^\infty \frac{i}{n}\mathbf{e}_\phi \cdot \nabla_\perp A_n^* \times \nabla_\perp A_n \tag{7.61}$$

Equation (7.57) is the desired GJ limit of the HBS model.

7.4.3 The Greene–Johnson model

The derivation of the Greene–Johnson model also requires a substantial amount of analysis, similar in spirit to the HBS calculation in Appendix E. Derivations of the GJ model can be found in the references (Greene and Johnson, 1961; Freidberg, 1987). For the present purposes of comparison it is sufficient to simply state the original results. After converting to the notation used in Eq. (7.57) one finds that the GJ model can be written as

$$\nabla_\perp^2\psi = -J - \frac{d\beta}{d\psi}(x - \langle x\rangle) + \nabla_\perp^2\left(\sum_1^\infty \frac{i}{n}\mathbf{e}_\phi \cdot \nabla_\perp A_n^* \times \nabla_\perp A_n\right) + \frac{\varepsilon N}{2}\frac{d\beta}{d\psi}\sum_1^\infty\left[\nabla_\perp^2|A_n|^2 - \langle\nabla_\perp^2|A_n|^2\rangle\right] \tag{7.62}$$

In the overlap region $\varepsilon N \sim \varepsilon^{1/2} \ll 1$ and the last term can be neglected. The two models, given by Eqs. (7.57) and (7.62), then coincide showing that the physics does indeed overlap. In the original GJ ordering $\varepsilon N \sim 1$ and the last term must be maintained.

7.4.4 Summary

The discussion above has shown that the high β stellarator model overlaps with the Greene–Johnson model in a regime of physical interest corresponding to helical fields that are wound neither too loosely nor too tightly. This adds further confirmation about the reliability of the high β stellarator model.

7.5 Vacuum flux surfaces

In this section and the ones that follow the high β stellarator model is solved for several special cases in order to acquire some intuition about the MHD equilibrium properties of stellarators. The present section focuses on the calculation of vacuum flux surfaces. As previously stated a stellarator has well-defined flux surfaces with a unique magnetic axis even in the vacuum limit $\beta \to 0$.

The problem is surprisingly complex in a 3-D geometry. For example, even when a simple set of vacuum magnetic fields is specified, such as a combined $l = 2$, $l = 3$ system, there is no simple closed form solution for the flux surfaces. In the examples examined below some analytic and numerical solutions are presented that describe different configurations. A primary goal is to show that there is a maximum limit to the helical field amplitude to avoid the appearance of a separatrix on the surface of the $\beta \to 0$ plasma.

7.5.1 Single helicity – the limiting helical field amplitude

The first example of interest involves a single helicity stellarator. In this case, because of the helical symmetry, an exact solution to the high β stellarator model can be found. The starting point is the second of the normalized high β stellarator equations evaluated in the limit $\beta \to 0$. From Eq. (7.35) it follows that

$$\left(\frac{\partial}{\partial \phi} + \mathbf{e}_\phi \times \nabla_\perp A \cdot \nabla_\perp\right) \nabla_\perp^2 A = 0 \tag{7.63}$$

For a vacuum field the solution is

$$\nabla_\perp^2 A = 0 \tag{7.64}$$

Assume now that the helical component of the magnetic field consists only of a single harmonic with poloidal periodicity l. For this case A is given by

$$\begin{aligned} A(\rho, \theta, \phi) &= \frac{\Delta_l}{l} \rho^l \cos(l\theta + \phi) \\ \Delta_l &= \frac{\delta_l}{N\varepsilon} \end{aligned} \tag{7.65}$$

where $l > 0$ and δ_l is defined by setting $(|B_p|/B_0)_{\rho = 1} = \delta_l$.

Consider next the first of the high β stellarator equations. A flux function ψ is introduced so that $\beta = \beta(\psi)$. Precisely which flux (e.g., poloidal, helical, toroidal) ψ corresponds to is discussed shortly. Also, the single helicity assumption is invoked implying that $\psi(\rho, \theta, \phi) = \psi(\rho, \alpha)$ with $\alpha = l\theta + \phi$. The first high β stellarator equation reduces to

$$\left(1 + \frac{l}{\rho}\frac{\partial A}{\partial \rho}\right)\frac{\partial \psi}{\partial \alpha} - \frac{l}{\rho}\frac{\partial A}{\partial \alpha}\frac{\partial \psi}{\partial \rho} = 0 \tag{7.66}$$

which, after multiplying by 2ρ, is further simplified by substituting A from Eq. (7.65),

$$\frac{\partial \psi}{\partial \alpha}\frac{\partial}{\partial \rho}(\rho^2 + 2\Delta_l \rho^l \cos\alpha) - \frac{\partial \psi}{\partial \rho}\frac{\partial}{\partial \alpha}(\rho^2 + 2\Delta_l \rho^l \cos\alpha) = 0 \tag{7.67}$$

The general solution to this equation is

$$\rho^2 + 2\Delta_l \rho^l \cos\alpha = G(\psi) \tag{7.68}$$

The function $G(\psi)$ is shown here to be proportional to the helical flux ψ_h first defined for the straight stellarator in Chapter 6. This definition, applied to the large aspect ratio vacuum surfaces in the high β stellarator model, is given by

$$\frac{\partial \psi_h}{\partial r} = lB_\theta + hrB_z \approx -l\frac{\partial A_1}{\partial r} + \frac{NB_0}{R_0} r \tag{7.69}$$

This equation can be easily integrated and converted to normalized coordinates. One finds

$$\psi = \rho^2 + 2\Delta_l \rho^l \cos\alpha \tag{7.70}$$

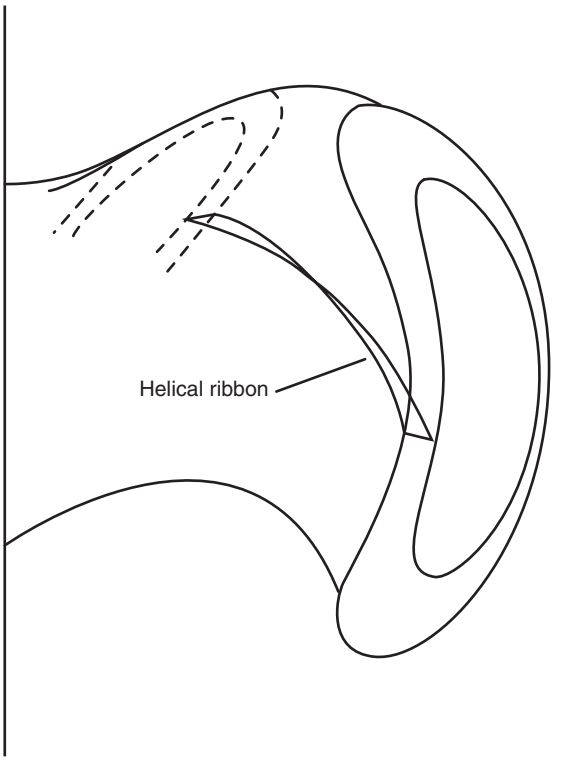

Figure 7.3 Helical flux passing through a rotating helical ribbon whose surface is defined by $\alpha = l\theta + \phi =$ constant.

where $\psi = (2R_0/NB_0a^2)\ \psi_h$ is the normalized helical flux implying that in Eq. (7.68) $G(\psi) = \psi$. Physically the helical flux is the flux passing through a rotating helical ribbon whose surface is defined by $l\theta - N\hat{\phi} =$ constant in un-normalized coordinates or $\alpha = l\theta + \phi =$ constant in normalized coordinates (see Fig. 7.3).

Equation (7.70) is the desired solution for the flux surfaces in a single helicity stellarator. The basic properties of this configuration can now be easily ascertained. The first point to notice is that the solution given by Eq. (7.70) coincides with the vacuum solution for a loosely wound straight stellarator as evidenced by a comparison with Eq. (7.51). This is perhaps not surprising since toroidal effects enter the high β stellarator only through the $\nabla_\perp \beta \cdot \mathbf{e}_Z$ term which vanishes in the limit of a vacuum field.

Next it is of interest to plot the flux contours for several values of l as illustrated in Fig. 7.4. These contours rotate helically along ϕ, the basic signature of a stellarator magnetic geometry. As might be expected $l = 2$ leads to elliptical surfaces, $l = 3$ to triangular surfaces, and $l = 4$ to square surfaces.

It is also worth noting from Eq. (7.35) that in the limit $\beta \to 0$ the appearance of the mirror ratio M vanishes from the high β stellarator equations for ψ and

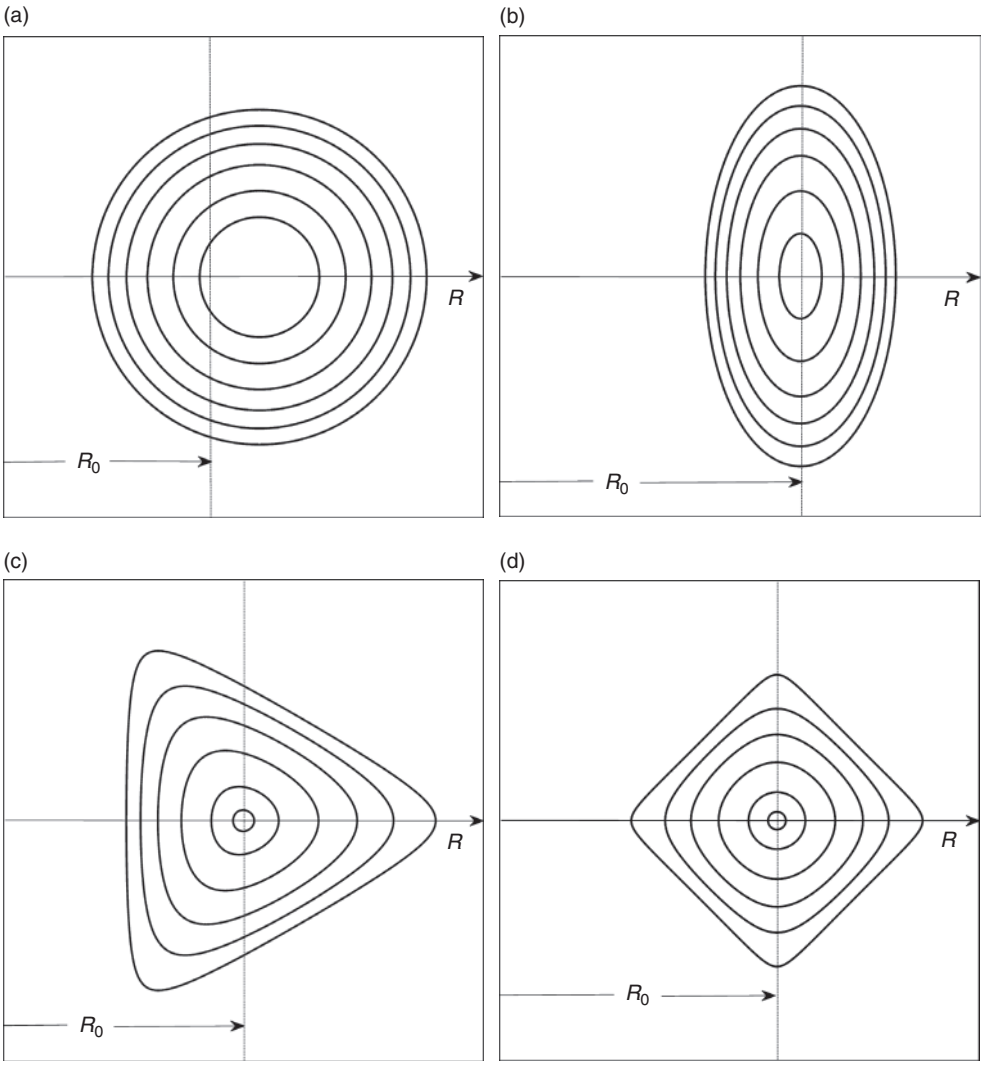

Figure 7.4 Vacuum helical flux surfaces for (a) $l = 1$, (b) $l = 2$, (c) $l = 3$, and (d) $l = 4$ stellarators.

A. Therefore the solution given by Eq. (7.70) still applies. The only difference when $M \neq 1$ is that the transformation back to the un-normalized laboratory coordinates is now given by $\rho = M^{1/2}(r/a)$.

Lastly, a critical feature of the single helicity vacuum surfaces is the existence of a maximum allowable helical amplitude. This limit arises because of the appearance of a separatrix on the plasma surface when the helical field becomes too large. The limiting amplitude can be easily calculated analytically by setting both components of $\nabla\psi$ to zero on the plasma surface.

The only slightly subtle point is defining the value of ψ that corresponds to the $\beta \to 0$ plasma surface. The reason is that the plasma surface has a complicated shape and may be situated in a comparably complicated 3-D vacuum chamber. Where exactly does the plasma make first contact with the surrounding wall, limiter, or diverter which defines the edge of the plasma? For present purposes this difficulty is overcome by defining the $\beta \to 0$ plasma surface to correspond to $r = a$ in the limit of a vanishing small helical field. The plasma surface is thus defined as

$$\psi = 1 \tag{7.71}$$

In this limit the location of the separatrix X-point is given by the simultaneous solution of

$$\begin{aligned} \frac{\partial \psi}{\partial \alpha}\bigg|_{\psi=1} &= 0 \\ \frac{\partial \psi}{\partial \rho}\bigg|_{\psi=1} &= 0 \end{aligned} \tag{7.72}$$

A short calculation shows that the separatrix moves onto the plasma surface when

$$\begin{aligned} \alpha &= \pi \\ \rho &= \left(\frac{1}{l\Delta_l}\right)^{\frac{1}{l-2}} \end{aligned} \tag{7.73}$$

One now sets $\psi = 1$ and substitutes Eq. (7.73) into Eq. (7.70). The result is that in order to avoid a separatrix on the plasma surface the amplitude of the helical field is limited by

$$\Delta_l = \frac{\delta_l}{N\varepsilon} \leq g(l) \equiv \frac{1}{l}\left(\frac{l-2}{l}\right)^{\frac{l-2}{2}} \tag{7.74}$$

For various values of l one finds that $g(2) = 0.5$, $g(3) = 0.192$, and $g(4) = 0.125$. The flux surfaces for an $l = 3$ system at the equilibrium limit are illustrated in Fig. 7.5 to show the appearance of the separatrix.

Physically, the equilibrium limit can be explained as follows. For small radii the flux surfaces are closed since they are dominated by the toroidal field; that is, for $\rho \ll 1$ the flux scales as $\psi \propto \rho^2$. As the radius increases the helical field starts to dominate. The reason is that for any $l \geq 3$, the radial dependence of the helical field, proportional to ρ^l, increases more rapidly than ρ^2. In the region of large ρ the flux surfaces open up because of the oscillatory behavior of the helical field. The separatrix represents the transition surface separating the regions between where the toroidal field or the helical field dominates the flux surface behavior.

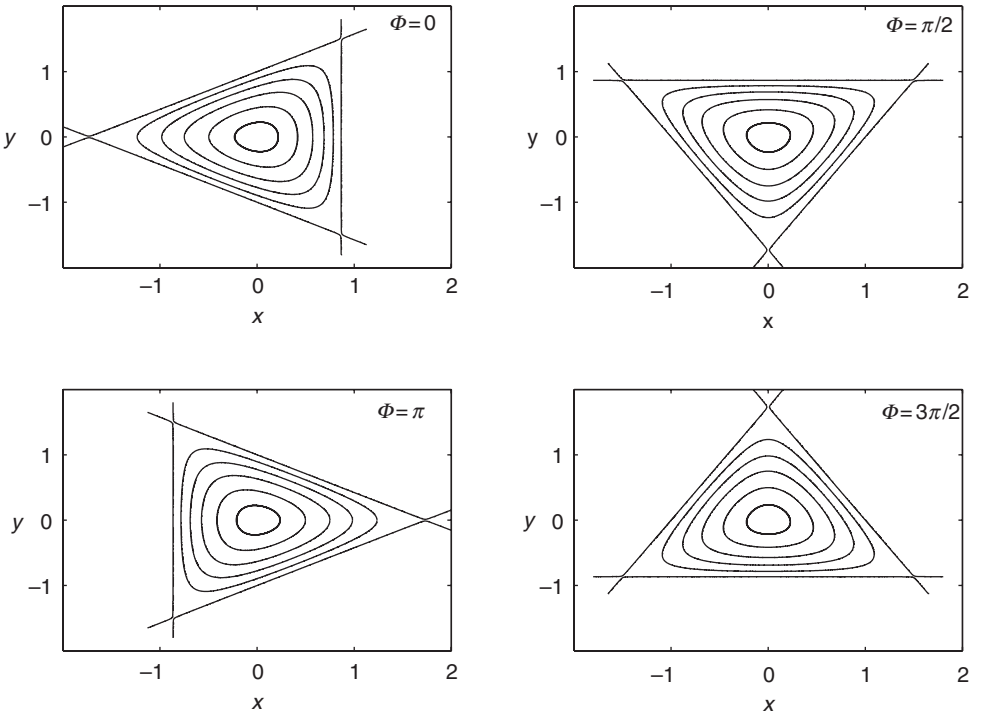

Figure 7.5 Vacuum flux surfaces for an $l = 3$ stellarator at the equilibrium limit showing the separatrix.

In summary, single helicity vacuum surfaces can be calculated analytically. These surfaces are closed out to the edge of the plasma for a sufficiently small helical field amplitude. The surfaces coincide with those calculated for the straight stellarator in Chapter 6.

7.5.2 Multiple helicity stellarators

The next step in building MHD intuition about stellarators involves examining the vacuum flux surfaces in a multiple helicity configuration. The problem is far more difficult than one might imagine. In fact it is not possible to obtain analytic solutions even for a system with only two helical harmonics, for instance $l = 2$ and $l = 3$. The reason is associated with the fact that even in the large aspect ratio, high β stellarator ordering, the problem remains truly three dimensional.

The solution to this problem involves, perhaps not surprisingly, a numerical calculation. There are several numerical procedures that can determine the vacuum surfaces in a fast and accurate manner. These methods are discussed elsewhere allowing the focus here to remain on results (Bauer *et al.*, 1987; Hirshman and Whitson, 1983; Reiman and Greenside, 1986). As an example, results are

presented for an $l = 2$, $l = 3$ stellarator. Of interest is the fact that there is now a finite allowable parameter region in Δ_2, Δ_3 space where flux surfaces exist without the appearance of a separatrix within the plasma.

The numerical formulation

The starting point for the analysis is again the second of the normalized high β stellarator equations evaluated in the vacuum limit $\beta \to 0$, given by

$$\nabla_\perp^2 A = 0 \tag{7.75}$$

In general, the vector potential $A(\rho, \theta, \phi)$ consists of a sum of terms, each one of the form $(\Delta_{l,n}/l)\,\rho^l \cos(l\theta + n\phi + n\phi_{l,n})$. It is assumed that the amplitude $\Delta_{l,n}$, phase $\phi_{l,n}$, and toroidal periodicity number, n, are known for each term. In other words, the applied vacuum helical field is assumed to be fully specified. For the $l = 2$, $l = 3$ example under consideration $A(\rho, \theta, \phi)$ is given by

$$A(\rho, \theta, \phi) = \frac{\Delta_2}{2}\rho^2 \cos(2\theta + \phi) + \frac{\Delta_3}{3}\rho^3 \cos(3\theta + \phi) \tag{7.76}$$

This expression is substituted into the first of the high β stellarator equations leading to

$$\frac{\partial \psi}{\partial \phi} + \frac{1}{\rho}\frac{\partial A}{\partial \rho}\frac{\partial \psi}{\partial \theta} - \frac{1}{\rho}\frac{\partial A}{\partial \theta}\frac{\partial \psi}{\partial \rho} = 0 \tag{7.77}$$

Equation (7.77) is solved numerically subject to the boundary condition of regularity within the plasma region. Since this is a first-order partial differential equation one is not allowed to also specify the shape of the boundary flux surface. In other words, the solution generates free boundary flux surfaces.

Numerical results

A numerically generated plot of the flux surfaces for the values $\Delta_2 = 0.25$ and $\Delta_3 = 0.03$ is illustrated in Fig. 7.6 for several values of ϕ. Observe that the surfaces have a strong combination of elliptical plus triangular deformations as expected. The deformations are finite in extent showing that simple analytic expansions would have a difficult time accurately approximating the solutions.

A second calculation investigates the transition region of parameter space where surfaces exist with and without the presence of a separatrix in the plasma. This region can be determined as follows. The plasma surface in the limit of low β is again chosen as $\psi = 1$. Next, a value of Δ_3 is chosen that satisfies $\Delta_3 < 0.231$, the limiting value for a single helicity $l = 3$ stellarator. Over a series of computer runs the value of Δ_2 is slowly increased from zero until a separatrix appears on the $\psi = 1$ plasma surface. This is the limiting value of Δ_2 for the given Δ_3. The

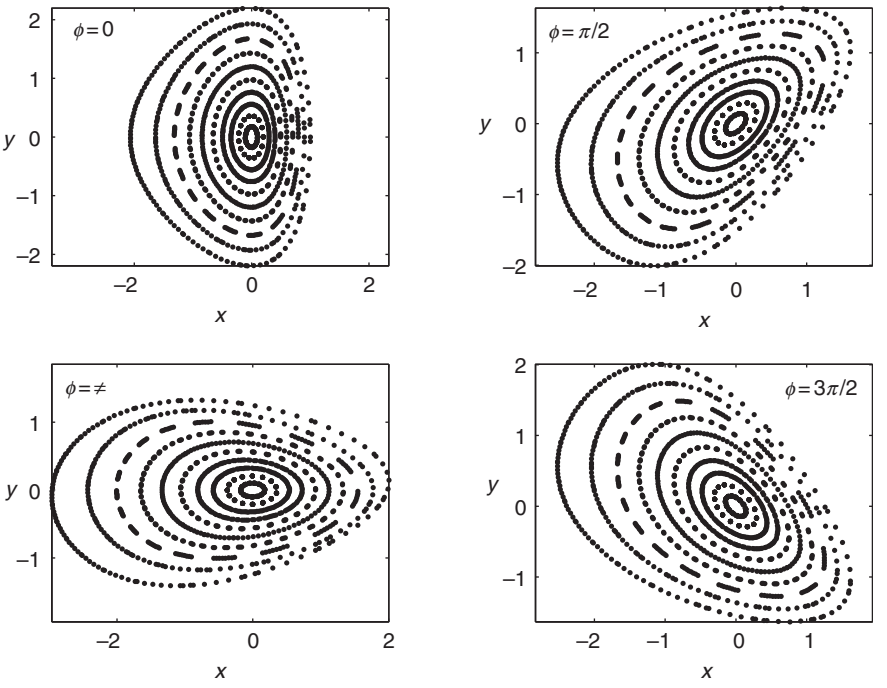

Figure 7.6 Numerically computed vacuum flux surfaces for an $l = 2, 3$ stellarator.

procedure is then repeated for a sequence of different Δ_3 values. The end result is a curve of Δ_2 vs. Δ_3 that defines the separatrix free region of operation and is illustrated in Fig. 7.7. The behavior is qualitatively similar but more difficult to calculate as compared to the pure single helicity stellarator.

Summary

In this subsection it has been shown that a stellarator has closed nested flux surfaces even in the vacuum limit $\beta \to 0$. For a single helicity system, vacuum surfaces can be found analytically. For a multi-helicity system, the vacuum surfaces must be calculated numerically. In general, there is a maximum limit to the size of the helical fields relative to the dominant toroidal field in order to prevent a separatrix from moving onto the plasma surface.

7.6 Effects of finite β

In the previous section the basic properties of vacuum flux surfaces in a stellarator have been derived. The goal of the present section is to determine the effects of

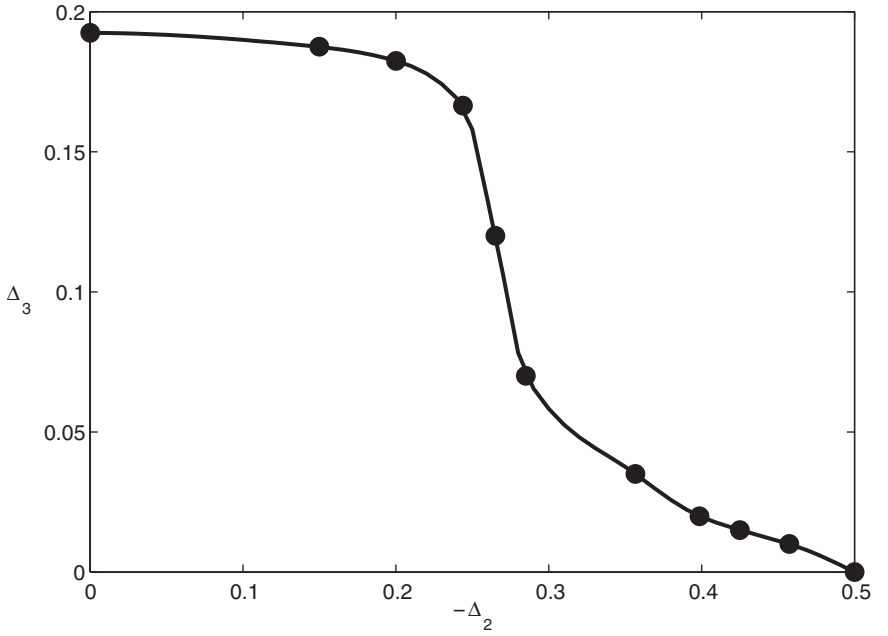

Figure 7.7 Boundary of operation without a separatrix in a Δ_3, Δ_2 space assuming the surface-to-volume ratio of all separatrices is fixed.

finite β on the vacuum surfaces. As might be expected, for reasons of mathematical simplicity, much of the discussion is focused on configurations where the applied vacuum field has only a single helicity, e.g., $\psi = \psi(r, 2\theta + \phi)$. Even so, once finite pressure is included the problem becomes truly three dimensional since toroidal β effects couple through terms proportional to cos θ.

The results of this section show that finite β stellarator equilibria exist even when there is zero net toroidal current flowing in the plasma. Also, finite β shifts the magnetic axis outward with respect to the vacuum magnetic axis. In this connection a simple physical picture is presented that demonstrates how in a current-free stellarator, a helical field produces an inward toroidal force along R to compensate the outward tire tube and $1/R$ forces.

It is also well known and directly demonstrated that in a stellarator with zero net current a vertical field produces no restoring force. This fact raises an apparent paradox since it is well known experimentally that applying a vertical field can indeed shift the plasma inward or outward along R. An explanation is presented that resolves this paradox, based on a dynamical model that takes into account induced, time-varying surface currents.

Interestingly, it is shown that a stellarator has a high β equilibrium limit similar to that in a high β tokamak. Further calculation shows that a flux conserving

stellarator can avoid the equilibrium limit by the natural induction of a net current as β is raised. Lastly numerical solutions are presented that solve the high β stellarator equations for a multi-helicity system.

7.6.1 Low β single helicity solutions

The first problem of interest investigates the equilibrium of a single helicity stellarator with a small but finite β. By assuming that β is small it is possible to derive a simple analytic solution for the flux surfaces from which it is possible to gain some physical insight into the properties of current-free stellarator equilibria.

The basic equations

The analysis is based on the Greene–Johnson overlap model, described by Eq. (7.57). In order to directly relate the solutions to the vacuum flux surfaces previously derived Eq. (7.57) must be renormalized back to the original HBS normalization. The easiest way to do this is to imagine that every term in Eq. (7.57) has a subscript "GJ." The renormalized variables will then have no subscripts and represent the original HBS normalization. The renormalization can be summarized as follows:

$$\begin{aligned} A_{GJ} &= N^{1/2}A = -\frac{A_1}{aB_0N^{1/2}\varepsilon} \\ \beta_{GJ} &= N^2\beta = \frac{2\mu_0 p_1}{\varepsilon B_0^2} \\ J_{GJ} &= NJ = -\frac{\mu_0 R_0}{B_0}\langle J_\phi \rangle \\ \psi_{GJ} &= N\psi = \frac{\psi_p}{2\pi a^2 B_0} \end{aligned} \tag{7.78}$$

In terms of the original HBS variables the overlap equation for the flux becomes

$$\nabla_\perp^2 \psi = -J - \frac{d\beta}{d\psi}(x - \langle x \rangle) + \nabla_\perp^2 \left(\sum_1^\infty \frac{i}{n} \mathbf{e}_\phi \cdot \nabla_\perp A_n^* \times \nabla_\perp A_n \right) \tag{7.79}$$

which is formally identical to Eq. (7.57) although the variables have different definitions.

The low β expansion

Equation (7.79) is solved by first setting $J = 0$, corresponding to a stellarator with zero net current on every flux surface. Next, it is assumed that the vacuum fields correspond to a single helicity. For this case the vector potential amplitude A_n is easily obtained from Eq. (7.65), repeated here for convenience,

$$\begin{aligned} A(\rho,\theta,\phi) &= A_n(\rho,\theta)\, e^{i\phi} + A_n^*(\rho,\theta)\, e^{-i\phi} = \frac{\Delta_l}{l}\rho^l \cos(l\theta+\phi) \\ A_n(\rho,\theta) &= \frac{\Delta_l}{2l}\rho^l e^{il\theta} \end{aligned} \tag{7.80}$$

Equation (7.79) reduces to

$$\nabla_\perp^2 \psi = -2(l-1)^2\Delta_l^2\rho^{2l-4} - \frac{d\beta}{d\psi}(x - \langle x\rangle) \tag{7.81}$$

Note that in the context of the overlap expansion $\Delta_l \sim \delta_l/N\varepsilon \sim \varepsilon^{1/4}$. Mathematically Δ_l must therefore be treated as a small parameter although practically this is not a very good assumption.

Even with these simplifications the 2-D equation is quite difficult to solve – it is still a non-linear partial differential equation. An approximate solution can be obtained by further assuming that β is smaller than assumed in the overlap ordering. The appropriate expansion is to assume that $\psi \sim \Delta_l^2$ and that $\beta/\Delta_l^4 \sim \beta/\varepsilon \ll 1$. Under these assumptions Eq. (7.81) can be solved by expanding

$$\psi(\rho,\theta) = \psi_0(\rho) + \psi_1(\rho,\theta) + \cdots \tag{7.82}$$

where $\psi_1/\psi_0 \sim \beta/\Delta_l^4$. The expansion is qualitatively similar to the low β ohmic tokamak expansion discussed in Chapter 6.

Zeroth-order solution

The zeroth-order equation for ψ_0 is given by

$$\frac{1}{\rho}\frac{d}{d\rho}\left(\rho\frac{d\psi_0}{d\rho}\right) = -2(l-1)^2\Delta_l^2\rho^{2l-4} \tag{7.83}$$

The solution is easily found and is given by

$$\psi_0(\rho) = -\frac{\Delta_l^2}{2}\rho^{2l-2} \tag{7.84}$$

To leading order the ϕ averaged flux surfaces are circular.

First-order solution

The first-order equation which determines ψ_1 can be written as

$$\nabla_\perp^2 \psi_1 = -\frac{d\beta}{d\psi_0}(x - \langle x \rangle) \tag{7.85}$$

Note that for circular flux surfaces the poloidally averaged $\langle x \rangle = \langle \rho \cos\theta \rangle = 0$. One now sets $x = \rho \cos\theta$ implying that $\psi_1(\rho, \theta) = \overline{\psi}_1(\rho) \cos\theta$. Also $\beta(\rho)$ replaces $\beta(\psi_0)$ as the free function. This leads to an equation for $\overline{\psi}_1$ given by

$$\frac{1}{\rho}\frac{d}{d\rho}\left(\rho \frac{d\overline{\psi}_1}{d\rho}\right) - \frac{\overline{\psi}_1}{\rho^2} = -\frac{d\beta}{d\rho}\frac{\rho}{d\psi_0/d\rho} \tag{7.86}$$

which simplifies to

$$\frac{1}{\rho^2}\frac{d}{d\rho}\left[\rho^3 \frac{d}{d\rho}\left(\frac{\overline{\psi}_1}{\rho}\right)\right] = \frac{1}{(l-1)\Delta_l^2 \rho^{2l-4}}\frac{d\beta}{d\rho} \tag{7.87}$$

Two boundary conditions must be specified. The first requires regularity on the axis $\rho = 0$. The second follows from the observation that ψ_0 contains the response to the applied vacuum helical fields while ψ_1 describes the diamagnetic modifications due to finite β. For a confined plasma the diamagnetic contributions must vanish far from the plasma which translates into the condition $\overline{\psi}_1(\infty) \to 0$.

The solution for $\overline{\psi}_1$ is easily obtained by integrating Eq. (7.87) twice and applying the boundary conditions. The result is

$$\overline{\psi}_1(\rho) = -\frac{\rho}{(l-1)\Delta_l^2}\int_\rho^\infty \frac{dx}{x^3}\int_0^x \frac{dy}{y^{2l-6}}\frac{d\beta}{dy} \tag{7.88}$$

Observe that for the solution to be well behaved near the origin for $l \geq 3$, the pressure profile must be very flat. The reason is that high l stellarator fields are very small near $\rho = 0$ (i.e., $B_p \propto \rho^{l-1}$) and are thus incapable of providing radial pressure balance. Specifically, for well-behaved solutions β must vary as $c_1 - c_2\rho^{4l-6}$.

The full solution

The solution is completed by adding the helical modulation to the flux surfaces obtained by setting the full $\psi_{tot}(\rho, \theta, \phi) = [\psi_0(\rho) + \overline{\psi}(\rho) \cos\theta] + \psi_{hel}(\rho, \theta, \phi) =$ constant. The quantity ψ_{hel} has been evaluated in Appendix E, Eq. (E.9), and can be written as

$$\begin{aligned}\psi_{hel}(\rho, \theta, \phi) &= \sum_{n\neq 0}\frac{i}{n}(\mathbf{e}_\phi \cdot \nabla_\perp A_n \times \nabla_\perp \psi_0)\, e^{in\phi} \\ &= -(l-1)\Delta_l^3 \rho^{3l-4} \cos(l\theta + \phi)\end{aligned} \tag{7.89}$$

The full solution is obtained by adding the terms from Eqs. (7.84), (7.88), and (7.89). The final form is simplified by assuming that $\beta = \beta_0(1 - \rho^{4l-6})$ for $0 \le \rho \le 1$. The end result for $l = 2$ is given by

$$\begin{aligned} \psi_{tot} &= -\frac{\Delta_2^2}{2}\left[\rho^2 + 2\Delta_2\rho^2\ \cos(2\theta+\phi) - \frac{\beta_0}{2\Delta_2^4}(2\rho-\rho^3)\ \cos\theta\right] && \rho \le 1 \\ \psi_{tot} &= -\frac{\Delta_2^2}{2}\left[\rho^2 + 2\Delta_2\rho^2\ \cos(2\theta+\phi) - \frac{\beta_0}{2\Delta_2^4}\frac{\cos\theta}{\rho}\right] && \rho \ge 1 \end{aligned} \tag{7.90}$$

Discussion

There are several important conclusions that can be drawn from Eq. (7.90). First and foremost, the solution given by Eq. (7.90) shows that closed nested flux surfaces exist in a small but finite β stellarator having zero net current on every flux surface. In the context of the low β expansion used in the analysis these flux surfaces are nearly circular with a small toroidal shift along R (the $\cos\theta$ term) and a small rotating helical ellipticity (the $\cos(2\theta+\phi)$ term). Even in this simple model the flux surfaces are three dimensional.

The perturbation to the circular flux surfaces, denoted by σ, can be determined by expanding $\rho = \overline{\rho} + \sigma(\overline{\rho}, \theta, \phi)$ with $\sigma/\overline{\rho} \ll 1$. Substituting into Eq. (7.90) yields

$$\begin{aligned} \sigma &= -\Delta_2\overline{\rho}\ \cos(2\theta+\phi) + \frac{\beta_0}{4\Delta_2^4}(2-\overline{\rho}^2)\cos\theta && \overline{\rho} \le 1 \\ \sigma &= -\Delta_2\overline{\rho}\ \cos(2\theta+\phi) + \frac{\beta_0}{4\Delta_2^4}\frac{1}{\overline{\rho}^2}\cos\theta && \overline{\rho} \ge 1 \end{aligned} \tag{7.91}$$

As stated the elliptical modulation due to the helical fields rotates as one moves along ϕ around the torus.

The toroidal shift is outward along R since the coefficient of the $\cos\theta$ term is positive. The shift continuously decreases for large $\overline{\rho} \gg 1$ since, as one expects, diamagnetic effects become smaller away from the plasma. Within the plasma (i.e., $\rho \le 1$), it is of interest to calculate the toroidal shift $\overline{\sigma}$ (which is the actual shift normalized to the plasma radius a) near the magnetic axis and at the plasma edge. These shifts are defined as follows:

$$\begin{aligned} \overline{\sigma}(\text{axis}) \equiv \overline{\sigma}_0 &= \frac{1}{2\pi}\int \sigma(0,0,\phi)d\phi = \frac{\beta_0}{2\Delta_2^4} \\ \overline{\sigma}(\text{edge}) \equiv \overline{\sigma}_a &= \frac{1}{2\pi}\int \overline{\sigma}(1,0,\phi)d\phi = \frac{\beta_0}{4\Delta_2^4} \end{aligned} \tag{7.92}$$

Observe that $\overline{\sigma}(\text{axis}) > \overline{\sigma}(\text{edge})$. The magnetic axis is shifted outward with respect to the edge of the plasma.

Now that the existence of MHD equilibria in a current-free stellarator has been established the next task is to understand physically how a helical magnetic field can produce a restoring force along R to balance the outward tire tube and $1/R$ forces. This is the topic of the next subsection.

7.6.2 Toroidal force balance in a current-free stellarator

In Chapter 6 it was shown that toroidal force balance in a tokamak is achieved by the application of a vertical field which interacts with the net toroidal current in the plasma. This interaction generates an inward force along R of magnitude $2\pi R_0 B_V I$ that balances the outward tire tube, $1/R$, and hoop forces.

In a current-free stellarator the hoop force and most importantly the vertical field force both vanish. How then does a stellarator compensate for the remaining tire tube and $1/R$ forces? Answering this question is the goal of the present subsection. Specifically, one wants to learn which magnetic field $\mathbf{B}$ and current $\mathbf{J}$ interact to produce the inward restoring force required to achieve toroidal force balance. It is shown below that it is the interaction of the vacuum helical magnetic field with the helical modulation of the Pfirsch–Schluter current that produces the restoring force.

Formulation of the toroidal force balance problem

The basic idea used to explain toroidal force balance is straightforward. One starts with the ideal MHD momentum equation, calculates the local toroidal force (i.e., the component along R), and then integrates over the entire plasma volume to obtain the total toroidal force. In this way the various global forces entering toroidal balance can be understood. Mathematically, this procedure can be stated as follows:

$$\int (\mathbf{J} \times \mathbf{B} - \nabla p) \cdot \mathbf{e}_R \, d\mathbf{r} = 0 \tag{7.93}$$

To help obtain physical intuition it is helpful to decompose $\mathbf{B}$ and $\mathbf{J}$ into poloidal and toroidal components,

$$\begin{aligned} \mathbf{B} &= \mathbf{B}_p + B_\phi \mathbf{e}_\phi \\ \mathbf{J} &= \mathbf{J}_p + J_\phi \mathbf{e}_\phi \end{aligned} \tag{7.94}$$

Equation (7.93) then reduces to

$$\int (J_\phi \mathbf{e}_\phi \times \mathbf{B}_p + B_\phi \mathbf{J}_p \times \mathbf{e}_\phi - \nabla p) \cdot \mathbf{e}_R \, d\mathbf{r} = 0 \tag{7.95}$$

Note that there is no $\mathbf{J}_p \times \mathbf{B}_p \cdot \mathbf{e}_R$ contribution since $\mathbf{J}_p \times \mathbf{B}_p$ points in the $\mathbf{e}_\phi$ direction. Next, each of the terms in Eq. (7.95) is evaluated. The first term corresponds to the helical restoring force, the second to the $1/R$ force, and the last to the tire tube force.

The tire tube force

The tire tube force exists in any toroidal geometry and can be evaluated without taking into account the detailed properties of the configuration under investigation. The calculation proceeds by using some simple vector identities

$$\begin{aligned} \nabla p \cdot \mathbf{e}_R &= \nabla p \cdot \nabla R \\ &= \nabla \cdot (p \nabla R) - p \nabla^2 R \\ &= \nabla \cdot (p \nabla R) - \frac{p}{R} \end{aligned} \tag{7.96}$$

The divergence term integrates to zero by Gauss's theorem assuming that p vanishes at large r.

In the large aspect ratio limit the tire tube force can thus be written as

$$F_{TT} = -\int \nabla p \cdot \mathbf{e}_R \, d\mathbf{r} = \int \frac{p}{R} \, d\mathbf{r} \approx \frac{1}{R_0} \int p \, d\mathbf{r} \tag{7.97}$$

Since $F_{TT} > 0$ the tire tube force points outward as expected.

*The 1/*R *force*

The $1/R$ force is also quite general, depending only on toroidicity but not the details of the configuration under consideration. The force is again easily calculated using some simple vector identities,

$$\begin{aligned} B_\phi \mathbf{J}_p \times \mathbf{e}_\phi \cdot \mathbf{e}_R &= -\frac{B_\phi}{\mu_0 R} \nabla (R B_\phi) \cdot \nabla R \\ &= \frac{1}{2\mu_0} \nabla (R^2 B_\phi^2 - R_0^2 B_0^2) \cdot \nabla \frac{1}{R} \\ &= \frac{1}{2\mu_0} \nabla \cdot \left[(R^2 B_\phi^2 - R_0^2 B_0^2) \nabla \frac{1}{R} \right] - \frac{1}{2\mu_0} (R^2 B_\phi^2 - R_0^2 B_0^2) \nabla^2 \frac{1}{R} \end{aligned} \tag{7.98}$$

The divergence term again integrates to zero by Gauss's theorem since $RB_\phi \to R_0 B_0$ for large r. The remaining term is evaluated by (1) recalling from Eq. (7.11) that in a low β stellarator $RB_\phi \approx R_0 B_0 + R_0 B_{\phi 1}$ and (2) that $\nabla^2 (1/R) = 1/R^3$. This leads to

$$F_{1/R} = \int B_\phi \mathbf{J}_p \times \mathbf{e}_\phi \cdot \mathbf{e}_R \, d\mathbf{r} \approx -\frac{1}{\mu_0} \int \frac{R_0^2 B_0 B_{\phi 1}}{R^3} \, d\mathbf{r} \approx -\frac{1}{\mu_0 R_0} \int B_0 B_{\phi 1} d\mathbf{r} \quad (7.99)$$

The last step makes use of the fact that radial pressure balance in a stellarator is similar to that in a θ-pinch. Specifically, Eq. (7.15) shows that $p_1 + B_0 B_{\phi 1}/\mu_0 = 0$. This leads to the final form of the $1/R$ force which can be written as

$$F_{1/R} \approx \frac{1}{R_0} \int p \, d\mathbf{r} \quad (7.100)$$

Observe that the $1/R$ force is equal in sign and magnitude to the tire tube force.

The helical restoring force

The helical restoring force depends on the details of the stellarator magnetic field, and thus requires some additional analysis. The first step is to calculate the quantities $\mathbf{B}_p$ and J_ϕ that appear in the remaining term of toroidal force balance.

In a low β system the only term in $\mathbf{B}_p$ that enters force balance corresponds to the vacuum helical field, denoted by $\hat{\mathbf{B}}_p$. This term is easily evaluated and for $l = 2$ is given by

$$\begin{aligned} \hat{\mathbf{B}}_p &= \nabla_\perp \hat{A}_1 \times \mathbf{e}_\phi \\ &= -haB_0 \nabla_\perp \left[\frac{\Delta_l}{l} \rho^l \cos(l\theta + \phi) \right] \times \mathbf{e}_\phi \\ &= hB_0 \Delta_2 r [\sin\alpha \, \mathbf{e}_r + \cos\alpha \, \mathbf{e}_\theta] \end{aligned} \quad (7.101)$$

where $\alpha = 2\theta + \phi$. It then follows that the combination $\mathbf{e}_\phi \times \mathbf{B}_p \cdot \mathbf{e}_R$ can be written as

$$\begin{aligned} \mathbf{e}_\phi \times \mathbf{B}_p \cdot \mathbf{e}_R &= hB_0 \Delta_2 r \, \mathbf{e}_\phi \times (\sin\alpha \, \mathbf{e}_r + \cos\alpha \, \mathbf{e}_\theta) \cdot (\cos\theta \, \mathbf{e}_r - \sin\theta \, \mathbf{e}_\theta) \\ &= -hB_0 \Delta_2 r (\cos\alpha \cos\theta + \sin\alpha \sin\theta) \end{aligned} \quad (7.102)$$

The next step describes the evaluation of J_ϕ which must be calculated to leading and first order in Δ_2. The reason is that the leading-order term will be shown to average to zero when integrating over ϕ. The basic equation determining J_ϕ is obtained by recalling that $\mu_0 J_\phi = -\nabla_\perp^2 A_1$ where $\nabla_\perp^2 A_1$ satisfies Eq. (7.32) with $M = 1$,

$$\left(hB_0 \frac{\partial}{\partial \phi} - \mathbf{e}_\phi \times \nabla_\perp A_1 \cdot \nabla_\perp \right) \nabla_\perp^2 A_1 = -\frac{2\mu_0}{R_0} \nabla_\perp p_1 \cdot \mathbf{e}_Z \quad (7.103)$$

This equation can be simplified by writing $A_1 = \hat{A}_1 + \tilde{A}_1$ where $\hat{A}_1$ is the vacuum helical field and $\tilde{A}_1$ is the diamagnetic contribution due to the pressure. It then

follows that $\nabla_\perp^2 \hat{A}_1 = 0$, $\nabla_\perp^2 \tilde{A}_1 = -\mu_0 J_\phi$ and, in the limit of small but finite pressure, $\tilde{A}_1/\hat{A}_1 \sim \beta \ll 1$. After again substituting $\hat{A}_1 = -(hB_0\Delta_2/2)\, r^2 \cos\alpha$ one finds that Eq. (7.103) reduces to

$$\left[\frac{\partial}{\partial\phi} + \Delta_2\left(\cos\alpha\frac{\partial}{\partial\theta} + r\,\sin\alpha\frac{\partial}{\partial r}\right)\right] J_\phi = \frac{2}{hR_0B_0}\nabla_\perp p_1 \cdot \mathbf{e}_Z \tag{7.104}$$

The task now is to solve this equation for the current density by expanding $J_\phi = J_{\phi 0} + J_{\phi 1} + J_{\phi 2} + \cdots$ where Δ_2 is the small expansion parameter. Ultimately it is necessary to calculate both $J_{\phi 0}$ and $J_{\phi 1}$. The leading-order equation is given by

$$\frac{\partial J_{\phi 0}}{\partial\phi} = 0 \tag{7.105}$$

which implies that

$$J_{\phi 0}(r,\theta,\phi) = \overline{J}_{\phi 0}(r,\theta) \tag{7.106}$$

This quantity will be calculated from a higher-order integrability constraint.

The first-order equation determines $J_{\phi 1}$ and can be written as

$$\frac{\partial J_{\phi 1}}{\partial\phi} = -\Delta_2\left(\cos\alpha\frac{\partial}{\partial\theta} + r\,\sin\alpha\frac{\partial}{\partial r}\right)\overline{J}_{\phi 0} \tag{7.107}$$

which has as its solution

$$J_{\phi 1} = \tilde{J}_{\phi 1} + \overline{J}_{\phi 1} = -\Delta_2\left(\sin\alpha\frac{\partial}{\partial\theta} - r\,\cos\alpha\frac{\partial}{\partial r}\right)\overline{J}_{\phi 0} + \overline{J}_{\phi 1}(r,\theta) \tag{7.108}$$

The second-order equation contains the first appearance of the pressure and leads to an expression for $\overline{J}_{\phi 0}$ by means of a periodicity constraint. The second-order equation is obtained by noting that within the context of the Δ_2 expansion the right-hand side of Eq. (7.104) reduces to

$$\begin{aligned}\frac{2}{hR_0B_0}\nabla_\perp p_1 \cdot \mathbf{e}_Z &= \frac{2}{hR_0B_0}\frac{dp_1}{d\psi}\left(\frac{\partial\psi}{\partial r}\,\sin\theta + \frac{1}{r}\frac{\partial\psi}{\partial\theta}\cos\theta\right)\\ &\approx \frac{2}{hR_0B_\phi}\frac{dp_1}{dr}\left[\sin\theta + O(\Delta_2)\right]\end{aligned} \tag{7.109}$$

where use has been made of the fact that $\psi \propto r^2[1 + O(\Delta_2)]$ and $p_1(r)$ rather than $p_1(\psi)$ now serves as the free function. The second-order equation is thus given by

$$\frac{\partial J_{\phi 2}}{\partial\phi} = -\Delta_2\left(\cos\alpha\frac{\partial}{\partial\theta} + r\,\sin\,\alpha\frac{\partial}{\partial r}\right)J_{\phi 1} + \frac{2}{hR_0B_0}\frac{dp_1}{dr}\,\sin\theta \tag{7.110}$$

For $J_{\phi 2}$ to be periodic the average value of the right-hand side over one period in ϕ (or equivalently α) must vanish. After the expression for $J_{\phi 1}$ is substituted into Eq. (7.110) a straightforward evaluation of the periodicity constraint yields

$$\overline{J}_{\phi 0}(r,\theta) = \frac{2}{hR_0B_0\Delta_2^2}\frac{dp_1}{dr}\ \cos\theta = 2\frac{q_H}{B_0}\frac{dp_1}{dr}\ \cos\theta \tag{7.111}$$

This expression is just the Pfirsch–Schluter current first obtained for a tokamak in Eq. (6.97) except that the safety factor corresponds to the vacuum helical transform (i.e., $q_H = 2\pi/\iota = 1/hR_0\Delta_2^2$) rather than the tokamak safety factor (i.e., $q = rB_0/R_0B_\theta$). Equation (7.111) is next substituted into Eq. (7.108) yielding an explicit expression for $J_{\phi 1}$

$$J_{\phi 1} = \tilde{J}_{\phi 1} + \overline{J}_{\phi 1} = \frac{2}{hR_0B_0\Delta_2}\left(\frac{dp_1}{dr}\sin\alpha\ \sin\theta + r\frac{d^2p_1}{dr^2}\ \cos\alpha\ \cos\theta\right) + \overline{J}_{\phi 1}(r,\theta) \tag{7.112}$$

The quantities required to evaluate the helical restoring force have now been calculated. If one makes use of the fact that $d\mathbf{r} = R_0 r dr d\theta d\phi = R_0 r dr d\theta d\alpha$ then the helical restoring force F_H can be evaluated from the definition

$$\begin{aligned} F_H &= \int J_\phi(\mathbf{e}_\phi \times \mathbf{B}_p \cdot \mathbf{e}_R)\, d\mathbf{r} \\ &\approx \int (\overline{J}_{\phi 0} + \tilde{J}_{\phi 1} + \overline{J}_{\phi 1})(\mathbf{e}_\phi \times \hat{\mathbf{B}}_p \cdot \mathbf{e}_R) R_0 r dr d\theta d\alpha \end{aligned} \tag{7.113}$$

The $\overline{J}_{\phi 0}$ and $\overline{J}_{\phi 1}$ terms average to zero over α. Only the $\tilde{J}_{\phi 1}$ contributes to the helical force. The expressions for $\tilde{J}_{\phi 1}$ and $\mathbf{e}_\phi \times \hat{\mathbf{B}}_p \cdot \mathbf{e}_R$ are substituted into Eq. (7.113) and the integrals over θ and α are evaluated. The expression for F_H reduces to

$$F_H = -2\pi^2 \int \left(r^2\frac{dp_1}{dr} + r^3\frac{d^2p_1}{dr^2}\right)dr \tag{7.114}$$

After several integration by parts this expression can be rewritten as

$$F_H = -8\pi^2 \int prdr = -\frac{2}{R_0}\int pd\mathbf{r} \tag{7.115}$$

where the subscript "1" has been suppressed from p_1. Equation (7.115) is the desired expression for the helical restoring force.

Discussion

After combining the expressions for the tire tube force (Eq. (7.97)), the $1/R$ force (Eq. (7.100)), and the helical force (Eq. (7.115)) one finds that

$$F_H = F_{TT} + F_{1/R} \tag{7.116}$$

The helical field does indeed provide an inward toroidal restoring force that balances the outward tire tube and $1/R$ forces. Force balance occurs at a location which is slightly shifted from the natural center of the vacuum helical magnetic axis because of the plasma pressure.

The field and current that interact to produce the helical restoring force are $\hat{\mathbf{B}}_p$ and $\tilde{J}_{\phi 1}\mathbf{e}_\phi$. Here, $\hat{\mathbf{B}}_p$ is the vacuum helical field and $\tilde{J}_{\phi 1}$ is a toroidal current arising from the helical modulation of the Pfirsch–Schluter current.

7.6.3 How does a vertical field shift a stellarator with no net current?

As is well known, an applied vertical field does not produce an inward or outward force along R in a current-free stellarator. This can be easily seen by calculating the force due a uniform vertical field $\mathbf{B} = B_V\mathbf{e}_Z$ as follows:

$$\begin{aligned} F_V &= \int (\mathbf{J} \times \mathbf{B_V}) \cdot \mathbf{e}_R \, d\mathbf{r} \\ &= B_V \int J_\phi R \, r dr \, d\theta \, d\phi \\ &\approx B_V \int R_0 d\phi \int J_\phi \, r dr \, d\theta \\ &= 2\pi R_0 B_V I \end{aligned} \tag{7.117}$$

Equation (7.117) is the expected result which shows that in a current-free stellarator (defined by $I = 0$), the vertical field force $F_V = 0$. The zero force result leads to an apparent paradox. It is well known experimentally that a current-free stellarator can be shifted inward or outward along R by changing the applied vertical field. However, if a vertical field produces no toroidal force how then can changing B_V shift the plasma?

The answer is associated with the fact that during the time when the vertical field is changing there is, in the context of ideal MHD, a transiently induced toroidal surface current

$$\mathbf{K} = K\mathbf{e}_\phi = (K_I + K_D \cos\theta)\mathbf{e}_\phi \tag{7.118}$$

The amplitude K consists of two components: (1) a net current K_I and (2) a dipole current $K_D \cos\theta$. These interact with the applied helical field and the changing vertical field in a somewhat complex manner, the end result nevertheless being a transient toroidal restoring force which shifts the plasma to a new position. Once the vertical field reaches its final steady state value, the restoring force and the corresponding surface current vanish. This is how a vertical field shifts the

plasma. A summary of the interactions that lead to the transient restoring force is as follows.

A convenient way to understand the basic physics is to think of the plasma as a perfectly conducting wire which at time $t = 0$ carries no electric current. A vertical field is then applied in the Z direction. If the wire is straight with its cross section lying in the R, Z plane then a dipole current is induced on the plasma surface to cancel the applied vertical field within the wire. The interior of a perfectly conducting wire is completely shielded from the applied magnetic field.

If the wire instead has the shape of a circular loop then, in addition to the dipole current, there is a component of net current. The magnitude and sign of the net current are determined by the requirement that the flux passing through the hole in the loop remains constant at its initial value. The flux passing through a closed perfectly conducting wire cannot change.

Now, the net current flowing on the surface K_I produces both a vertical field force and a hoop force along R. The combination of these two forces can be shown to be always inward causing the ring to try and collapse on itself. Since K_I is proportional to B_V,[4] this inward force is proportional to $K_I B_V \propto B_V^2$. Consequently, for small B_V the K_I force is small compared to the dipole force which is shown to be linearly proportional to B_V. For simplicity of presentation the effects of the net surface current are hereafter neglected.

The restoring force arising from the dipole current is slightly subtle. The situation is as follows. The interaction of the surface dipole current with the vertical field makes no net toroidal force on the wire – the force averages to zero over θ. Similarly, the interaction of the dipole current with the applied helical magnetic field would also average to zero over ϕ if the minor cross section of the wire was circular. But, the actual plasma cross section is circular plus a helical modulation. This modulation causes the average value of the helical field $\langle \mathbf{B}_h \rangle$ on the plasma surface to be non-zero. Indeed, it is $\langle \mathbf{B}_h \rangle$ that generates the rotational transform. The interaction of the surface dipole current with $\langle \mathbf{B}_h \rangle$ on the helically modulated surface produces the dominant toroidal restoring force. This force can be either inward or outward depending upon the sign of B_V.

A simple model is presented below that translates these ideas into a quantitative prediction of the dynamical motion of the plasma as it moves from one state to another.

The flux function in the presence of a vertical field

The dynamical model is derived by modifying the low β solution to the Greene–Johnson overlap equations derived in Section 7.6.1 to include the effect of an

[4] The current required to cancel the vertical field flux is given by $LI = \pi R_0^2 B_V$, which implies that $I \propto K_I \propto B_V$.

applied-time varying vertical field. For analytic simplicity attention is again focused on a single helicity $l = 2$ stellarator in which the free pressure function is chosen as $\beta(\rho) = \beta_0(1 - \rho^2)$. The inclusion of an applied vertical field requires that homogeneous solutions be added to the solutions given by Eq. (7.90). The corresponding amplitudes are determined by a modified set of boundary conditions.

Based on the discussion above, the homogeneous solutions include the effect of the dipole surface current but neglect those due to the net surface current. The dipole contribution to the flux appears in both the interior and exterior of the plasma. The interior contribution is not automatically zero but has a value to cancel the contribution arising from the plasma shift. The modified solutions can be written as

$$\begin{aligned}
&\rho \le 1 \\
&\quad \psi_{tot} = -\frac{\Delta_2^2}{2}\left[\rho^2 + 2\Delta_2\rho^2\ \cos(2\theta+\phi) - \frac{\beta_0}{2\Delta_2^4}(2\rho-\rho^3)\ \cos\theta\right] + c_1\rho\ \cos\theta \\
&\rho \ge 1 \\
&\quad \psi_{tot} = -\frac{\Delta_2^2}{2}\left[\rho^2 + 2\Delta_2\rho^2\ \cos(2\theta+\phi) - \frac{\beta_0}{2\Delta_2^4}\frac{\cos\theta}{\rho}\right] + \left(c_2\rho + \frac{c_3}{\rho}\right)\ \cos\theta
\end{aligned} \tag{7.119}$$

The terms labeled by the coefficients $c_j = c_j(t)$ are the time-varying homogeneous dipole solutions.

The unknown coefficients are determined by a set of boundary conditions that must be satisfied by the toroidally averaged flux function

$$\overline{\psi}_{tot}(\rho,\theta,t) = \frac{1}{2\pi}\int_0^{2\pi} \psi_{tot}\, d\phi \tag{7.120}$$

From Eq. (7.119) one sees that

$$\begin{aligned}
\overline{\psi}_{tot} &= -\frac{\Delta_2^2}{2}\left[\rho^2 - \frac{\beta_0}{2\Delta_2^4}(2\rho-\rho^3)\ \cos\theta\right] + c_1\rho\ \cos\theta \qquad \rho \le 1 \\
\overline{\psi}_{tot} &= -\frac{\Delta_2^2}{2}\left[\rho^2 - \frac{\beta_0}{2\Delta_2^4}\frac{\cos\theta}{\rho}\right] + \left(c_2\rho + \frac{c_3}{\rho}\right)\ \cos\theta \qquad \rho \ge 1
\end{aligned} \tag{7.121}$$

The boundary conditions on $\overline{\psi}_{tot}$ are as follows. First, note that the plasma–vacuum interface is a slightly shifted circle. The shift, as discussed, arises from the forces generated by the surface current. This is in addition to the initial

shift generated by the tire tube and $1/R$ forces. For a small vertical field the shift is also small, implying that the shape of the plasma–vacuum interface can be written as

$$\rho_S(\theta,t) = 1 + \overline{\sigma}_a(t)\ \cos\theta \tag{7.122}$$

where, from Eq. (7.92), $\overline{\sigma}_a(0) = \beta_0/4\Delta_2^2$. The shift $\sigma_a(t) \ll 1$ is the basic unknown in the problem. The main goal of the model is to calculate $\overline{\sigma}_a(t)$ as a function of $B_V(t)$.

The first boundary condition requires continuity of flux across the interface and is given by

$$[\![\,\overline{\psi}_{tot}(\rho_S,\theta,t)\,]\!] = 0 \tag{7.123}$$

Here, $[\![\ ]\!]$ denotes the jump across the surface.

The second boundary condition specifies the change in flux far from the plasma due to the vertical field $B_V(t)$. This change from its initial value is denoted by $\delta\overline{\psi}_{tot}(\rho,\theta,t)$ where $\delta\overline{\psi}_{tot}(\rho,\theta,t) = \overline{\psi}_{tot}(\rho,\theta,t) - \overline{\psi}_{tot}(\rho,\theta,0)$. In terms of the present notation the boundary condition has the form

$$\delta\overline{\psi}_{tot}(\rho,\theta,t)\big|_{\rho\gg 1} \rightarrow \frac{B_V(t)}{haB_0}\rho\ \cos\theta \tag{7.124}$$

The third and last boundary condition corresponds to conservation of flux in the plasma. A useful way to view the situation is as follows. Initially the plasma is in equilibrium with the helical field force balancing the tire tube and $1/R$ forces. The fields have diffused into the plasma leading to the low β solutions given by Eq. (7.90). The vertical field is now applied. Its rise time is slow compared to the ideal MHD time but fast compared to the resistive diffusion time. During the evolution the plasma, therefore, behaves like a perfect conductor with respect to the vertical field. In other words, the flux in the plasma at any instant of time must always equal its initial value. This is the third boundary condition which can be expressed as

$$\overline{\psi}_{tot}[\rho_S(t),\theta,t] = \overline{\psi}_{tot}[\rho_S(0),\theta,0] \tag{7.125}$$

The problem has now been fully specified. Next, to determine the desired dynamical equations requires the following steps: (1) apply the boundary conditions to Eq. (7.121) to evaluate the homogeneous solution coefficients $c_j(t)$; (2) use the resulting solution to calculate the jump in the poloidal field across the plasma surface, which then yields the induced surface current; (3) from the surface current it is straightforward to calculate the net body force on the plasma $F_R(t)$; and (4) the dynamical equations follow from balancing the body force with the plasma inertial force.

The final dynamical equation has the form of a differential equation for $\overline{\sigma}_a(t)$ driven by a forcing term proportional to $B_V(t)$. The solution to this equation is easily obtained showing how a vertical field shifts the plasma in a current-free stellarator.

Applying the boundary conditions

It is a straightforward matter to apply the boundary conditions and evaluate the c_j. The jump condition given by Eq. (7.123) requires that

$$c_1 = c_2 + c_3 \tag{7.126}$$

The far field condition defined by Eq. (7.124) implies that

$$c_2 = \frac{B_V(t)}{haB_0} \tag{7.127}$$

Lastly, keeping in mind that $\rho_S = 1 + \overline{\sigma}_a \cos\theta$ must be expanded for small $\overline{\sigma}_a$ on the surface, one sees that conservation of flux within the plasma as given by Eq. (7.125) yields

$$c_1 = \Delta_2^2[\overline{\sigma}_a(t) - \overline{\sigma}_a(0)] \tag{7.128}$$

The resulting solutions for the c_j are substituted into Eq. (7.121) leading to the following expressions for the plasma flux including the effects of the applied vertical field:

$$\rho \le 1$$
$$\overline{\psi}_{tot} = -\frac{\Delta_2^2}{2}\left[\rho^2 - \frac{\beta_0}{2\Delta_2^4}(2\rho - \rho^3)\cos\theta\right] + \Delta_2^2(\overline{\sigma}_a - \overline{\sigma}_{a0})\rho\cos\theta$$
$$\rho \ge 1$$
$$\overline{\psi}_{tot} = -\frac{\Delta_2^2}{2}\left[\rho^2 - \frac{\beta_0}{2\Delta_2^4}\frac{\cos\theta}{\rho}\right] + \frac{B_V}{haB_0}\rho\cos\theta + \left[\Delta_2^2(\overline{\sigma}_a - \overline{\sigma}_{a0}) - \frac{B_V}{haB_0}\right]\frac{\cos\theta}{\rho} \tag{7.129}$$

where $\overline{\sigma}_{a0} = \overline{\sigma}_a(0) = \beta_0/4\Delta_2^2$.

The dipole surface current

From the flux one can easily calculate the jump in poloidal magnetic field on the surface and the corresponding dipole surface current. In terms of the present notation the jump in poloidal magnetic field is given by

$$\begin{aligned}\llbracket B_\theta \rrbracket &= haB_0\left[\left.\frac{\partial\psi_{tot}}{\partial\rho}\right|_{S_+} - \left.\frac{\partial\psi_{tot}}{\partial\rho}\right|_{S_-}\right] \\ &= 2[B_V - haB_0\Delta_2^2(\overline{\sigma}_a - \overline{\sigma}_{a0})]\cos\theta\end{aligned} \tag{7.130}$$

The dipole surface current is obtained directly from Ampere's law and has the form

$$\mu_0 \mathbf{K}_D = \mu_0 \overline{K}_D \cos\theta \, \mathbf{e}_\phi = [\![B_\theta]\!] \mathbf{e}_\phi = 2[B_V - haB_0\Delta_2^2(\overline{\sigma}_a - \overline{\sigma}_{a0})] \cos\theta \mathbf{e}_\phi \tag{7.131}$$

The surface current body force

The next step is to calculate the net toroidal body force arising from the dipole surface current. As stated this force arises from the interaction of the surface current with the applied helical field on the helically modulated surface and can be written as

$$\begin{aligned} F_R &= \int \mathbf{J} \times \mathbf{B} \cdot \mathbf{e}_R \, d\mathbf{r} \\ &= -\int J_D dr (B_{hr} \sin\theta + B_{h\theta} \cos\theta) R_0 r \, d\theta \, d\phi \\ &= -R_0 \int \overline{K}_D \cos\theta [r B_{hr} \sin\theta + r B_{h\theta} \cos\theta]_S d\theta d\phi \end{aligned} \tag{7.132}$$

where $J_D dr = \overline{K}_D \cos\theta$ is the usual surface current relation and $\mathbf{B}_h$ is the applied helical field. Also, since $\overline{K}_D$ is a surface current the term in the square bracket must be evaluated on S defined by $\rho = 1 + \sigma_h \cos\alpha$.

The applied helical fields have been given in Eq. (7.101), and when evaluated on S have the form

$$\begin{aligned} r B_{hr}|_S &= hB_0\Delta_2 r^2 \sin\alpha|_S \approx ha^2 B_0 \Delta_2 (1 + 2\sigma_h \cos\alpha) \sin\alpha \\ r B_{h\theta}|_S &= hB_0\Delta_2 r^2 \cos\alpha|_S \approx ha^2 B_0 \Delta_2 (1 + 2\sigma_h \cos\alpha) \cos\alpha \end{aligned} \tag{7.133}$$

Here, σ_h is the helical modulation of the plasma surface which has already been calculated in Eq. (7.91). One sees that $\sigma_h = \overline{\sigma}_h \cos\alpha = -\Delta_2 \cos\alpha$.

The quantities $\overline{K}_D$ and $\mathbf{B}_h$ are substituted into Eq. (7.132) to evaluate the body force. Only the term containing the $B_{h\theta}$ modulation survives the averaging over θ and ϕ leading to

$$\begin{aligned} F_R &= -2ha^2 R_0 B_0 \Delta_2 \int \overline{\sigma}_h \overline{K}_D \cos^2\theta \cos^2\alpha \, d\theta d\phi \\ &= -4\pi^2 h^2 a^3 R_0 \Delta_2^4 \frac{B_0^2}{\mu_0} \left(\overline{\sigma}_a - \overline{\sigma}_{a0} - \frac{B_V}{haB_0\Delta_2^2} \right) \end{aligned} \tag{7.134}$$

The dynamical equations of motion

The dynamical equations of motion are now obtained directly from Newton's law

$$M \frac{d^2 R}{dt^2} = F_R \tag{7.135}$$

For a uniform density one sets $M = (m_i n_0)(2\pi^2 R_0 a^2)$ and notes that $R = R_0 + a(1 + \overline{\sigma}_a)$. Equation (7.135) reduces to

$$\frac{d^2\overline{\sigma}_a}{dt^2} + 2h^2 V_a^2 \Delta_2^4 \left(\overline{\sigma}_a - \overline{\sigma}_{a0} - \frac{B_V}{haB_0\Delta_2^2} \right) = 0 \tag{7.136}$$

Observe that the evolution of $\overline{\sigma}_a$ is determined by the solution to a second order differential equation driven by a forcing term proportional to B_V. To obtain some insight into the behavior assume that the vertical field starts at zero and monotonically increases to a finial value B_{Vf}. Specifically, assume that

$$B_V(t) = B_{Vf}(1 - e^{-t/t_V}) \tag{7.137}$$

where t_V is the characteristic rise time of the vertical field. If one now introduces a normalized time $\tau = t/t_V$ then the equation for $\overline{\sigma}_a$ simplifies to

$$\frac{d^2\overline{\sigma}_a}{d\tau^2} + \Omega_V^2 \, (\overline{\sigma}_a - \overline{\sigma}_{a0}) = b_V(1 - e^{-\tau}) \tag{7.138}$$

Here, $\Omega_V^2 = 2(\iota_H/2\pi)^2 (V_A t_V/R_0)^2$, $b_V = \Omega_V^2(2\pi/\iota_H\varepsilon)(B_{Vf}/B_0)$, $\iota_H/2\pi = hR_0\Delta_2^2$ is helical transform, and $V_A^2 = B_0^2/\mu_0 m_i n_0$ is the square of the Alfven speed. The parameter Ω_V represents the ratio of the vertical field rise time to the MHD time and for typical experimental parameters $\Omega_V^2 \gg 1$. The initial conditions for a plasma that starts at rest are

$$\begin{aligned} \overline{\sigma}_a(0) &= \overline{\sigma}_{a0} \\ \frac{d\overline{\sigma}_a(0)}{d\tau} &= 0 \end{aligned} \tag{7.139}$$

The solution is easily found and is given by

$$\begin{aligned} \overline{\sigma}_a(\tau) - \overline{\sigma}_{a0} &= \frac{b_V}{\Omega_V^2 \, (1 + \Omega_V^2)} [1 + \Omega_V^2 - \Omega_V^2 e^{-\tau} - \cos(\Omega_V \tau) - \Omega_V \sin(\Omega_V \tau)] \\ &\approx \frac{b_V}{\Omega_V^2} \left[1 - e^{-\tau} - \frac{1}{\Omega_V} \sin(\Omega_V \tau) \right] \end{aligned} \tag{7.140}$$

The approximate form corresponds to the limit $\Omega_V^2 \gg 1$.

Discussion

The dynamical behavior can be understood by plotting the solution given by Eq. (7.140) in Fig. 7.8 for the case $\Omega_V^2 = 25$ and $b_V/\Omega_V^2 = 0.75\overline{\sigma}_{a0}$. One can see that within the context of ideal MHD, $\overline{\sigma}_a(\tau) - \overline{\sigma}_{a0}$ essentially tracks the applied vertical

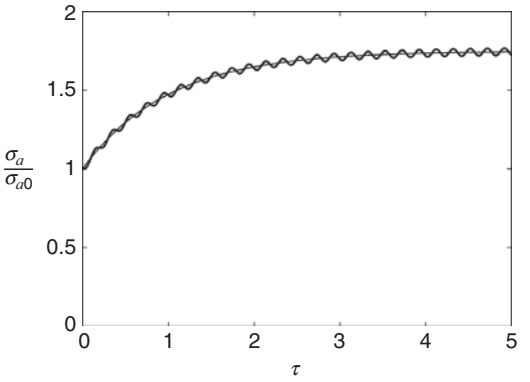

Figure 7.8 Dynamical trajectory of the plasma surface under the action of a time varying vertical field.

field with a small superimposed oscillation of relative amplitude $1/\Omega_V$. A small dissipation would cause these oscillations to damp. Once the vertical field reaches its final value the net toroidal body force on the plasma vanishes and $\overline{\sigma}_a$ reaches a new steady state value given by

$$\overline{\sigma}_a(\infty) = \overline{\sigma}_{a0} + \frac{b_V}{\Omega_V^2} \tag{7.141}$$

or in real units

$$\overline{\sigma}_a(\infty) = \frac{2\pi}{\iota_H}\left[\frac{\mu_0 p_1(0)}{2NB_0^2} + \frac{B_{Vf}}{\varepsilon B_0}\right] \tag{7.142}$$

The overall conclusion is that a vertical field produces a net body force only during the transient period when it is changing from its initial value to its final value. In the final steady state the stellarator remains current-free with no toroidal force produced by the vertical field. This analysis resolves the apparent paradox.

7.6.4 The equilibrium β limit in a stellarator

The goal of this subsection is to demonstrate that a current-free stellarator has an equilibrium β limit similar to that in a high β tokamak. The limit may be potentially more important in a stellarator than a tokamak. The reason is that without a net current stellarators are less susceptible to MHD instabilities and thus may be able to operate closer to the equilibrium limit. In other words, the β limit may be ultimately set by equilibrium rather than stability considerations (see for instance Kikuchi *et al.*, 2012, and Helander *et al.*, 2012).

The reason for the existence of an equilibrium β limit is similar to the tokamak. In a current-free stellarator as β increases the plasma surface is shifted outward due to the tire tube and $1/R$ forces. Assuming that the vacuum helical field is held fixed, then in order to keep the plasma centered about the natural helical magnetic axis one must apply a vertical field. Eventually, when β becomes sufficiently large, the resulting vertical field on the plasma surface B_V exceeds the surface averaged helical field $\langle \mathbf{B}_h \rangle$ causing the appearance of a separatrix. When this occurs the stellarator has reached its equilibrium β limit.

The analysis required to calculate the β limit is again based on the Greene–Johnson overlap equations. The problem is more difficult than for the low β equilibrium because the surface shifts become finite; that is, β effects enter in leading order implying that an expansion in β will not be effective. Still, by making several reasonable assumptions it becomes possible to calculate in a simple way the equilibrium β limit in a stellarator.

The assumptions required are as follows. (1) Attention is again focused on a single helicity $l = 2$ configuration. (2) To solve the overlap equations one assumes Solov'ev profiles for the free functions. (3) The plasma is allowed to carry a net current I which is set to zero at the end of the calculation. This will be important in the next subsection that describes the flux conserving stellarator. (4) Most importantly, the normalized pressure is treated as a finite quantity. Specifically, it is assumed that in terms of the overlap equation notation $\beta \sim \Delta_2^4$ which in real units is equivalent to $2\mu_0 p/B_0^2 \sim \varepsilon$.

The calculation of the β limit is similar to the high β tokamak analysis. One minor difference is the choice of sign for the free functions, which are now chosen so that the net current and helical transform both have the same sign for a positive h. The choices are not essential and can be switched, but the present choice makes the algebra a little neater. The analysis is now described below.

Simplification of the overlap equations

The starting model corresponds to the Greene–Johnson overlap equation given by Eq. (7.57). The assumptions described above are now applied and correspond to setting

$$\begin{aligned} A_n(\rho,\theta) &= \frac{\Delta_2}{4}\rho^2 e^{i2\theta} \\ \frac{d\beta}{d\psi} &= C \\ J &= A + C\langle x \rangle \end{aligned} \tag{7.143}$$

This leads to the following form of the overlap equation,

$$\nabla_\perp^2 \psi = -A - 2\Delta_2^2 - C\rho \cos\theta \tag{7.144}$$

The boundary conditions are based on the idea that the solutions to Eq. (7.144) should describe a sequence of equilibria corresponding to increasing values of β. At low β the shape of the toroidally averaged flux function ψ is a circle. In fact, by symmetry it follows that at low β the surface is a circle for any value of l. Now, as β is increased one must imagine that the vertical field is also increased to keep the plasma surface centered about $\rho = 0$. The surface will remain approximately circular. To keep the calculation simple it is further assumed that small shaping fields are externally applied that keep the surface exactly circular. The formulation is thus transformed from a free boundary to a fixed boundary problem with the boundary condition given by

$$\psi(1, \theta) = 0 \tag{7.145}$$

Note that without loss in generality, the free additive constant to the flux has been chosen so that $\psi = 0$ on the plasma surface.

The solution to the reduced overlap equation is easily found and is given by

$$\psi = (1 - \rho^2)\left[\frac{1}{4}(A + 2\Delta_2^2) + \frac{C}{8}\rho \cos\theta\right] \tag{7.146}$$

The solution is formally similar to Eq. (6.101) for the high β tokamak. The next task is to express the constants A and C in terms of physical quantities.

Relation of A *and* C *to physical quantities*

The constant A is related to the net current I flowing in the plasma. The desired relation is obtained by recalling that

$$I_\phi = \int \langle J_\phi \rangle \, dS = -\frac{NB_0 a^2}{\mu_0 R_0} \int J\rho \; d\rho \, d\theta \tag{7.147}$$

where the integral is carried out over the cross section of the plasma. Next, the function J is eliminated by means of Eq. (7.143) noting that $\langle x \rangle = \langle \rho \cos\theta \rangle = 0$ on a circular plasma. A short calculation then yields

$$\frac{\iota_I}{2\pi} \equiv \hat{\imath}_I = \frac{\mu_0 R_0 I_{\hat{\phi}}}{2\pi a^2 B_0} = -\frac{\mu_0 R_0 I_\phi}{2\pi a^2 B_0} = \frac{1}{2} h R_0 A \tag{7.148}$$

Here, $\hat{\imath}_I = 1/q_*$ is the inverse kink safety factor associated with the net plasma current.

The constant C is related to the plasma beta, which is approximately equal to the toroidal beta β_t defined by

$$\beta_t = \frac{1}{\pi a^2}\int \frac{2\mu_0 p}{B_0^2}\, dS = \frac{\varepsilon N^2}{\pi}\int \beta\rho\, d\rho\, d\theta \tag{7.149}$$

One now substitutes the relation $\beta(\psi) = C\psi$ with ψ given by Eq. (7.146). Another short calculation leads to

$$\beta_t = \frac{\varepsilon N^2}{8}(A + 2\Delta_2^2)C = \frac{ha}{4}(\hat{\imath}_I + \hat{\imath}_H)C \tag{7.150}$$

where $(\iota_H/2\pi) \equiv \hat{\imath}_H = hR_0\Delta_2^2$ is the normalized rotational transform due to the vacuum helical field.

The flux function, the rotational transform, and the equilibrium β *limit*

The expressions for A and C are substituted into the solution for ψ which simplifies to

$$\begin{aligned} \psi &= \frac{\hat{\imath}_I + \hat{\imath}_H}{2hR_0}(1-\rho^2)(1 + \nu\rho\cos\theta) \\ \nu &= \frac{\beta_t}{\varepsilon(\hat{\imath}_I + \hat{\imath}_H)^2} \end{aligned} \tag{7.151}$$

As with the high β tokamak, in order to calculate the equilibrium β limit it is necessary to evaluate the safety factor, or equivalently the rotational transform, on the plasma surface. This task can be readily carried out by using the definition of the safety factor given by Eq. (6.33) and keeping in mind that in the context of the present ordering assumptions the helical component of the flux function is smaller than the toroidally averaged component (see Table 7.2). In other words, the rotational transform is essentially determined by ψ as given by Eq. (7.151). A short calculation using the fact that $B_p = |B_\theta|$ on the plasma surface shows that Eq. (6.33) reduces to

$$q_a \approx -\frac{\varepsilon B_0}{2\pi}\int_0^{2\pi}\frac{d\theta}{B_\theta} = -\frac{1}{2\pi hR_0}\int_0^{2\pi}\frac{d\theta}{[\partial\psi/\partial\rho]_{\rho=1}} \tag{7.152}$$

The integral can be easily evaluated and is given by

$$\frac{\iota_a}{2\pi} \equiv \hat{\imath}_a = \frac{1}{q_a} = (\hat{\imath}_I + \hat{\imath}_H)(1-\nu^2)^{1/2} \tag{7.153}$$

One sees that in order avoid a separatrix moving onto the plasma surface it is necessary that $v^2 \leq 1$. This corresponds to the equilibrium β limit, which can be written as

$$\begin{aligned} \beta_t &\leq \varepsilon(\hat{\imath}_I + \hat{\imath}_H)^2 && \text{Hybrid stellarator/tokamak} \\ \beta_t &\leq \varepsilon\hat{\imath}_I^2 && \text{Pure tokamak} \\ \beta_t &\leq \varepsilon\hat{\imath}_H^2 && \text{Pure stellarator} \end{aligned} \tag{7.154}$$

Equation (7.154) shows that there is a great similarity between the equilibrium β limits in a tokamak and a stellarator with a smooth connection between them. Although the expressions are formally similar there are still some observations that can be made with respect to actual practical values. For both configurations the critical β is proportional to $\varepsilon\iota^2$. Stellarators tend to have a smaller ε but a larger ι. Tokamaks, because of their simpler geometry tend to have a higher maximum magnetic field at the toroidal field coils. However, the $1/R$ fall off of the toroidal field is stronger in a tokamak because of the tighter aspect ratio. Overall, the magnetic field in the center of the plasma, which is the critical location in terms of the plasma physics, can be comparable. Actual numerical comparisons of the β limit depend upon the details of the design but are typically at least as large for a stellarator as a tokamak.

7.6.5 The flux conserving stellarator

As discussed in Chapter 6 a tokamak operating in a flux conserving mode does not actually have an equilibrium limit. The reason is that in order to keep a flux conserving plasma centered in the discharge chamber as β is increased both the plasma current and the vertical field increase. This shared contribution to toroidal force balance delays the appearance of the separatrix on the plasma surface thereby avoiding the equilibrium limit. If the current is held fixed the entire burden falls on the vertical field and in this case a separatrix appears.

A similar situation occurs for the flux conserving stellarator, although in this case the result is a bit more dramatic. To visualize the situation consider starting with a low β plasma in current-free stellarator designed without an ohmic transformer. Auxiliary heating power is supplied on a time scale slow compared to the ideal MHD time but fast compared to the resistive diffusion time, corresponding to conserving operation. As β increases due to the heating a net current must begin to flow in the plasma in order to conserve the flux. Thus, even in the absence of an ohmic transformer and without any effort made to deliberately drive current with microwaves or beams, a net current flows in the plasma – more dramatic than a tokamak which already has a large current and an ohmic transformer. Ultimately the stellarator current will die away on the resistive diffusion time, but even so it will persist for a substantial period of time.

The amount of current that flows in a flux conserving stellarator can be calculated in a straightforward way from the results just derived in subsection 7.6.4. All that is required is to re-interpret the solutions so that they correspond to flux conserving operation. The critical step is to assume that during the entire flux conserving evolution the rotational transform $\hat{\imath}_a$ is held fixed at its initial value. This replaces the condition $\hat{\imath}_I = 0$ which describes a sequence of current-free stellarators.

Now, if the initial low β stellarator starts off current-free then flux conservation requires that $\hat{\imath}_a = \hat{\imath}_H$ during the entire heating evolution. Here, $\hat{\imath}_H$ is the initial helical transform which is assumed to remain constant during the evolution; that is, the helical field amplitude does not change as the heating power is applied. Equation (7.153) subject to the constraint $\hat{\imath}_a = \hat{\imath}_H$ implies that

$$v^2 = 1 - \left(\frac{\hat{\imath}_H}{\hat{\imath}_I + \hat{\imath}_H}\right)^2 \tag{7.155}$$

The parameter v is related to β_t by Eq. (7.151). For flux conservation it makes sense to introduce a heating parameter H consistent with the physics,

$$H \equiv \frac{\beta_t}{\varepsilon \hat{\imath}_H^2} = \frac{(\hat{\imath}_I + \hat{\imath}_H)^2}{\hat{\imath}_H^2} v \tag{7.156}$$

The parameter H is useful since as heat is applied β_t must increase since $\hat{\imath}_H$ remains constant. Thus $\beta_t \propto H$.

The desired relation is obtained by substituting v from Eq. (7.156) into Eq. (7.155). The resulting relation is easily solved for $\hat{\imath}_I/\hat{\imath}_H$ as a function of H

$$\frac{\hat{\imath}_I}{\hat{\imath}_H} = \left\{\frac{1}{2}\left[1 + (1 + 4H^2)^{1/2}\right]\right\}^{1/2} - 1 \tag{7.157}$$

This expression shows how much transform due to net current must be induced relative to the initial helical transform as heat is applied on a flux conserving time scale.

Equation (7.157) is plotted in Fig. 7.9. The main conclusion is that there is no equilibrium β limit. As β_t continually increases a progressively larger net current is induced to hold the plasma in equilibrium. In terms of specific scaling relations observe that for

$$\begin{aligned} H &\ll 1 \qquad \hat{\imath}_I/\hat{\imath}_H \approx H^2/2 \\ H &\gg 1 \qquad \hat{\imath}_I/\hat{\imath}_H \approx H^{1/2} \\ H &= 1 \qquad \hat{\imath}_I/\hat{\imath}_H \approx 0.27 \end{aligned} \tag{7.158}$$

Although the net current transform does not dominate for typical regimes of operation it can become substantial. One must take care to make sure that

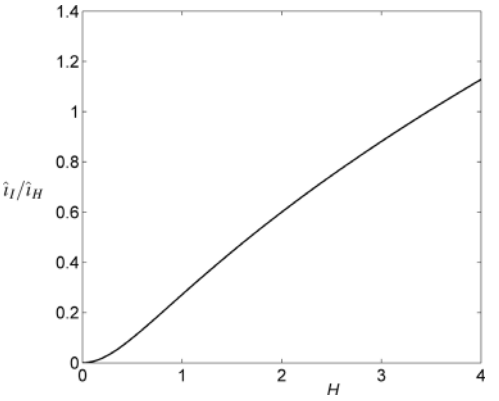

Figure 7.9 Induced normalized net current $\hat{\imath}_I/\hat{\imath}_H$ vs. the heating parameter H in a flux conserving stellarator.

current-driven kink modes are not excited before the net current diffuses away. Likewise, once the current does diffuse away either the helical field and/or the vertical field must be increased to keep the plasma centered while making sure that the equilibrium limit is not violated.

7.6.6 Multiple helicity, finite β stellarators

The previous analyses of finite β effects in a stellarator have focused on a single helicity, $l = 2$ configuration described by the simplified Greene–Johnson overlap equations. This approach has led to a number of analytic results. The present subsection considers the general HBS model which allows multiple helicities and larger values for the helical field amplitudes and plasma β. This is the more realistic experimental situation and clearly, because of the inherent 3-D nature of the problem, an efficient numerical procedure is required. As with the vacuum case several numerical procedures exist that generate fast and accurate solutions to the HBS equations. These methods are described in the references listed under Further reading at the end of the chapter. For present purposes it is assumed that such a numerical code has been written and used to produce the results described below.

Numerical formulation

To demonstrate the behavior of the flux surfaces in a finite β stellarator attention is focused on two practical examples, specifically the Large Helical Device (LHD) in Japan and the W7-X device in Germany. LHD is predominantly an $l = 2$ heliotron with small additional helical and vertical fields to optimize performance. W7-X is currently under construction and has a more complicated magnetic field

configuration aimed at improving transport. It does this by means of a series of linked mirrors with transport optimized "elbows" connecting each mirror.

The form of the HBS equations which have been solved numerically are obtained from Eq. (7.35) and can be written as

$$\left[\frac{\partial}{\partial\phi} + \mathbf{e}_\phi \times \nabla_\perp(\hat{A} + \tilde{A}) \cdot \nabla_\perp\right]\psi = 0$$

$$\left[\frac{\partial}{\partial\phi} + \mathbf{e}_\phi \times \nabla_\perp(\hat{A} + \tilde{A}) \cdot \nabla_\perp\right]\nabla_\perp^2\tilde{A} = \frac{1}{M^{3/2}}\frac{d\beta}{d\psi}\nabla_\perp\psi \cdot \mathbf{e}_Z \tag{7.159}$$

$$\hat{A} = \sum_l \frac{\Delta_l}{l}\rho^{|l|}\cos(l\theta + \phi)$$

where $\hat{A}$ is the known vacuum vector potential and $\tilde{A}$ is the diamagnetic response due to the plasma currents. The boundary conditions require that ψ and $\tilde{A}$ be regular everywhere and that $\tilde{A} \to 0$ far from the plasma since it is a diamagnetic response.

Numerical results

Flux surfaces from the numerical solutions to Eq. (7.159) are illustrated in Figs. 7.10 and 7.11. The first set of flux surfaces represents an LHD-like equilibrium. This is not an especially challenging equilibrium to calculate since it is

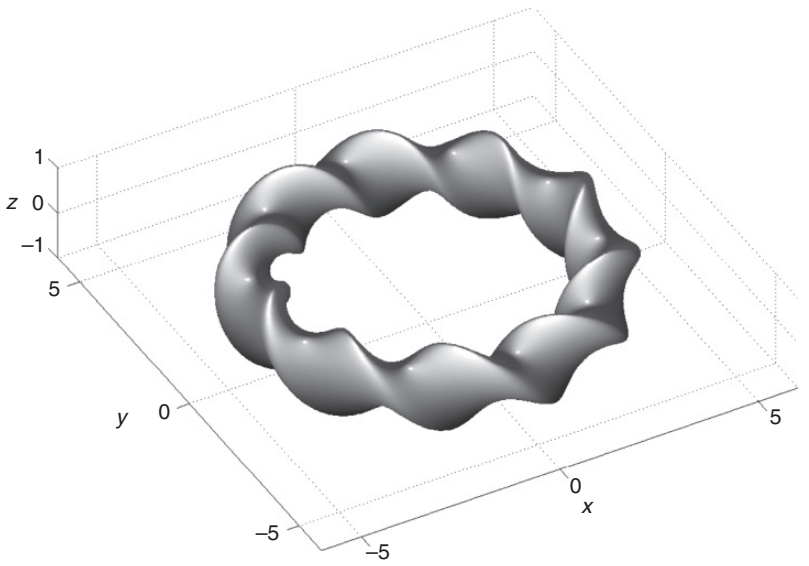

Figure 7.10 Numerically calculated boundary surface for a finite β, LHD-like plasma from the high β stellarator model.

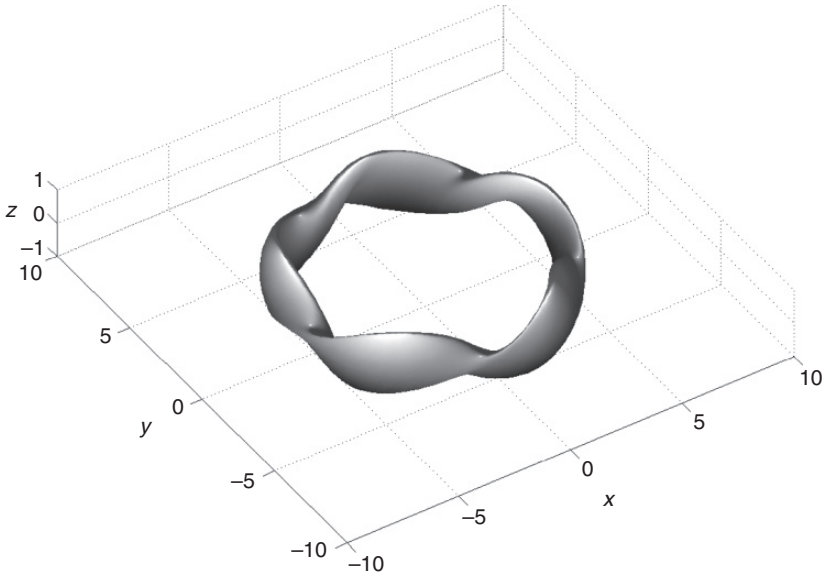

Figure 7.11 Numerically calculated boundary surface for a finite β, W7-X-like plasma from the high β stellarator model.

dominated by a large $l = 2$ field. The flux surfaces have a rotating elliptical structure.

The W7-X-like flux surfaces are more complicated and change substantially at different toroidal locations. At one toroidal location the cross section has the appearance of an elongated "boomerang." In a different toroidal location it looks like a "bullet."

These configurations are discussed in more detail in Section 7.8 following the description of neoclassical transport. The main conclusion is that realistic 3-D stellarator equilibria can be calculated numerically using the HBS expansion. The results are quite similar to numerical solutions obtained from "exact" codes which use no expansions. Detailed comparisons are more difficult than one might imagine, largely due to the differences used in specifying the vacuum magnetic fields.

7.7 Neoclassical transport in stellarators

The previous sections in Chapter 7 have described many of the basic MHD equilibrium properties of stellarators. Even so, one cannot in good conscience complete the discussion without understanding the impact of neoclassical transport on the MHD design of stellarators. The reason is that neoclassical transport in an un-optimized stellarator can substantially exceed anomalous transport. In contrast,

neoclassical transport in a tokamak almost always is smaller than anomalous transport. If the situation cannot be improved, the implication is that stellarators will always have poorer confinement than tokamaks, not a good prospect for the future development of the stellarator concept.

Fortunately, the physics of neoclassical transport in stellarators is now reasonably well understood (Helander and Sigmar, 2002; Helander *et al*., 2012; Kikuchi *et al*., 2012). This knowledge has led to the development of several very clever ideas to mitigate the problem. These involve the ideas of "omnigenity," "quasi-isodynamics," and "quasi-symmetry." The goal in this subsection is to motivate and explain these basic ideas.

The strategy for accomplishing the goal starts with a review of neoclassical transport in a tokamak in the low collisionality "banana regime," the one of most interest to fusion plasmas. This discussion is also valuable for predicting neoclassical transport in a stellarator. In addition an anomalous "gyro-Bohm" transport estimate is presented which describes the approximate real-world operation of many tokamaks.

With these serving as references it is then possible to describe the problem that arises because of the inherent 3-D nature of a stellarator. Once the problem has been identified, various mitigating ideas (i.e., quasi-omnigenity, quasi-isodynamics, and quasi-symmetry) are presented which substantially improve single-particle confinement and neoclassical transport. Most importantly these ideas are expressed in terms of constraints on the magnetic field which then place the solution in the domain of MHD. In practice MHD design optimization is carried out numerically and several optimized configurations are discussed in Section 7.8.

7.7.1 Review of transport in a tokamak

General neoclassical transport procedure

Readers should keep in mind that the present textbook is focused on MHD and that a self-contained description of transport would require an entire textbook of its own. Several very good ones are listed in the references. Consequently, to keep the discussion in this section relatively brief, simple semi-quantitative ideas are used and in certain places results are simply quoted, the assumption being that readers have some knowledge of neoclassical transport theory in a tokamak (Helander and Sigmar, 2002).

The discussion begins with a summary of the general procedure used to estimate neoclassical transport – the random walk approximation. Attention is focused on the ion thermal diffusivity coefficient χ_i which is responsible for determining the energy confinement time $\tau_E \sim a^2/\chi_i$, one of the critical parameters defining concept desirability.

In general, χ_i is estimated from the random walk approximation given by

$$\chi_i \approx f_{eff} \nu_{eff} \overline{(\Delta r^2)} \tag{7.160}$$

Here, Δr is the step size associated with ion energy transport (i.e., the distance that a single ion's energy is transported after each collision). The quantity $\overline{(\Delta r^2)}$ is the collision averaged step size squared and enters quadratically because of the random nature of collisions resulting in a diffusive rather than a convective transport of energy. The quantity ν_{eff} is the effective rate of collisions. Often, ν_{eff} is just the inverse of the ion–ion Coulomb time. However, in the banana regime where thermal diffusion is dominated by trapped particles, ν_{eff} is higher since fewer collisions are needed to de-trap an ion causing its energy to be transported over a distance Δr. Lastly, f_{eff} is the fraction of the total particle population responsible for energy transport. In many cases all the particles contribute to energy transport and $f_{eff} \approx 1$. In contrast, when transport is dominated by the small fraction of trapped particles, then $f_{eff} \ll 1$.

The random walk approximation is now used to estimate χ_i for the reference case of banana transport in a tokamak.

Neoclassical transport in a tokamak – overview

Energy transport in a tokamak, or any torus for that matter, is substantially more complicated than in a cylinder and is referred to as "neoclassical transport." In a tokamak neoclassical transport, which arises solely from collisions (and not micro-instabilities), has three distinct regimes of behavior, known as the "banana" regime, the "plateau" regime, and the "Pfirsch–Schluter" regime. The regimes are distinguished by the relative size of the ion–ion collision frequency compared to the bounce frequency of trapped particles. Fusion plasmas operate predominantly in the banana regime corresponding to low collisionality.

On top of this complexity is the fact that energy transport over most of the plasma is anomalously large due to turbulence driven by micro-instabilities. The dominant micro-instabilities have been identified although a corresponding analytic expression for χ_i is still to be determined. Even so, basic scaling relations derived from the properties of the micro-instabilities under consideration have been proposed. Often the scaling information is viewed as more important than the hard-to-determine multiplicative numerical coefficients. Nonetheless, a simple expression for the anomalous χ_i is also presented here for the sake of reference. This expression describes the so-called "gyro-Bohm" diffusivity which seems to agree as well as any with experimental measurements.

Neoclassical transport in a tokamak – the banana regime

Banana diffusion corresponds to the low collisionality regime of neoclassical transport. It is dominated by trapped particle collisions. The reason is that the mean step size and effective collision frequency are much larger than for passing particle collisions. Competing with these effects is the fact that trapped particles only constitute a small fraction of the total number of particles. The first two effects win out causing the overall transport to be dominated by trapped particles.

The basic assumption required to estimate banana diffusion is that trapped particles are able to execute many bounce periods before having a collision. The maximum collisionality that defines the transition out of the banana regime into the plateau regime corresponds to the situation where a trapped particle has just one collision during a bounce period. This critical collisionality is estimated as follows.

Trapped particles, because of the condition for mirroring, all have a small parallel velocity $v_{\|} \sim \varepsilon^{1/2} v \sim \varepsilon^{1/2} V_{Ti}$. This leads to a collisionless bounce time between mirror points $\delta t \sim L_{\|}/v_{\|} \sim qR/v_{\|} \sim qR/\varepsilon^{1/2} V_{Ti}$. Next, note that the effective collision time is shorter than τ_{ii} since a trapped particle must only undergo a small angle (not a 90 degree) collision of magnitude $\delta\alpha \sim (v_{\|}/v)(\pi/2) \sim \varepsilon^{1/2}(\pi/2)$ to become de-trapped. This is the change in angle necessary for a particle to jump one banana width because of a collision. Specifically, since angular scattering is a diffusive process the effective collision time is $\delta t \sim [\delta\alpha/(\pi/2)]^2 \tau_{ii} \sim \varepsilon\tau_{ii}$. The transition collision frequency where a trapped particle has one collision during a bounce period is obtained by equating the two expressions for δt. The result is $\nu_{ii} \sim \varepsilon^{8/2} V_{Ti}/qR$. The conclusion is that banana transport occurs when

$$\nu_{ii} < \varepsilon^{3/2} \frac{V_{Ti}}{qR} \tag{7.161}$$

The banana thermal diffusivity coefficient can now be easily estimated. To use the random walk approximation one needs to calculate ν_{eff}, $(\Delta r)^2$, and f_{eff}. The effective collision frequency has already been estimated. It is the inverse of the time necessary for a particle to diffuse through an angle $\delta\alpha \sim (v_{\|}/v)(\pi/2)$; that is $\nu_{eff} \sim \nu_{ii}/\varepsilon$.

To calculate Δr recall that the time it takes a trapped particle to execute one banana orbit scales as $\delta t \sim qR/v_{\|} \sim qR/\varepsilon^{1/2} V_{Ti}$. In the banana regime a particle will not experience a collision during this time, implying that its drift off the flux surface can be estimated as $\Delta r \sim V_D \delta t \sim (q/\varepsilon^{1/2}) r_{Li}$. Here, $V_D \sim V_{Ti}(r_{Li}/R)$ is the $1/R$ grad-B guiding center drift off the surface.

Lastly, the fraction of trapped particles can also be easily estimated by calculating the portion of phase space where such particles exist: $f_{eff} \sim \delta\alpha/(\pi/2) \sim (v_{\|}/v) \sim \varepsilon^{1/2}$. Combining these results one finds that the thermal diffusivity coefficient for the banana regime is given by

$$\chi_i \equiv \chi_{NC} \sim f_{eff} v_{eff} \overline{(\Delta r^2)} \sim \varepsilon^{1/2}(v_{ii}/\varepsilon)(q r_{Li}/\varepsilon^{1/2})^2 \sim (q^2/\varepsilon^{3/2})\, v_{ii} r_{Li}^2 \quad (7.162)$$

Observe that banana diffusivity is larger by a factor $q^2/\varepsilon^{3/2} \sim 50$ than the pure cylindrical value $v_{ii} r_{Li}^2$.

Anomalous transport in a tokamak – gyro-Bohm diffusion

Even with the neoclassical increase by a factor of about 50, this is still not sufficient to explain experimental observations which are even more pessimistic. The reason is that thermal transport is anomalous, driven by various micro-instabilities such as the ion and electron temperature gradient modes and the trapped electron mode. Progress is being made both analytically and computationally to quantify the turbulent transport due to these instabilities but, at the time of this writing, this is still a work in progress.

Many researchers in the fusion community use the "gyro-Bohm" diffusivity as a simple estimate for anomalous transport (see for instance Miyamoto, 2005, and Stacey, 2012). The same estimate is used here. The gyro-Bohm thermal diffusivity coefficient scales as

$$\chi_i \equiv \chi_{GB} \sim \frac{V_{Ti}^2}{\omega_{ci}} \frac{r_{Li}}{a} \sim \frac{V_{Ti}}{a} r_{Li}^2 \quad (7.163)$$

Note that the diffusivity is independent of collision frequency, not a surprise since turbulence replaces collisions as the transport mechanism.

Transport in a tokamak – summary

Thermal transport in a tokamak can be conveniently summarized by plotting thermal diffusivity vs. collision frequency. For plotting purposes the quantities are normalized as follows. The vertical axis illustrates χ_i/χ_{GB}. Thermal diffusivity is normalized to the gyro-Bohm value given by Eq. (7.163). The horizontal axis illustrates the ratio of the trapped particle effective collision frequency to the trapped particle bounce frequency. This ratio is usually called ν_* and is given by $\nu_* \equiv (qR/\varepsilon^{3/2} V_{Ti}) \nu_{ii}$. Banana transport corresponds to $\nu_* < 1$. Thus, for neoclassical transport corresponding to $\chi_i = \chi_{NC}$, one finds that $\chi_{NC}/\chi_{GB} \approx \varepsilon q \nu_* \propto 1/T^2$ showing a linear scaling with normalized collision frequency.

The thermal diffusivity curve for a tokamak operating in the banana regime is shown in Fig. 7.12. Also shown is the classical result for a cylinder. Readers should focus on the scaling trends rather than on specific numerical values since all multiplicative constants have been set to unity for simplicity. There are several important conclusions that can be drawn from Fig. 7.12 after having substituted typical experimental values:

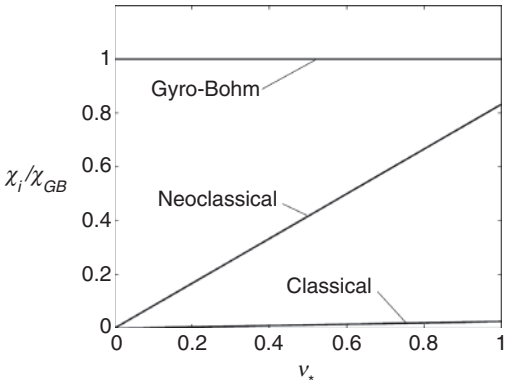

Figure 7.12 Comparison of neoclassical diffusivity in a toroidal and straight tokamak as a function of collisionality for $\varepsilon = 1/3$ and $q = 2.5$.

(1) Neoclassical transport is always substantially higher than cylindrical transport.
(2) Tokamaks operating in the high temperature fusion regime lie almost entirely in the low ν_* banana regime.
(3) In the banana regime anomalous transport dominates over neoclassical transport.
(4) A fusion tokamak can just about reach ignition assuming anomalous transport prevails, but there is not a large margin of safety.

These conclusions along with Fig. 7.12 serve as a useful reference for understanding the problems that arise with neoclassical transport in a stellarator.

7.7.2 The problem with neoclassical transport in a stellarator

Consider now a standard un-optimized stellarator operating in a high temperature, low collisionality regime, equivalent to the banana regime for tokamaks. A major problem arises with the trapped particles because of the helical modulation of B along the parallel motion of a particle's trajectory. This modulation is shown schematically in Fig. 7.13.

The existence of this modulation can be seen explicitly by expanding B to second order using the HBS model,

$$\frac{B}{B_0} \approx 1 + \frac{B_{\phi 1}}{B_0} + \frac{B_{\phi 2}}{B_0} + \frac{1}{2}\frac{B_{r1}^2 + B_{\theta 1}^2}{B_0^2} \tag{7.164}$$

As an example, for a single helicity, vacuum $l = 3$ field this expression reduces to

$$\frac{B}{B_0} \approx 1 - \varepsilon\rho\ \cos\theta + \varepsilon^2\left[\rho^2\ \cos^2\theta + \frac{N^2\Delta_3^2}{2}\rho^4 + \frac{N^2\Delta_3}{3}\rho^2\ \cos(3\theta + \phi)\right] \tag{7.165}$$

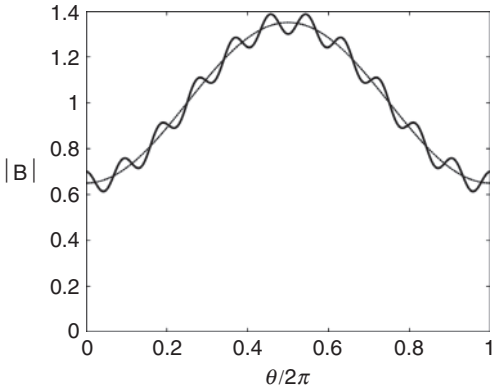

Figure 7.13 Helical modulation of $|B|$ in a toroidal stellarator.

where the helical contribution to $B_{\phi 2}/B_0 \approx (\varepsilon^2 N^2 \Delta_3/3)\rho^2 \cos(3\theta + \phi)$ has been obtained from $\mathbf{e}_r \cdot \nabla \times \mathbf{B} = 0$. The helical part of $B_{\theta 2}/B_0$ appears as the last term in the equation and represents the helical modulation.

As a particle free streams along the field line it sees, in addition to the $1/R$ dependence of the toroidal field, local mirror fields due to the helical modulation. Particles can get trapped in these local mirror fields *virtually anywhere* in the poloidal cross section. A simple physical picture can be obtained by assuming a particle is deeply trapped in such a local mirror in the vicinity of $\rho = \rho_0$, $\theta = \theta_0$ which correspond to the magnetic field minimum. In this case, the dominant variation in B that a particle sees as it tries to stream along the field is due to the ϕ dependence of the helical modulation. Under this assumption Eq. (7.165) reduces to

$$\begin{aligned}\frac{B(\phi)}{B_0} &\approx 1 - \varepsilon\rho_0 \cos\theta_0 + \varepsilon^2 \left[\rho_0^2 \cos^2\theta_0 + \frac{N^2\Delta_3^2}{2}\rho_0^4 + \frac{N^2\Delta_3}{3}\rho_0^2 \cos(3\theta_0 + \phi)\right] \\ &\approx 1 + \varepsilon_H \rho_0^2 \cos(3\theta_0 + \phi)\end{aligned} \tag{7.166}$$

Here, $\varepsilon_H = \varepsilon^2 N^2 \Delta_3/3$ measures the helical mirror ratio $B_{\max}/B_{\min} = (1 + \varepsilon_H)/(1 - \varepsilon_H)$.

It is the fact that particles can get mirror trapped anywhere in the poloidal cross section, i.e., at any value of θ_0, that causes stellarators to have problems. To understand the reason, recall that the grad-B and curvature drifts perpendicular to the flux surface are always uni-directional (either up or down), and are due primarily to the $1/R$ dependence of the toroidal field. The helical fields also produce perpendicular guiding center drifts but these oscillate in sign (are not unidirectional) giving rise to helical bananas which correspond to confined orbits.

What is the consequence of having trapped particles centered about an arbitrary θ_0? For reference, in a tokamak, which has toroidal symmetry, $\theta_0 = 0$ for all trapped particles. Therefore "up" is away from the plasma half of the time and towards the plasma the other half of the time (see Fig. 7.14a). The drift off the flux surface averages to zero over one bounce period thereby implying that trapped particles are confined. Consequently, until a trapped particle has a collision, however long that time may be, its guiding center will continue to execute bounce motion with its maximum excursion off a flux surface equal to its banana width. In other words, when a collision does finally occur, the mean random walk step size is simply $\Delta r \sim V_D \tau_B \sim V_D/\nu_B$ where $V_D \sim V_{Ti} r_{Li}/R$ is the drift velocity and $\tau_B \sim qR/\varepsilon^{1/2} V_{Ti}$ is the bounce period.

Turning to the stellarator, one sees a much different picture. If a particle is trapped for example, at a θ_0 in the first quadrant of the poloidal plane, it continuously and monotonically drifts upward off the surface because of the unidirectional drifts. There is no opportunity to have its drift canceled since it does not sample the entire poloidal cross section. In fact in the limit of zero collisions most trapped particles would simply drift out of the plasma and strike the first wall. This behavior is illustrated in Fig. 7.14b. When such a particle finally does have a collision its step size will be much, much larger than the banana width characterizing tokamak behavior. A trapped stellarator particle will have drifted a distance equal to $\Delta r \sim V_D \tau_{eff} = V_D/\nu_{eff}$. In the low collisionality regime $\tau_{eff} \gg \tau_B$ leading to a much larger neoclassical energy loss rate for a stellarator.

A semi-quantitative estimate of neoclassical transport in an un-optimized stellarator can be easily obtained by using a set of analogous approximations as for the tokamak. To begin, note that the trapped particles have a small parallel velocity, related to the helical mirror ratio: $v_\parallel \sim \varepsilon_H^{1/2} v \sim \varepsilon_H^{1/2} V_{Ti}$. Therefore, a trapped particle must only scatter through a small angle to become de-trapped and jump a distance equal to the mean step size. This angle is given by $\delta\alpha \sim (v_\parallel/v)(\pi/2) \sim \varepsilon_H^{1/2}(\pi/2)$. Since angular scattering is a diffusive process, the implication is that the effective collision time (and effective collision frequency) are given by $\tau_{eff} = 1/\nu_{eff} \sim [\delta\alpha/(\pi/2)]^2 \, \tau_{ii} \sim \varepsilon_H \tau_{ii}$.

Next, the value of f_{eff} is equal to the portion of phase space occupied by trapped particles. A simple calculation yields $f_{eff} \sim \delta\alpha/(\pi/2) \sim (v_\parallel/v) \sim \varepsilon_H^{1/2}$. Observe that the values of ν_{eff} and f_{eff} are the same as for the tokamak with ε replaced by ε_H.

The main difference from the tokamak is in the mean step size. In a tokamak the step size is equal to the banana width: $\Delta r \sim V_D \tau_B$, where V_D is the grad-B drift velocity and τ_B is the bounce period. In a stellarator, where particles drift unidirectionally until they finally have a collision the step size is $\Delta r \sim V_D \tau_{eff}$. In the low collisionality regime $\tau_{eff} \gg \tau_B$ implying a much larger step size for a stellarator. The value of Δr for a stellarator thus scales as $\Delta r \sim (V_{Ti} r_{Li}/R)(\varepsilon_H/\nu_{ii})$.

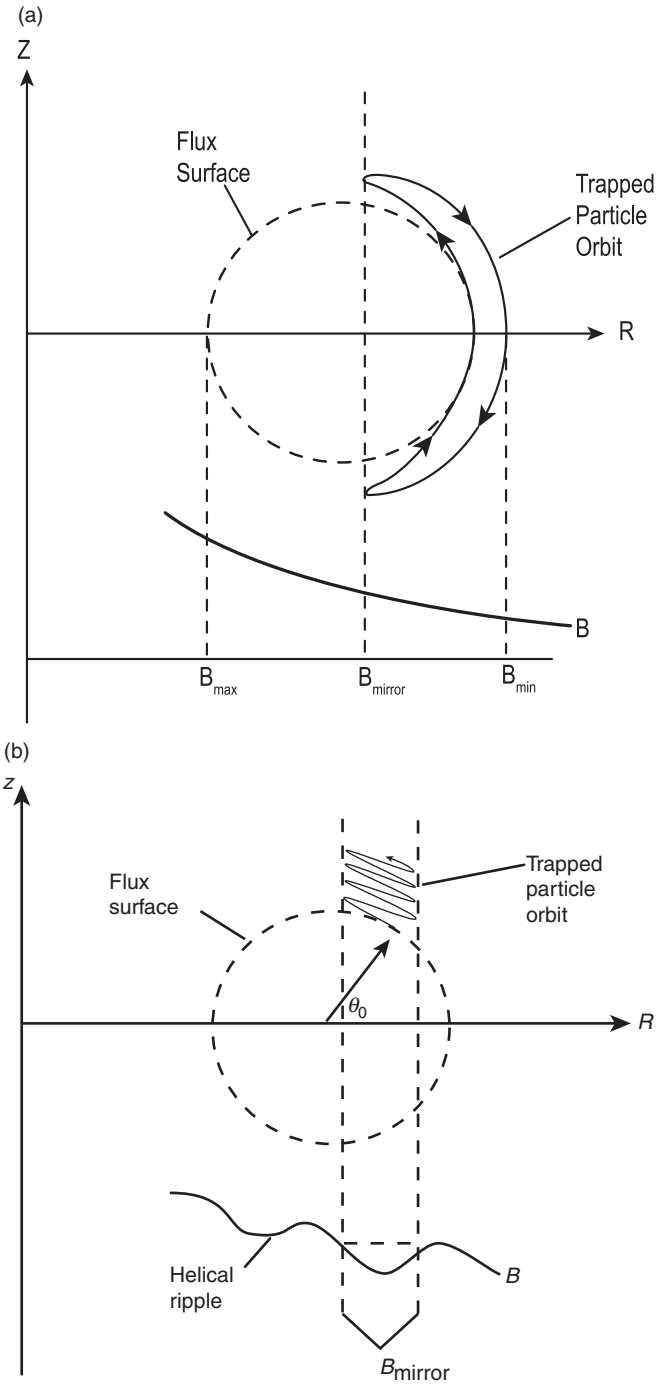

Figure 7.14 (a) Cancellation of the ∇B and curvature drifts in a tokamak leading to trapped particle banana orbits. (b) Direct loss of helically trapped particles in a stellarator because the drift is always away from the surface.

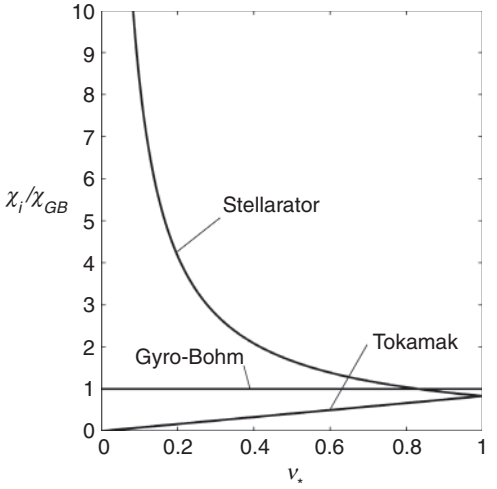

Figure 7.15 Thermal diffusivity in the banana regime of a tokamak and a stellarator vs. collisionality. Note the poorer performance of the stellarator.

These results can be combined leading to the following estimate for neoclassical transport in an un-optimized stellarator,

$$\chi_i \equiv \chi_{NC} \sim \frac{\varepsilon_H^{3/2} V_{Ti}^2}{R^2} \frac{r_{Li}^2}{\nu_{ii}} \tag{7.167}$$

The critical feature is that $\chi_{NC} \sim 1/\nu_{ii}$ as compared to $\chi_{NC} \sim \nu_{ii}$ for a tokamak. Consequently, in the high temperature, low collisionality regime stellarator transport is inherently worse than in a tokamak.

A more quantitative comparison can be made by introducing the expression for ν_* and normalizing the diffusivity to the tokamak gyro-Bohm value:

$$\begin{aligned} \frac{\chi_{NC}}{\chi_{GB}}\bigg|_{\text{Tok}} &\sim q\varepsilon\nu_* \\ \frac{\chi_{NC}}{\chi_{GB}}\bigg|_{\text{Stel}} &\sim (\varepsilon_H/\varepsilon)^{3/2} \frac{q\varepsilon}{\nu_*} \end{aligned} \tag{7.168}$$

Here, q is the tokamak safety factor. For comparable mirror ratios (i.e., $\varepsilon_H \sim \varepsilon$), one sees that neoclassical transport in a stellarator and tokamak are comparable when $\nu_* \approx 1$. As the temperature increases then ν_* decreases, implying that transport improves in a tokamak and gets worse in a stellarator, as illustrated in Fig. 7.15. The specific scalings with temperature for the three thermal diffusivities are given by

$$\begin{aligned} \chi_{NC}|_{\text{Tok}} &\propto 1/T^{1/2} \\ \chi_{GB} &\propto T^{3/2} \\ \chi_{NC}|_{\text{Stel}} &\propto T^{5/2} \end{aligned} \tag{7.169}$$

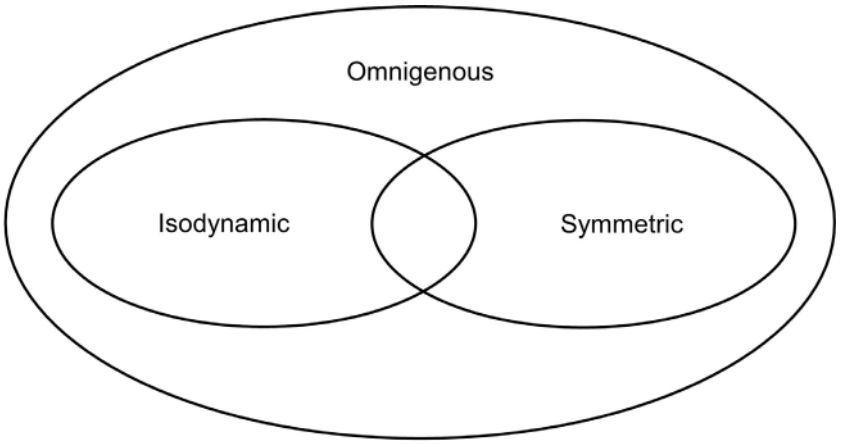

Figure 7.16 Venn diagram relation between ideal omnigenous, ideal isodynamic, and ideal symmetric stellarators.

Since $q\varepsilon \sim 1$ in most tokamaks, the implication is that the neoclassical losses in a low collisionality, un-optimized stellarator are much larger than those produced by anomalous transport. This is the basic problem faced by stellarators.

7.7.3 One solution – the omnigenous stellarator

The previous discussion has shown that greatly enhanced neoclassical transport can occur in un-optimized stellarators because of the unidirectional drift experienced by particles trapped in poloidally localized helical mirror fields. How can one improve this situation? Three related ideas have been proposed: the quasi-omnigenous stellarator, the quasi-isodynamic stellarator, and the quasi-symmetric stellarator. These topics are nicely reviewed in Mynick (2006), Landreman and Catto (2012), and Helander *et al*. (2012).

In terms of an overview it is useful to think of quasi-omnigenous stellarators as a special subclass of general stellarators. Quasi-isodynamic and quasi-symmetric stellarators are then separate subclasses of quasi-omnigenous stellarators. This overview is illustrated schematically in Fig. 7.16. The present subsection is focused on quasi-omnigenous stellarators. The additional subclasses are discussed in the following two subsections.

The goal here is to define and show how the property of omnigenity improves neoclassical transport in a stellarator. The result is the ideal-omnigenity constraint which can be translated into requirements on the magnetic field structure, thereby placing it into the domain of MHD.

The constraint of ideal-omnigenity

The basic idea is to identify the critical geometric requirement on the magnetic field that would prevent particles from being helically trapped in a local section of the poloidal plane. In other words, poloidally localized helical mirror fields must be eliminated. If this could be achieved trapped particles would then behave in a manner similar to a tokamak. In the absence of collisions they would execute confined banana orbits with a low level of neoclassical transport.

The strategy to accomplish this goal is to calculate the net guiding center drift of a banana center from its initial to final flux surface during a single bounce period and then set it equal to zero for all trapped particles. This is equivalent to forcing a particle's upward drift to be away from the plasma half the time and towards the plasma the other half, thereby canceling any net upward motion. A stellarator which exactly satisfies this constraint is defined as having the property of "ideal-omnigenity."

The desired constraint is quantified by calculating the flux surface jump $\Delta\psi$ that is accrued over a single bounce period. This value of $\Delta\psi$ is then easily converted into the mean step size required for the random walk estimate. The quantity $\Delta\psi$ is determined by transforming from r, θ, ϕ to ψ, θ, ϕ coordinates so that ψ now represents the "radial" position of the particle.

The equation of motion for the particle's guiding center ψ position is given by

$$\frac{d\psi}{dt} = \frac{\partial\psi}{\partial t} + \mathbf{V}_D \cdot \nabla\psi = \mathbf{V}_D \cdot \nabla\psi \tag{7.170}$$

Here, $\mathbf{V}_D = d\mathbf{r}_g/dt$ is the guiding center drift velocity and the $\partial\psi/\partial t$ term has been set to zero because of the assumption of equilibrium. The quantity $\mathbf{V}_D$ is dominated by the grad-B drift which is proportional to $v_\perp^2$. The curvature drift is small because it is proportional to $v_\parallel^2$ and the particles of interest are trapped and thus have small $v_\parallel^2$. Single-particle guiding center theory shows that the term $\mathbf{V}_D \cdot \nabla\psi$ for the grad-B drift for ions can be written as

$$\mathbf{V}_D \cdot \nabla\psi = \frac{m_i v_\perp^2}{2eB^3}(\mathbf{B} \times \nabla B \cdot \nabla\psi) = \frac{\mu}{eB^2}(\mathbf{B} \times \nabla B \cdot \nabla\psi) \tag{7.171}$$

Here, $\mu = m_i v_\perp^2/2B$ is the usual adiabatic invariant. (A more complete form of $\mathbf{V}_D$ including the curvature and $\mathbf{E} \times \mathbf{B}$ drifts is given in Section 7.7.6 and leads to the same overall conclusions derived below.)

The flux jump $\Delta\psi$, is obtained by integrating Eq. (7.170) over one bounce period. One finds

$$\Delta\psi = \oint \mathbf{V}_D \cdot \nabla\psi \, dt = \frac{\mu}{e}\oint \frac{1}{B^2}(\mathbf{B} \times \nabla B \cdot \nabla\psi) \, dt \tag{7.172}$$

The constraint of ideal-omnigenity requires that

$$\Delta\psi = 0 \tag{7.173}$$

for all trapped particles. (The criterion can be shown to be automatically satisfied for all passing particles which, by definition, sample the entire flux surface.)

Equation (7.172) is cumbersome to evaluate because a detailed knowledge of the trapped particle's guiding center trajectory is required. The evaluation can be substantially simplified by assuming that the trapped particle banana width Δr_B is much less than the minor radius of the plasma: $\Delta r_B \sim (q/\varepsilon^{1/2}) r_{Li} \ll r$, usually a very good approximation experimentally. Then, the integrand I, which is a function of the guiding center trajectory $\mathbf{r}_g$ can be expanded as

$$I[\mathbf{r}_g(\mathbf{r},t)] = I[\mathbf{r} + \Delta\mathbf{r}_B(\mathbf{r},t)] \approx I(\mathbf{r}) + O(\Delta r_B/r) \approx I(\mathbf{r}) \tag{7.174}$$

where $\mathbf{r}$ represents the location of the central magnetic field line that longitudinally bisects the banana orbit.

Similarly, the small Δr_B assumption allows the integration path in Eq. (7.172) to be accurately approximated by

$$dt = \frac{dl}{v_\parallel} = \frac{dl}{(2/m_i)^{1/2}[E - \mu B(\mathbf{r}_g)]^{1/2}} \approx \frac{dl}{(2/m_i)^{1/2}[E - \mu B(\mathbf{r})]^{1/2}} \approx \tag{7.175}$$

Here, $E = (m_i/2)(v_\perp^2 + v_\parallel^2)$ is the particle's energy, also a constant of the motion and l is arc length along the magnetic field.

The evaluation of $\Delta\psi$ now only requires an integral along the magnetic field line and not the actual particle trajectory, a major reduction in complexity. Another useful simplification is that in the small Δr_B limit the integral along the outer leg of the banana orbit is approximately equal to the return integral along the inner leg.

These results can be combined leading to the following expression for the ideal-omnigenity constraint,

$$\Delta\psi(\psi,\theta_0) \approx 2\frac{\mu}{e}\left(\frac{m_i}{2}\right)^{1/2} \int_{l_1}^{l_2} \frac{(\mathbf{B}\times\nabla B\cdot\nabla\psi)}{B^2(E-\mu B)^{1/2}}\, dl = 0 \tag{7.176}$$

where l_1, l_2 are the turning points of the banana orbit: $E - \mu B(l_{1,2}) = 0$. Also without loss in generality we can assume that all field lines start their trajectory at $\phi_0 = 0$.

The quasi-omnigenous stellarator

There are several important consequences from Eq. (7.176) that lead to the transformation of the ideal-omnigenous constraint into the more practical quasi-omnigenous constraint. These are as follows.

The ideal-omnigenous constraint has been expressed solely in terms of the magnetic field in physical space coordinates. No detailed information about the guiding center trajectories is required. Consequently, Eq. (7.176) is in a convenient form for MHD analysis. Unfortunately, it is not possible to exactly satisfy Eq. (7.176) experimentally, or even theoretically, for a truly 3-D configuration.

Instead, Eq. (7.176) can only be approximately satisfied by various optimization procedures. The resulting configurations are thus called "quasi-omnigenous." The procedure for generating a quasi-omnigenous equilibrium requires the evaluation of $\Delta\psi = \Delta\psi(\psi, \theta_0, E, \mu)$ for a wide range of trapped particles (i.e., a wide range of E, μ). Actually, since transport is a diffusive process, the quantity that is actually needed is a distribution function weighted average of $(\Delta\psi)^2$ including an additional average over all poloidal angles θ_0:

$$[\Delta\psi_{av}(\psi)]^2 = \frac{\int (\Delta\psi)^2 \dfrac{f(E,\mu,\psi)}{(E-\mu B)^{1/2}}\, dEd\mu d\theta_0}{\int \dfrac{f(E,\mu,\psi)}{(E-\mu B)^{1/2}}\, dEd\mu d\theta_0} \tag{7.177}$$

If ψ is now chosen to correspond to the poloidal flux/2π then the equivalent random walk step size is easily related to $(\Delta\psi_{av})^2$ by the expression

$$[\Delta r(\psi)]^2 \sim \left(\frac{\delta r_D}{\tau_B}\tau_{eff}\right)^2 \sim \frac{(\Delta\psi_{av})^2}{\langle(\nabla\psi)^2\rangle}\frac{\tau_{eff}^2}{\tau_B^2} \sim \frac{(\Delta\psi_{av})^2}{\langle R^2 B_p^2\rangle}\frac{\tau_{eff}^2}{\tau_B^2} \tag{7.178}$$

Here, δr_D is the average distance that a banana center moves after one bounce period τ_B and is directly proportional to $\Delta\psi_{av}$. For particles trapped in helical ripples τ_B is shorter than for a tokamak because of the shorter helical wavelength; that is $\tau_B \sim L_H/v_{\|} \sim 2\pi R/N\varepsilon_H^{1/2}V_{Ti}$. The quantity $\langle R^2 B_p^2\rangle$ is the flux surface average of $R^2 B_p^2$. Physically, the ratio $\delta r_D/\tau_B$ is the unidirectional guiding center drift velocity of the banana center leading to enhanced transport.

The step size in Eq. (7.178) can then be used to estimate the neoclassical thermal diffusivity:

$$\chi_{NC}(\psi) \sim f_{eff}(\Delta r)^2 \nu_{eff} \sim \frac{N^2\varepsilon_H^{5/2}}{4\pi^2 R^2}\frac{(\Delta\psi_{av})^2}{\langle R^2 B_p^2\rangle}\frac{V_{Ti}^2}{\nu_{ii}} \tag{7.179}$$

Equation (7.179) is a similar but more accurate scaling relation than the simpler estimate given by Eq. (7.167). The value of χ_{NC} does not have to reduce to the neoclassical value for a tokamak to achieve success. It must only be reduced to the size of the gyro-Bohm coefficient, which sets the practical limit for tokamak transport. Qualitatively, stellarator neoclassical transport is improved by designing magnetic geometries which tend to minimize $(\Delta\psi_{av})^2$.

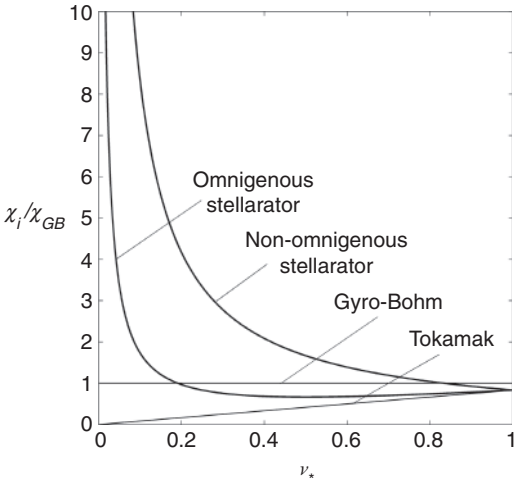

Figure 7.17 Schematic diagram showing the improvement in thermal diffusivity vs. collisionality in an omnigenous stellarator.

Even so, the geometrically optimized value of $\chi_{NC} \propto T^{5/2}$ is still larger for high temperatures. The reasons are that (1) the grad-B drift is proportional to $v_\perp^2 \propto T$ and (2) high energy particles drift a longer time because of their lower collision frequency $\nu_{eff} \propto 1/T^{3/2}$. Therefore, if omnigenity is not perfect (i.e., $(\Delta\psi_{av})^2 \neq 0$), high energy particles drift further off the flux surface than low energy particles. The implication is that the optimized thermal diffusivity will evolve towards the un-optimized value as the temperature increases. Even so, significant gains are possible over a large portion of the plasma. This behavior is shown schematically in Fig. 7.17.

The procedure just described demonstrates how the thermal diffusivity can be calculated and then compared to gyro-Bohm diffusion. MHD optimization requires that this procedure be repeated many times with different helical field amplitudes, phases and helicities. Optimization corresponds to minimizing $\chi_{NC}(\psi)$, or alternatively maximizing some simpler related parameter such as the global energy confinement time τ_E with respect to the helical field parameters. Often times the optimization leads to configurations with multiple helicities and a non-planar magnetic axis.

Lastly, the fact that no exact 3-D ideal-omnigenous equilibria have been found suggests that a range of widely different stellarator configurations might lead to a comparably optimized configuration in terms of neoclassical transport. To narrow down the range one needs additional constraints. This recognition has led to the ideas of the quasi-isodynamic and quasi-symmetric stellarator and it is here that specific optimized designs appear. The next task is to investigate the ideas behind these additional constraints.

7.7.4 The isodynamic stellarator

The idea of the isodynamic stellarator has been developed by German fusion scientists and has served as a guide to their past and future experimental programs (Gori *et al.*, 1996; Helander and Nuhrenberg, 2009; and Nuhrenberg, 2010). Currently the $1B class W7-X stellarator is under construction at Max Planck Institute for Plasma Physics in Greifswald, Germany and is designed to approximately satisfy the isodynamic constraint. This subsection describes the philosophy behind the constraint. It also provides corresponding mathematical definitions of ideal-isodynamic and quasi-isodynamic stellarators expressed in terms of the properties of the magnetic field. One simple conclusion from the discussion is that an ideal-isodynamic stellarator by definition automatically satisfies the constraint of ideal-omnigenity. The opposite is not true.

Philosophy

There are many additional constraints that can be imposed over and above omnigenity that, if satisfied, would likely lead to improved stellarator performance. In the author's view the philosophy that has led the Germans to the isodynamic constraint is founded on a basic mistrust of plasma behavior as β is increased.

Two potentially undesirable transport effects can happen at high β, even assuming good high β MHD stability. First, the flux surfaces may become more delicate, perhaps forming large islands or stochastic regions of magnetic field, both very detrimental to transport. Also, finite β driven shifts in the flux surface location can impair the performance of the divertor, a more difficult problem in a 3-D than 2-D configuration.

Second, as the pressure increases in a stellarator there is a natural transport-driven net current induced in the plasma, known as the bootstrap current. Thus, even if a stellarator has zero net current at low β a substantial current might flow of its own accord at high β. This current, if large enough, could drive kink instabilities leading to disruptions, thereby eliminating one of the main advantages of the stellarator.

An examination of many years of experimental data would seem to indicate that the German philosophy does indeed have significant merit. How is this philosophy translated into the isodynamic design constraint? Numerical studies have shown that flux surface robustness is related to the size of the bootstrap current. Similarly MHD kink stability is closely coupled to the net toroidal bootstrap current. Therefore eliminating the bootstrap current would alleviate both concerns discussed above.

To summarize: An ideal-isodynamic stellarator is one which satisfies the ideal-omnigenity constraint while simultaneously setting the bootstrap current to zero.

For context, it is worth noting that a stellarator design based on isodynamic optimization usually leads to a large aspect ratio device, $R_0/a \sim 10$.

With the philosophy now defined, the next step is to translate the isodynamic constraint into a mathematical criterion.

The ideal-isodynamic constraint

The ideal-isodynamic constraint requires the derivation of an expression for the bootstrap current in a general stellarator and then setting it equal to zero. Such an expression has been calculated and is presented shortly, but as will be seen it is quite complicated. A simpler constraint is presented here that follows from the basic physics of the bootstrap current. This definition differs from others appearing in the literature, but is used, nevertheless, to keep the concept as simple as possible.

To begin assume that the stellarator of interest satisfies the ideal-omnigenity constraint. Trapped particles now execute helical banana orbits but no longer drift from flux surface to flux surface after every bounce period. Each trapped particle orbit is characterized by a banana width Δr_B. The first point to note is that since Δr_B is finite this leads to a diamagnetic current flowing parallel to the magnetic field.

The diamagnetic effect is illustrated in Fig. 7.18, which shows co ($v_\| > 0$) and counter ($v_\| < 0$) banana orbits for two trapped particles with the same E, μ that are tangent on the same (dotted) flux surface. If there is a density gradient ($dn/d\psi < 0$) there are more inner than outer bananas resulting in a diamagnetic current flowing parallel to the magnetic field on the flux surface. A similar argument holds if there is a temperature gradient ($dT/d\psi < 0$).

The actual bootstrap current J_B is larger than the trapped particle diamagnetic current J_T and results from friction between trapped and passing particles. Specifically, in order to conserve overall momentum, this friction sets up a differential flow between passing and trapped electrons which generates the actual bootstrap current. The relation between bootstrap current and the trapped particle diamagnetic current is approximately given by

$$J_B \sim \frac{1}{\varepsilon} J_T \tag{7.180}$$

The conclusion to be drawn from Eq. (7.180) is that in order to completely eliminate the bootstrap current one must set $J_T = 0$. Now, the trapped particle diamagnetic current is clearly proportional to the banana width of the orbits. Therefore, a sufficient condition for setting $J_T = 0$ is to require the banana width of all particles to be zero. This condition actually represents substantial "overkill." It is mostly the case that both positive and negative diamagnetic currents flow within a given flux surface. Minimizing J_B then requires designing a magnetic geometry such that the contributions cancel when averaged over a flux surface.

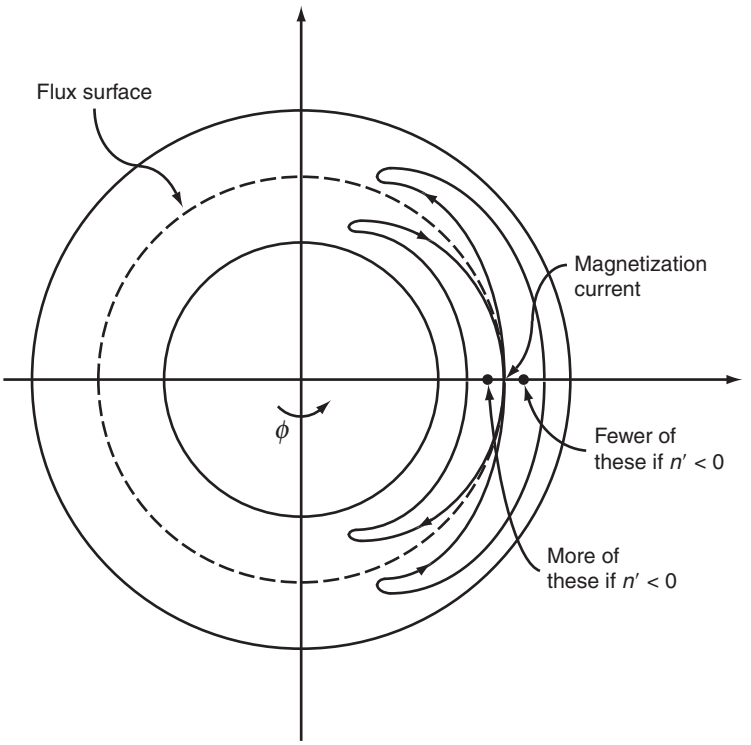

Figure 7.18 Diamagnetic effect of trapped particles due to a density gradient that ultimately leads to the generation of the bootstrap current.

Even so, the expression for the bootstrap current is sufficiently complicated that it is convenient to adopt the "overkill" condition as the definition of the ideal-isodynamic constraint. The condition can never be satisfied theoretically or experimentally but it does point in the right direction. It also helps address the important issue of alpha-particle confinement in reactor scale devices.

Mathematically, the finite banana width arises from the trapped particle grad-B drift off the flux surface. If the magnetic field can be designed so that a trapped particle's grad-B drift is zero along its entire banana orbit, then its banana width will be zero and there will be no bootstrap current. From Eq. (7.176) one sees that this requirement, which corresponds to the ideal-isodynamic constraint, can be written as

$$\mathbf{B} \times \nabla B \cdot \nabla \psi = 0 \tag{7.181}$$

Equation (7.181) is a very strict condition. It obviously implies that an ideal-isodynamic stellarator automatically satisfies the ideal-omnigenous constraint; that is, isodynamic stellarators are a subset of omnigenous stellarators.

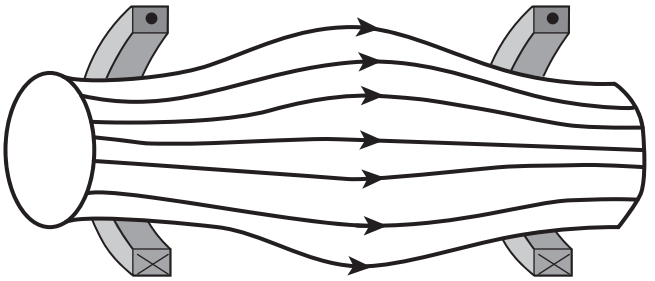

Figure 7.19 A 2-D symmetric mirror that exactly satisfies the ideal isodynamic constraint. Trapped particles never leave the flux surface and thus generate no bootstrap current.

The German approach to satisfy this constraint has been to try and design a magnetic configuration in which **B** and ∇B are parallel. A simple 2-D configuration that exactly satisfies Eq. (7.181) is a linear symmetric mirror machine as shown in Fig. 7.19. In this configuration a particle's grad-B drift is in the θ direction, and by symmetry, its guiding center orbit never drifts off the flux surface. Of course the simple mirror is known to be MHD unstable and all "passing" particles are lost through the ends. Still, in the context of a stellarator, the mirror geometry has the proper features with respect to the trapped particle orbits.

The German design of its new W7-X experiment does indeed have the appearance of a series of linked mirrors, but this is slightly misleading since most of the sophisticated optimization involves the plasma "elbows" which connect one straight section to another. Qualitatively, the W7-X geometry attempts to have the toroidally averaged helical curvature drift cancel the $1/R$ toroidal drift as much as possible. This reduces the bootstrap current and to a certain extent $\Delta\psi_{av}$.

Even with $J_B \rightarrow 0$, the $1/\nu_*$ dependence of χ_{NC} persists since trapped particles still do not sample the entire flux surface, particularly for vacuum fields. However, as β is increased a substantial diamagnetic ∇B drift arises due to the r dependence of $B(r)$ which causes the particles to poloidally drift around the flux surfaces. Therefore, to the extent that the magnetic geometry can be designed such that B does not vary with poloidal angle (i.e., there is no poloidal mirroring), the trapped particles can remain trapped toroidally but still sample the entire flux surface because of the poloidal $\nabla B(r)$ drift. Clearly a sophisticated design effort is required to satisfy these multiple constraints. The W7-X stellarator experiment is discussed in more detail in the next section.

The last point worth reiterating is that the ideal-isodynamic constraint given by Eq. (7.181) cannot be satisfied exactly experimentally or theoretically. Its real purpose is to serve as an idealized design target. Consequently, it is necessary to define a quantitative metric that measures how closely a realistic design comes to satisfying the ideal constraint. This leads to the idea of the quasi-isodynamic stellarator.

The quasi-isodynamic stellarator

The idea behind the quasi-isodynamic stellarator is in principle quite simple. One calculates the bootstrap current as a function of the amplitudes, phases, and helicities of the applied stellarator field. Next, some appropriate form of multi-function optimization is carried out that simultaneously attempts to minimize the thermal diffusivity $\chi_{NC}(\psi)$ and the bootstrap current density $J_B(\psi)$. Alternatively, simpler parameters could be used such as the energy confinement time τ_E and the total bootstrap current I_B. The result of such an optimization is a "quasi-isodynamic" stellarator, a configuration that is as close to being omnigenous as possible while simultaneously minimizing the bootstrap current.

The main technical difficulty in the procedure is the amount of work required to evaluate $J_B(\psi)$. There is an analytic expression for $J_B(\psi)$ for a general stellarator geometry, but it is quite complicated and requires the solution of several magnetic differential equations. Still, the burden of work falls on the computer and not the scientist.

The complexity can be appreciated by examining the actual expression for $J_B(\psi)$ after making the simplifying assumption that $T_i = T_e = T$ and setting the charge number $Z = 1$ (see for instance Landreman and Catto, 2011), and references therein,

$$J_B(\psi) \equiv \frac{\langle J_\parallel B\rangle}{\langle B\rangle} = -6.8\,\frac{f_{eff}}{1-f_{eff}}\,\frac{\langle G\rangle}{\langle B\rangle}\left(T\frac{\partial n}{\partial \psi} + 0.04n\frac{\partial T}{\partial \psi}\right) \tag{7.182}$$

Here, $\langle\ \rangle$ denotes flux surface average and the complicated function $\langle G\rangle$ is given by

$$\langle G\rangle = \frac{1}{f_{eff}}\left(\langle h_1\rangle - \frac{3}{4}\langle B^2\rangle\int_0^{1/B_{\max}}\frac{\langle h_2\rangle}{\langle g\rangle}\lambda\, d\lambda\right) \tag{7.183}$$

with $g = (1 - \lambda B)^{1/2}$ and h_1, h_2 being solutions of the magnetic differential equations

$$\begin{aligned} \mathbf{B}\cdot\nabla\left(\frac{h_1}{B^2}\right) &= \frac{2}{B^3}\mathbf{B}\times\nabla B\cdot\nabla\psi \qquad h_1\big|_{B=B_{\max}} = 0 \\ \mathbf{B}\cdot\nabla\left(\frac{h_2}{g}\right) &= \frac{\lambda}{2g^3}\mathbf{B}\times\nabla B\cdot\nabla\psi \qquad h_2\big|_{B=B_{\max}} = 0 \end{aligned} \tag{7.184}$$

There are two points to note. First, when the ideal-isodynamic constraint is satisfied then $h_1 = h_2 = 0$ and, as expected $J_B = 0$. Second, although the procedure is complicated requiring a numerical evaluation, it is nonetheless expressed solely in terms of the magnetic field; no individual particle orbits have to be calculated.

The quasi-isodynamic stellarator is one of two special classes of stellarator geometries that have been suggested to greatly reduce neoclassical losses in a 3-D system.

7.7.5 The symmetric stellarator

The second class of stellarator geometries that has been suggested to reduce neoclassical losses is the "symmetric stellarator." This configuration has been studied by fusion scientists around the world but has received special attention in the United States. One example is the university scale helically symmetric stellarator experiment, HSX, at the University of Wisconsin (see for instance Canik *et al*., 2007). Also, there was a major effort to build a $100M class toroidally symmetric stellarator at the Princeton Plasma Physics Laboratory (Zarnstorff *et al*., 2001). However, to the great frustration of the US fusion community, this experiment, the National Compact Stellarator Experiment (NCSX) was canceled because of budget constraints.

The present subsection describes the basic idea behind the symmetric stellarator. The definition of an ideal-symmetric stellarator is presented as well as a more practical definition for the quasi-symmetric stellarator. Although not obvious, it is also shown that an ideal-symmetric stellarator is omnigenous.

Philosophy

Scientists in the US fusion program have adopted a different strategy than their German colleagues. In the United States, scientists are willing to live with a bootstrap current as long as it is not too large. Instead, the goal is to generate compact stellarator configurations that have both omnigenity and a large macroscopic flow velocity, on the order of the ion thermal speed. This flow velocity, and in particular the corresponding velocity shear, is expected to reduce plasma microturbulence. Thus, omnigenity would reduce neoclassical transport, and large velocity shear would reduce turbulent transport. Overall, the energy confinement time should show significant improvement, indeed a worthy goal.

Generating a large flow velocity in a general 3-D geometry is a difficult task. The reason is that neoclassical viscosity is usually large, and therefore would be expected to damp the flow velocity down to the order of the diamagnetic drift velocity. This velocity is smaller by a factor r_{Li}/a than the thermal velocity. However, by carefully designing the magnetic field, it is possible to dramatically reduce the viscosity, thereby allowing larger flow velocities.

This "careful design" corresponds to the symmetric stellarator configuration. It is important to recognize that stellarator designs optimized with respect to the symmetry constraint can be more compact than isodynamic stellarators. For

example, the NCSX design had an aspect ratio $R_0/a \sim 4$. From the US view compactness is an advantage since scaled-up reactor designs would be smaller and presumably more economical. From the German view compactness is apparently not as serious an issue. Instead the large aspect ratio can be viewed as an advantage because of engineering simplicity, lower wall loading, and easier access to the plasma. The best strategy has yet to be determined.

Consider now translating the symmetric stellarator constraint into a mathematical criterion.

The ideal-symmetric stellarator – general velocity constraints

The discussion begins with a description of the general constraints on the flow velocity in any 3-D configuration, temporarily ignoring omnigenity. Once these constraints are established, an additional constraint is introduced that minimizes the viscosity, thereby allowing for large flows. The viscosity constraint can be obtained from a collisionless kinetic MHD model (Helander, 2007), a collisional Braginskii transport model, or even to a large extent from ideal MHD. All lead to the same final result.

The approach adopted here makes use of the ideal MHD equations with flow including a single, but important, contribution from the Braginskii transport model. In addition the model restricts attention to the subclass of flows that are consistent with the assumption that the temperature satisfy $T = T(\psi)$. This constraint arises from hindsight reasoning and, as is shown, is important in showing that symmetric stellarators with large flows are also omnigenous. The constraint is plausible physically since the large parallel thermal conductivity would be expected to quickly equilibrate the temperature on any given flux surface. Still, $T = T(\psi)$ is an added constraint since it cannot be directly deduced from ideal MHD.

The derivation of the general flow constraints starts from the recognition that in steady state $\nabla \times \mathbf{E} = 0$ implying that

$$\mathbf{E} = -\nabla\Phi \tag{7.185}$$

Next, the parallel component of the ideal Ohm's law requires that $\mathbf{E} \cdot \mathbf{B} = -\mathbf{B} \cdot \nabla\Phi = 0$. The consequence is that

$$\Phi = \Phi(\psi) \tag{7.186}$$

where ψ is a flux surface label. The perpendicular component of Ohm's law then leads to an expression for the total velocity that can be written as

$$\mathbf{v} = \frac{\mathbf{E} \times \mathbf{B}}{B^2} + \frac{v_\parallel}{B}\mathbf{B} = -\frac{d\Phi}{d\psi}\frac{\nabla\psi \times \mathbf{B}}{B^2} + \frac{v_\parallel}{B}\mathbf{B} \tag{7.187}$$

The first general constraint on the velocity follows from forming the dot product of Eq. (7.187) with $\nabla\psi$. One obtains

$$\mathbf{v}\cdot\nabla\psi = 0 \tag{7.188}$$

The flow velocity must lie in the flux surface; that is, there is no cross field flow.

The second general constraint arises from the combined use of the ideal MHD energy equation and conservation of mass. The energy equation can be written as

$$\frac{d}{dt}\left(\frac{p}{n^{\gamma}}\right) = 2\mathbf{v}\cdot\nabla\left(\frac{T}{n^{\gamma-1}}\right) = 2\frac{T}{n^{\gamma-1}}\left[\frac{1}{T}\mathbf{v}\cdot\nabla T - \frac{\gamma-1}{n}\mathbf{v}\cdot\nabla n\right] = 0 \tag{7.189}$$

Since the flow is restricted to be consistent with $T = T(\psi)$ it automatically follows from Eq. (7.188) that $\mathbf{v}\cdot\nabla T = 0$. Thus, the conclusion from Eq. (7.189) is that

$$\mathbf{v}\cdot\nabla n = 0 \tag{7.190}$$

This relation is used in the conservation of mass equation

$$\frac{dn}{dt} + n\nabla\cdot\mathbf{v} = \mathbf{v}\cdot\nabla n + n\nabla\cdot\mathbf{v} = 0 \tag{7.191}$$

Application of Eq. (7.190) leads to the second important constraint on the velocity,

$$\nabla\cdot\mathbf{v} = 0 \tag{7.192}$$

The flow velocity in any 3-D system must be incompressible if one requires that $T = T(\psi)$.

Lastly, in terms of general properties observe that with the form of velocity given by Eq. (7.187) it follows that the steady state Faraday's law, $\nabla\times(\mathbf{v}\times\mathbf{B}) = 0$ is automatically satisfied.

The ideal-symmetric stellarator – the large flow velocity constraint

The large flow velocity constraint is based on the intuition that for such a flow to exist, the viscosity must be small. If not, viscous forces would greatly slow down the flow velocity to a much smaller value. One straightforward way to determine the constraint is to write down the viscosity tensor as, for instance, derived by Braginskii (1965). This is the approach used here. Since the Braginskii viscosity is a very complicated tensor, attention is focused on the largest, leading-order (in $1/\omega_{ci}\tau_{ii}$) contribution. For incompressible flows, the tensor is diagonal and can be written as

$$\begin{aligned}\boldsymbol{\Pi} &= \eta_0(\mathbf{I} - 3\mathbf{bb})(\mathbf{b}\cdot\nabla\mathbf{v}\cdot\mathbf{b})\\ \eta_0 &\approx 0.96nT\tau_{ii}\end{aligned} \tag{7.193}$$

The condition on the velocity for the viscosity to vanish for incompressible flows is thus given by

$$\mathbf{b} \cdot \nabla \mathbf{v} \cdot \mathbf{b} = 0 \tag{7.194}$$

Interestingly, the identical condition arises from a low collisionality treatment (Helander, 2007) using the kinetic MHD model. Equation (7.194) can be written in an alternate form by forming the dot product of Faraday's law with $\mathbf{B}$ and using the incompressibility constraint

$$\mathbf{B} \cdot \nabla \times (\mathbf{v} \times \mathbf{B}) = \mathbf{B} \cdot (\mathbf{B} \cdot \nabla \mathbf{v} - \mathbf{v} \cdot \nabla \mathbf{B}) = B^2 \mathbf{b} \cdot \nabla \mathbf{v} \cdot \mathbf{b} - B \mathbf{v} \cdot \nabla B = 0 \tag{7.195}$$

The large flow velocity constraint given by Eq. (7.194) is thus equivalent to

$$\mathbf{v} \cdot \nabla B = 0 \tag{7.196}$$

The constraint requires that the magnitude of $\mathbf{B}$ be constant along the direction of the flow velocity.

With hindsight this condition is perhaps not surprising. Intuitively, Eq. (7.196) implies that a large flow can exist when the plasma flows along a "smooth magnetic channel." A "corrugated magnetic channel" would produce a series of compressions and decompressions of the plasma which, in the presence of any dissipation, would damp the flow. If one had this intuition initially, then Eq. (7.196) could have simply been postulated as the definition of the large velocity constraint without explicitly bringing viscosity into the discussion. Such is the value of hindsight.

The ideal-symmetric stellarator

The constraints that must be satisfied by the velocity in a large flow system have now been determined. The next task is to transform these constraints into a corresponding condition on the magnetic field. This will define the ideal-symmetric stellarator. The basic constraints are summarized below:

$$\begin{aligned} \nabla \cdot \mathbf{v} &= 0 \qquad \text{General flow constraint} \\ \mathbf{v} \cdot \nabla \psi &= 0 \qquad \text{General flow constraint} \\ \mathbf{v} \cdot \nabla B &= 0 \qquad \text{Large flow constraint} \end{aligned} \tag{7.197}$$

To proceed note that the second and third constraints imply that the velocity can be written as

$$\mathbf{v} = g(\mathbf{r}) \nabla \psi \times \nabla B \tag{7.198}$$

The scalar function $g(\mathbf{r})$ is determined by recalling that the velocity can also be written in the form given by Eq. (7.187). One equates these two expressions and

forms the dot product first with ∇B and then with $\mathbf{B}$, leading to the following two relations:

$$\begin{aligned} \frac{d\Phi}{d\psi}\frac{\nabla\psi\times\mathbf{B}\cdot\nabla B}{B^2} &= -v_{\|}\frac{\mathbf{B}\cdot\nabla B}{B} \\ g\nabla\psi\times\mathbf{B}\cdot\nabla B &= -v_{\|}B \end{aligned} \tag{7.199}$$

Eliminating $v_{\|}$ yields

$$g(\mathbf{r}) = \frac{d\Phi}{d\psi}\frac{1}{\mathbf{B}\cdot\nabla B} \tag{7.200}$$

and

$$\mathbf{v} = \frac{d\Phi}{d\psi}\frac{\nabla\psi\times\nabla B}{\mathbf{B}\cdot\nabla B} \tag{7.201}$$

The desired constraint on the magnetic field geometry is now obtained by requiring that the flow be incompressible. Thus, setting $\nabla\cdot\mathbf{v}=0$ leads to the ideal-symmetric constraint

$$\nabla\psi\times\nabla B\cdot\nabla(\mathbf{B}\cdot\nabla B)=0 \tag{7.202}$$

This result, while quantitative, is not completely satisfactory in terms of providing physical intuition. There are two reasons. First, Eq. (7.202) is relatively complicated so that the magnetic field strategies required to satisfy the constraint are not immediately obvious. In particular it is not exactly clear what is "symmetric" in the ideal-symmetric stellarator. The second reason is that even if Eq. (7.202) is satisfied over the entire plasma it is not evident whether or not the corresponding configuration is omnigenous. These two issues are discussed below.

What is symmetric in an ideal-symmetric stellarator?

It is shown here that the ideal-symmetric stellarator constraint implies that the three-dimensional function $B=B(\mathbf{r})$ is actually a two-dimensional function of flux and magnetic field arc length: $B=B(\psi, l)$. Assuming that this can be proved then the symmetry is immediately obvious. The quantity $B(\psi, l)$ is symmetric with respect to the third coordinate denoted here as α.

The analysis begins with the introduction of a set of flux coordinates ψ, α, l. The flux satisfies the usual condition $\mathbf{B}\cdot\nabla\psi=0$. The arc length coordinate also satisfies the familiar condition $\mathbf{B}\cdot\nabla l=B$. The third coordinate can be fairly general. A good choice for α is an angle-like variable which is locally perpendicular to the magnetic field: $\mathbf{B}\cdot\nabla\alpha=0$. One can always find an α that satisfies this orthogonality property. For unconvinced readers, this is demonstrated explicitly in

the next subsection. The property $\mathbf{B} \cdot \nabla\alpha = 0$ is convenient because it leads to the following simplification: $\mathbf{B} \cdot \nabla = B(\partial/\partial l)$.

Introduction of these coordinates into the ideal-symmetric constraint given by Eq. (7.202) leads to

$$B\nabla\psi \times \nabla B \cdot \nabla\left(\frac{\partial B}{\partial l}\right) = 0 \tag{7.203}$$

The general solution to Eq. (7.203) is

$$\frac{\partial B}{\partial l} = F(\psi, B) \tag{7.204}$$

where $F(\psi, B)$ is an arbitrary function.

Next, Eq. (7.204) is first differentiated with respect to l and secondly to α resulting in two expressions,

$$\begin{aligned} \frac{\partial^2 B}{\partial l^2} &= \frac{\partial F}{\partial B}\frac{\partial B}{\partial l} \\ \frac{\partial^2 B}{\partial l \partial \alpha} &= \frac{\partial F}{\partial B}\frac{\partial B}{\partial \alpha} \end{aligned} \tag{7.205}$$

These expressions are divided, yielding

$$\frac{\partial}{\partial l}\ln\left(\frac{\partial B}{\partial l}\right) = \frac{\partial}{\partial l}\ln\left(\frac{\partial B}{\partial \alpha}\right) \tag{7.206}$$

This equation can be integrated with respect to l, leading to

$$\frac{\partial B}{\partial l} = H(\psi,\alpha)\frac{\partial B}{\partial \alpha} \tag{7.207}$$

where $H(\psi, \alpha)$ is arbitrary. Now introduce a new set of coordinates with a modified arc length

$$\begin{aligned} \psi' &= \psi \\ \alpha' &= \alpha \\ l' &= l + h(\psi, \alpha) \end{aligned} \tag{7.208}$$

with $h(\psi, \alpha)$ to be determined. Note that l' is still a proper arc length coordinate: $\mathbf{B} \cdot \nabla l' = B$. After substituting Eq. (7.208) into Eq. (7.207) one obtains

$$\left(1 - H\frac{\partial h}{\partial \alpha}\right)\frac{\partial B}{\partial l'} = H\frac{\partial B}{\partial \alpha'} \tag{7.209}$$

The function $h(\psi,\alpha)$ is chosen to satisfy $H(\partial h/\partial\alpha) = 1$ leading to the important conclusion

$$\frac{\partial B}{\partial \alpha'} = 0 \quad \rightarrow \quad B = B(\psi',l') \tag{7.210}$$

This completes the proof, explicitly demonstrating that the ideal-symmetric stellarator constraint corresponds to the symmetry requirement $B(\psi',\alpha',l') \rightarrow B(\psi',l')$.

Physically, the symmetry condition implies that large flows in a flux surface can only occur when B does not depend on the angle-like coordinate α. As the plasma flows around the torus it must, in spite of toroidal effects, encounter a uniform B corresponding to a smooth magnetic channel. If not, then corrugations in B would lead to a strong viscous damping.

Are ideal-symmetric stellarators omnigenous?

Although not obvious, the analysis below shows that an ideal-symmetric stellarator with large flow is also omnigenous. To demonstrate this result one rewrites the ideal quasi-symmetric constraint given by Eq. (7.202) in an alternate form consisting of two terms. One is shown to easily satisfy the omnigenity constraint. The other also satisfies the constraint but the proof requires some effort. The analysis begins by noting that the quantity $\mathbf{B} \times \nabla\psi$ can in general be vector decomposed as

$$\mathbf{B} \times \nabla\psi = g_1\mathbf{B} + g_2\nabla\psi \times \nabla B + g_3\nabla\psi = g_1\mathbf{B} + g_2\nabla\psi \times \nabla B \tag{7.211}$$

where $g_3 = 0$ because of the requirement that $\mathbf{B} \cdot \nabla\psi = 0$. Now form the dot product of this relation first with ∇B and then with $\mathbf{B}$ leading to the following two relations:

$$\begin{aligned} g_1 &= -\frac{\mathbf{B} \times \nabla B \cdot \nabla\psi}{\mathbf{B} \cdot \nabla B} \\ g_2 &= -\frac{B^2}{\mathbf{B} \cdot \nabla B} \end{aligned} \tag{7.212}$$

The next step is to take the divergence of Eq. (7.211). The result can be written in terms of the ideal-symmetric stellarator constraint which is then set to zero,

$$\mathbf{B} \cdot \nabla\left(\frac{\mathbf{B} \times \nabla B \cdot \nabla\psi}{\mathbf{B} \cdot \nabla B}\right) + \mu_0\mathbf{J} \cdot \nabla\psi = \frac{B^2}{(\mathbf{B} \cdot \nabla B)^2}\nabla\psi \times \nabla B \cdot \nabla(\mathbf{B} \cdot \nabla B) = 0 \tag{7.213}$$

The first term on the left-hand side of the constraint can be formally integrated with respect to arc length, yielding

$$\mathbf{B} \times \nabla B \cdot \nabla\psi = G(\psi)B\frac{\partial B}{\partial l} + \mu_0 B\frac{\partial B}{\partial l}\int_0^l \frac{\mathbf{J} \cdot \nabla\psi}{B}\, dl' \tag{7.214}$$

where $G(\psi)$ is a free integration function. Equation (7.214) is useful because $\mathbf{B} \times \nabla B \cdot \nabla \psi$ is precisely the quantity appearing in the ideal-omnigenous constraint given by Eq. (7.176).

One now observes that the term with $G(\psi)$ automatically satisfies the omnigenity constraint. This can be seen by writing the corresponding contribution to Eq. (7.176) as follows

$$\begin{aligned}\int_{l_1}^{l_2} \frac{(\mathbf{B} \times \nabla B \cdot \nabla \psi)_G}{B^2 (E - \mu B)^{1/2}}\, dl &\rightarrow G(\psi) \int_{l_1}^{l_2} \frac{1}{B(E - \mu B)^{1/2}} \frac{\partial B}{\partial l}\, dl \\ &= \frac{G(\psi)}{E^{1/2}} \int_{l_1}^{l_2} \frac{\partial}{\partial l} \ln \left[\frac{E - (E - \mu B)^{1/2}}{E + (E - \mu B)^{1/2}} \right] dl\end{aligned} \tag{7.215}$$

The term in the integrand is an exact differential which can be trivially integrated. Furthermore, the end points of the integration path represent the mirror points which by definition satisfy $B_{\max}(l_1) = B_{\max}(l_2)$. Therefore, as stated, this contribution vanishes.

The remaining contribution to the omnigenous constraint involves the quantity $\mathbf{J} \cdot \nabla \psi$. For systems with zero flow $\mathbf{J} \times \mathbf{B} = \nabla p$ implying that $\mathbf{J} \cdot \nabla \psi = 0$. Ideal-symmetric systems without flow are automatically omnigenous. This, however, defeats one main purpose of the ideal-symmetric system which is to achieve good neoclassical transport in the presence of large flow velocities. Therefore, a zero flow ideal-symmetric system, which is more difficult to create than an ideal-omnigenous system, would appear to offer no additional advantages. The increased difficulty is a consequence of the fact that symmetric systems must satisfy a 2-D local criterion in ψ,l, while omnigenous systems average over arc length leading to a 1-D criterion in ψ for many particles.

The quantity $\mathbf{J} \cdot \nabla \psi$ does not obviously vanish in a system with flow because of the inertial terms. However, a nice proof by Sugama *et al*. (2011) shows that $\mathbf{J} \cdot \nabla \psi$ does indeed vanish even in the presence of large flows. An outline of their proof is as follows.

One starts with the momentum equation, assuming that the zero viscosity constraint has been satisfied. Form the dot product of this equation first with $\mathbf{B}$ and then with $\mathbf{v}$. A short calculation that makes use of the previously derived flow constraints leads to two relations given by

$$\begin{aligned}\mathbf{B} \cdot \nabla \left(\frac{p}{\rho} \ln \rho - \frac{v^2}{2} \right) + \mathbf{v} \cdot \nabla (B v_{\|}) &= 0 \\ \rho \mathbf{v} \cdot \nabla \left(\frac{v^2}{2} \right) - \mathbf{B} \cdot \nabla (B v_{\|}) &= 0\end{aligned} \tag{7.216}$$

The goal now is to eliminate the $Bv_{\|}$ terms from Eq. (7.216). This task is accomplished by some simple differentiation that makes use of the commuting property between $\mathbf{B}\cdot\nabla$ and $\mathbf{v}\cdot\nabla$. Specifically, by making use of Faraday's law it follows that $\mathbf{B}\cdot\nabla(\mathbf{v}\cdot\nabla Q)=\mathbf{v}\cdot\nabla(\mathbf{B}\cdot\nabla Q)$. The resulting equation can be written as

$$(\mathbf{B}\cdot\nabla)^2\left(\frac{p}{\rho}\ln\rho-\frac{v^2}{2}\right)+\rho(\mathbf{v}\cdot\nabla)^2\left(\frac{v^2}{2}\right)=0 \tag{7.217}$$

Next, note that the quantity of interest $\mathbf{J}\cdot\nabla\psi$ can be expressed in terms of v^2 by rewriting the previously derived $\mathbf{v}$ component of the momentum equation as

$$\mathbf{J}\cdot\nabla\psi=-\frac{\rho}{d\Phi/d\psi}\mathbf{v}\cdot\nabla\left(\frac{v^2}{2}\right) \tag{7.218}$$

The proof continues by introducing flux coordinates ψ,α,l or more conveniently ψ,α,B. Now, recall that $\mathbf{v}\cdot\nabla\psi=\mathbf{v}\cdot\nabla B=0$ implying that

$$\mathbf{J}\cdot\nabla\psi=-\frac{\rho}{d\Phi/d\psi}(\mathbf{v}\cdot\nabla\alpha)\frac{\partial}{\partial\alpha}\left(\frac{v^2}{2}\right)=-\rho\frac{\partial}{\partial\alpha}\left(\frac{v^2}{2}\right) \tag{7.219}$$

where use has been made of the fact that $\mathbf{B}=\nabla\psi\times\nabla\,\alpha$ (also proven in Section 7.7.6). The final desired equation is obtained by differentiating Eq. (7.217) with respect to α and using the facts that $\rho=\rho(\psi,B)$, $p=p(\psi,B)$ and that for symmetric systems $B=B(\psi,l)$,

$$\left\{(\mathbf{B}\cdot\nabla B)\frac{\partial}{\partial B}\left[(\mathbf{B}\cdot\nabla B)\frac{\partial}{\partial B}\right]-\rho\Phi'^2\frac{\partial^2}{\partial\alpha^2}\right\}\frac{\partial v^2}{\partial\alpha}=0 \tag{7.220}$$

This is a single partial differential equation for $\partial v^2/\partial\alpha$. When solved subject to appropriate boundary conditions Sugama *et al.* (2011) pointed out that except for a very narrow class of uninteresting solutions, the only physically acceptable solution is $\partial v^2/\partial\alpha=0$ or $v^2=v^2(\psi,B)$. From Eq. (7.219) it then immediately follows that

$$\mathbf{J}\cdot\nabla\psi=0 \tag{7.221}$$

which is the desired result.

The overall conclusion is that the exact ideal-symmetric constraint given by Eq. (7.202) is equivalent to the more convenient form obtained from Eq. (7.214)

$$\mathbf{B}\times\nabla B\cdot\nabla\psi=G(\psi)\mathbf{B}\cdot\nabla B \tag{7.222}$$

which, as has been shown, proves that ideal-symmetric stellarators automatically satisfy the ideal-omnigenous constraint.

The quasi-symmetric stellarator

As for the other ideal constraints it is not possible to create, either theoretically or experimentally, an exact ideal-symmetric 3-D stellarator. In 2-D, however, a straight cylindrically symmetric mirror with purely poloidal flow satisfies the ideal-symmetric constraint.

To design a practical 3-D large flow stellarator one must define an appropriate set of metrics over which a multi-function optimization can be carried out that simultaneously minimizes the neoclassical transport and the viscous force. The result of this optimization is the "quasi-symmetric stellarator." As before, the thermal diffusivity $\chi_{NC}(\psi)$, given by Eq. (7.179), is a good measure of omnigenity and the associated local neoclassical transport losses. The energy confinement time τ_E is an alternate global parameter.

A useful metric for the viscous forces can be defined as follows. First, form the dot product of the momentum equation (including the Braginskii viscosity) with $\mathbf{v}$. After a short calculation the result can be expressed as

$$\nabla \cdot \left[\left(\frac{\rho v^2}{2} + p \right) \mathbf{v} + \frac{1}{\mu_0} \mathbf{E} \times \mathbf{B} + \Pi_0 (\mathbf{v} - 3 v_\parallel \mathbf{b}) \right] = -3 \frac{\eta_0}{B^2} (\mathbf{v} \cdot \nabla B)^2 \qquad (7.223)$$

Here, $\Pi_0 = \eta_0 (\mathbf{b} \cdot \nabla \mathbf{v} \cdot \mathbf{b}) = (\eta_0 / B)(\mathbf{v} \cdot \nabla B)$, $\eta_0 \approx 0.96 n T \tau_{ii}$, and use has been made of various equilibrium relations and the general velocity constraints. The large flow velocity constraint has not been used.

Next, Eq. (7.223) is integrated over a plasma volume bounded by a flux surface $\psi =$ constant. All the divergence terms are converted to surface integrals by Gauss' theorem. Each surface term vanishes by virtue of the general velocity constraints. What remains is the term on the right-hand side proportional to $(\mathbf{v} \cdot \nabla B)^2$ which would vanish if the large flow constraint was exactly satisfied.

If the constraint is not exactly satisfied the remaining non-zero term represents the viscous power attempting to slow down the velocity. In principle, one needs to solve the time-dependent problem to calculate the actual slowing down of the plasma flow. For design purposes this is not necessary. Instead, it makes sense to use the viscous power as a metric which has to be minimized to allow for the maximum flow. Mathematically, the quantity to be minimized can be written as

$$P_V(\psi) = 3 \int_\psi \frac{\eta_0}{B^2} (\mathbf{v} \cdot \nabla B)^2 d\mathbf{r} \qquad (7.224)$$

To utilize Eq. (7.224) one must substitute a desired flow velocity $\mathbf{v}(\mathbf{r})$ and then minimize with respect to the free stellarator harmonic parameters appearing in B. A simpler global parameter is the viscous power integrated over the entire plasma, $P_{Va} = P_V(\psi_a)$.

To summarize a quasi-symmetric stellarator is defined as one that has been optimized to be as close to omnigenous as possible while simultaneously minimizing the viscous force.

7.7.6 Boozer coordinates

Introduction

The previous discussion has led to three possible constraints on the magnetic field, any of which, if satisfied, would greatly improve neoclassical transport in a stellarator. These are summarized below:

$$\begin{aligned} &\int_{l_1}^{l_2} \frac{(\mathbf{B}\times\nabla B\cdot\nabla\psi)}{B^2(E-\mu B)^{1/2}}\,dl = 0 && \text{Omnigenous}\\ &\mathbf{B}\times\nabla B\cdot\nabla\psi = 0 && \text{Isodynamic}\\ &\mathbf{B}\times\nabla B\cdot\nabla\psi = G(\psi)(\mathbf{B}\cdot\nabla B) && \text{Symmetric} \end{aligned} \tag{7.225}$$

The constraints listed in Eq. (7.225) have the advantage of being written in a coordinate independent form and are each functions of the same quantity $\mathbf{B}\times\nabla B\cdot\nabla\psi$. Still, it is somewhat difficult to understand intuitively how to design a stellarator magnetic field that approximately satisfies any of these constraints. This is where flux coordinates make an important contribution. By transforming to a clever set of flux coordinates one can show that the constraints reduce to much simpler, easier to understand, forms. These forms are often used to help with the practical design of stellarators. They are also particularly useful for understanding neoclassical transport in a stellarator. Measured against these important benefits is one minor disadvantage. It requires a considerable effort, mainly computational, to actually carry out the transformation from real laboratory coordinates to flux coordinates. The main issues are discussed below.

The first part of the analysis presents a derivation of the Boozer coordinates. In the second part the Boozer coordinates are used to simplify the three neoclassical constraints listed in Eq. (7.225).

Boozer coordinates

The goal is to show that a coordinate transformation always exists that leads to a pair of co-variant and contra-variant representations for the magnetic field which have particularly simple forms. These forms in turn lead to the remarkable result that the perpendicular guiding center drift of a particle off a given flux surface is a function only of $B = |\mathbf{B}|$ and not the individual vector components. The transformed coordinates are known as Boozer coordinates (Boozer, 1982).

The discussion starts with a transformation from the familiar laboratory coordinates r,θ,ϕ to a general set of flux coordinates ψ, χ, ζ. Here, ψ is a radial-like coordinate, χ is a poloidal-like angle, and ζ is a toroidal-like angle. For intuition one can imagine writing the flux coordinates as

$$\begin{aligned}\psi &= \psi_0(r) + \sum_{m,n} \psi_{mn}(r)\, e^{i(m\theta+n\phi)} \\ \chi &= \theta + \sum_{m,n} \theta_{mn}(r)\, e^{i(m\theta+n\phi)} \\ \zeta &= \phi + \sum_{m,n} \phi_{mn}(r)\, e^{i(m\theta+n\phi)}\end{aligned} \tag{7.226}$$

Observe that χ increases by 2π when θ increases by 2π. Similarly for ζ and ϕ. This form of the transformation is, however, not explicitly needed for the analysis.

To obtain the desired contra-variant representation two pieces of information are required for $\mathbf{B}$: $\mathbf{B}\cdot\nabla\psi = 0$, $\nabla\cdot\mathbf{B} = 0$. One can now introduce a set of three independent basis vectors in terms of ψ, χ, ζ:

$$\nabla\psi\times\nabla\chi \qquad \nabla\zeta\times\nabla\psi \qquad \nabla\chi\times\nabla\zeta \tag{7.227}$$

These basis vectors always allow $\mathbf{B}$ to be written in a contra-variant (i.e., cross-product) form

$$\mathbf{B}(\mathbf{r}) = f_1\nabla\psi\times\nabla\chi + f_2\nabla\zeta\times\nabla\psi + f_3\nabla\chi\times\nabla\zeta \tag{7.228}$$

where $f_j = f_j(\psi,\chi,\zeta)$. Equation (7.228) can be simplified. The condition $\mathbf{B}\cdot\nabla\psi = 0$ requires that $f_3 = 0$. The condition $\nabla\cdot\mathbf{B} = 0$ leads to a constraint between f_1 and f_2,

$$\begin{aligned}\nabla\cdot\mathbf{B} &= J'\left(\frac{\partial f_1}{\partial\zeta} + \frac{\partial f_2}{\partial\chi}\right) = 0 \\ J' &= \nabla\psi\times\nabla\chi\cdot\nabla\zeta\end{aligned} \tag{7.229}$$

where $\boldsymbol{J}' \equiv 1/\boldsymbol{J}$ is the inverse Jacobian of the transformation; that is $d\mathbf{r} = \boldsymbol{J}d\psi d\chi d\zeta$. Equation (7.229) implies that f_1 and f_2 can be written in terms of a stream function. Specifically, the solution to Eq. (7.229) can be expressed as

$$\begin{aligned}f_1(\psi,\chi,\zeta) &= \overline{f}_1(\psi) + \sum_1^\infty \overline{f}_{1n}(\psi)\chi^n + \overline{\overline{f}}\,(\psi)\zeta + \frac{\partial\tilde{f}(\psi,\chi,\zeta)}{\partial\chi} \\ f_2(\psi,\chi,\zeta) &= \overline{f}_2(\psi) + \sum_1^\infty \overline{f}_{2n}(\psi)\zeta^n - \overline{\overline{f}}(\psi)\chi - \frac{\partial\tilde{f}(\psi,\chi,\zeta)}{\partial\zeta}\end{aligned} \tag{7.230}$$

The non-oscillatory terms have been explicitly displayed so that by definition $\langle\tilde{f}\rangle = 0$ over one period in χ and/or ζ. Periodicity constraints require that

$\overline{f}_{1n} = \overline{f}_{2n} = 0$ and $\overline{\overline{f}} = 0$. Consequently, the magnetic field given by Eq. (7.228) can be rewritten as

$$\mathbf{B}(\mathbf{r}) = \overline{f}_1 \nabla\psi \times \nabla\chi + \overline{f}_2 \nabla\zeta \times \nabla\psi + \nabla\psi \times \nabla\tilde{f} \tag{7.231}$$

An identical relation exists for $\mathbf{J}$ since $\mathbf{J} \cdot \nabla\psi = 0$ and $\nabla \cdot \mathbf{J} = 0$.

$$\mu_0 \mathbf{J}(\mathbf{r}) = \overline{h}_1 \nabla\psi \times \nabla\chi + \overline{h}_2 \nabla\zeta \times \nabla\psi + \nabla\psi \times \nabla\tilde{h} \tag{7.232}$$

Next, the desired co-variant (i.e., gradient) form of the magnetic field can be obtained from Eq. (7.232) by writing

$$\begin{aligned} \mu_0 \mathbf{J}(\mathbf{r}) &= \nabla \times [\overline{g}_1 \nabla\chi - \overline{g}_2 \nabla\zeta - \tilde{h} \nabla\psi] \\ \overline{h}_1 &= \frac{d\overline{g}_1}{d\psi} \\ \overline{h}_2 &= \frac{d\overline{g}_2}{d\psi} \end{aligned} \tag{7.233}$$

From Ampere's law, $\mu_0 \mathbf{J} = \nabla \times \mathbf{B}$, one sees that

$$\mathbf{B} = \overline{g}_1 \nabla\chi - \overline{g}_2 \nabla\zeta - \tilde{h} \nabla\psi + \nabla\tilde{g} \tag{7.234}$$

where $\tilde{g}(\psi,\chi,\zeta)$ is a free integration function.

Now, the critical step in the transformation to Boozer coordinates is the recognition that introduction of a new set of coordinates where χ and ζ are modified by carefully chosen periodic functions eliminates the appearance of the functions $\tilde{f}$ and $\tilde{g}$ in the two forms for $\mathbf{B}$. The new coordinates are defined as

$$\begin{aligned} \psi' &= \psi \\ \chi' &= \chi - \tilde{k}_\chi(\psi,\chi,\zeta) \\ \zeta' &= \zeta - \tilde{k}_\zeta(\psi,\chi,\zeta) \end{aligned} \tag{7.235}$$

where $\tilde{k}_\chi$ and $\tilde{k}_\zeta$ are to be determined. After substituting into Eqs. (7.231) and (7.234) one obtains the following representations for $\mathbf{B}$,

$$\begin{aligned} \mathbf{B}(\mathbf{r}) &= \overline{f}_1 \nabla\psi' \times \nabla\chi' + \overline{f}_2 \nabla\zeta' \times \nabla\psi' + \nabla\psi' \times \nabla(\tilde{f} + \overline{f}_1 \tilde{k}_\chi - \overline{f}_2 \tilde{k}_\zeta) \\ \mathbf{B}(\mathbf{r}) &= \overline{g}_1 \nabla\chi' - \overline{g}_2 \nabla\zeta' + \left(\frac{d\overline{g}_1}{d\psi} \tilde{k}_\chi - \frac{d\overline{g}_2}{d\psi} \tilde{k}_\zeta - \tilde{h} \right) \nabla\psi' + \nabla(\tilde{g} + \overline{g}_1 \tilde{k}_\chi - \overline{g}_2 \tilde{k}_\zeta) \end{aligned} \tag{7.236}$$

The functions $\tilde{k}_\chi$ and $\tilde{k}_\zeta$ are chosen so that the last terms in each equation are simultaneously set to zero. The appropriate choices are

$$\tilde{k}_\chi = -\left(\frac{\overline{g}_2}{\overline{f}_1\overline{g}_2 - \overline{f}_2\overline{g}_1}\right)\tilde{f} + \left(\frac{\overline{f}_2}{\overline{f}_1\overline{g}_2 - \overline{f}_2\overline{g}_1}\right)\tilde{g}$$
$$\tilde{k}_\zeta = -\left(\frac{\overline{g}_1}{\overline{f}_1\overline{g}_2 - \overline{f}_2\overline{g}_1}\right)\tilde{f} + \left(\frac{\overline{f}_1}{\overline{f}_1\overline{g}_2 - \overline{f}_2\overline{g}_{11}}\right)\tilde{g} \tag{7.237}$$

Observe that $\tilde{k}_\chi$ and $\tilde{k}_\zeta$ are periodic with respect to χ and ζ – there are no secular terms. Therefore, as χ, ζ change by 2π, so do χ', ζ'.

With these choices the two forms for **B** reduce to

$$\mathbf{B}(\mathbf{r}) = \nabla\psi \times \nabla(\overline{f}_1\chi - \overline{f}_2\zeta)$$
$$\mathbf{B}(\mathbf{r}) = \overline{g}_1\nabla\chi - \overline{g}_2\nabla\zeta + \tilde{k}\nabla\psi \tag{7.238}$$

where for convenience the primes have been suppressed and

$$\tilde{k}(\psi,\chi,\zeta) = \frac{d\overline{g}_1}{d\psi}\tilde{k}_\chi - \frac{d\overline{g}_2}{d\psi}\tilde{k}_\zeta - \tilde{h} \tag{7.239}$$

As will be shown the term containing $\tilde{k}$ does not play an important role in the analysis since its contribution is only in the $\nabla\psi$ direction. A very important feature of Eq. (7.238) is that the coefficients $\overline{f}_1$, $\overline{f}_2$, $\overline{g}_1$, $\overline{g}_2$ are functions only of ψ.

Equation (7.239) is almost in the desired final form for the Boozer coordinates. What remains is to relate the functions $\overline{f}_1$, $\overline{f}_2$, $\overline{g}_1, \overline{g}_2$ to more physical quantities.

Relation of $\overline{f}_1, \overline{f}_2, \overline{g}_1, \overline{g}_2$ to physical quantities

It is shown here that the quantities $\overline{f}_1$, $\overline{f}_2$, $\overline{g}_1, \overline{g}_2$ or equivalently $\overline{f}_1$, $\overline{f}_2$, $\overline{h}_1$, $\overline{h}_2$ are closely related to the magnetic fluxes and currents contained within a given pressure contour. The calculations are carried out by introducing the poloidal and toroidal differential surface areas required to calculate the fluxes and currents. These are illustrated in Fig. 7.20. The mathematical expressions for the poloidal and toroidal differential surface areas are given by their usual definitions

$$d\mathbf{A}_p = \frac{\partial\mathbf{r}}{\partial\zeta} \times \frac{\partial\mathbf{r}}{\partial\psi} d\zeta\, d\psi$$
$$d\mathbf{A}_t = \frac{\partial\mathbf{r}}{\partial\psi} \times \frac{\partial\mathbf{r}}{\partial\chi} d\chi\, d\psi \tag{7.240}$$

The various derivatives with respect to ψ,χ,ζ can be conveniently carried out in a rectangular coordinate system $x(\psi,\chi,\zeta)$, $y(\psi,\chi,\zeta)$, $z(\psi,\chi,\zeta)$. Thus, writing $\mathbf{r} = x(\psi,\chi,\zeta)\mathbf{e}_x + y(\psi,\chi,\zeta)\ \mathbf{e}_y + z(\psi,\chi,\zeta)\mathbf{e}_z$ one obtains

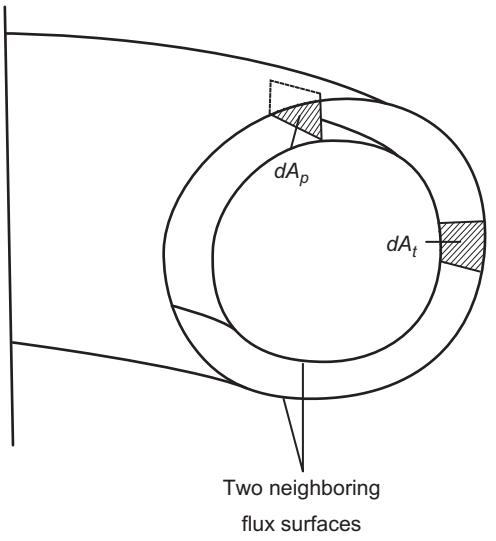

Figure 7.20 Differential poloidal and toroidal surface areas used to calculate fluxes and currents.

$$\begin{aligned}\frac{\partial \mathbf{r}}{\partial \psi} &= x_\psi\,\mathbf{e}_x + y_\psi\,\mathbf{e}_y + z_\psi\,\mathbf{e}_z \\ \frac{\partial \mathbf{r}}{\partial \chi} &= x_\chi\,\mathbf{e}_x + y_\chi\,\mathbf{e}_y + z_\chi\,\mathbf{e}_z \\ \frac{\partial \mathbf{r}}{\partial \zeta} &= x_\zeta\,\mathbf{e}_x + y_\zeta\,\mathbf{e}_y + z_\zeta\,\mathbf{e}_z\end{aligned} \tag{7.241}$$

Similarly the rectangular unit vectors can be written as

$$\begin{aligned}\mathbf{e}_x &= \nabla x = x_\psi \nabla\psi + x_\chi \nabla\chi + x_\zeta \nabla\zeta \\ \mathbf{e}_y &= \nabla y = y_\psi \nabla\psi + y_\chi \nabla\chi + y_\zeta \nabla\zeta \\ \mathbf{e}_z &= \nabla z = z_\psi \nabla\psi + z_\chi \nabla\chi + z_\zeta \nabla\zeta\end{aligned} \tag{7.242}$$

A straightforward but slightly tedious calculation then shows that

$$\begin{aligned}\frac{\partial \mathbf{r}}{\partial \zeta} \times \frac{\partial \mathbf{r}}{\partial \psi} &= J\nabla\chi \\ \frac{\partial \mathbf{r}}{\partial \psi} \times \frac{\partial \mathbf{r}}{\partial \chi} &= J\nabla\zeta\end{aligned} \tag{7.243}$$

where $\boldsymbol{J} = [x_\psi(y_\chi z_\zeta - z_\chi\, y_\zeta) + x_\chi\,(y_\zeta z_\psi - z_\zeta\, y_\psi) + x_\zeta\,(y_\psi z_\chi - z_\psi\, y_\chi)]$. The quantity $\boldsymbol{J}$ is the Jacobian of the coordinate transformation; that is, there are two equivalent ways to write $\boldsymbol{J}$. The first definition is

$$dx\ dy\ dz = J d\psi\ d\chi\ d\zeta = d\psi\ d\chi\ d\zeta/(\nabla\psi \times \nabla\chi \cdot \nabla\zeta) \tag{7.244}$$

The second equivalent definition in flux coordinates is

$$J = \begin{vmatrix} x_\psi & x_\chi & x_\zeta \\ y_\psi & y_\chi & y_\zeta \\ z_\psi & z_\chi & z_\zeta \end{vmatrix} = [x_\psi\,(y_\chi z_\zeta - z_\chi y_\zeta) + x_\chi\,(y_\zeta z_\psi - z_\zeta y_\psi) + x_\zeta\,(y_\psi z_\chi - z_\psi y_\chi)] \tag{7.245}$$

Combining these results leads to the following simple expressions for the differential surface areas

$$\begin{aligned} d\mathbf{A}_p &= (J\nabla\chi)d\zeta\, d\psi \\ d\mathbf{A}_t &= (J\nabla\zeta)d\chi\, d\psi \end{aligned} \tag{7.246}$$

Consider now the poloidal flux defined by

$$\Psi_p = \int \mathbf{B}\cdot d\mathbf{A}_p = \int_0^{2\pi}\int_0^{\psi} (\mathbf{B}\cdot\nabla\chi) J\, d\zeta\, d\psi \tag{7.247}$$

Using the contra-variant Boozer representation of $\mathbf{B}$ it follows that

$$\mathbf{B}\cdot\nabla\chi = \overline{f}_2\,(\nabla\zeta\times\nabla\psi)\cdot\nabla\chi = \frac{\overline{f}_2}{J} \tag{7.248}$$

The Jacobian factors cancel in the integrand and the ζ integral can be immediately evaluated yielding a factor of 2π. The poloidal flux reduces to

$$\Psi_p = 2\pi\int_0^{\psi} \overline{f}_2\, d\psi \tag{7.249}$$

Recall that ψ is defined as $\psi = \Psi_p/2\pi$. Thus, differentiating Eq. (7.249) with respect to ψ leads to the conclusion that

$$\overline{f}_2 = 1 \tag{7.250}$$

A completely analogous calculation for the toroidal flux shows that

$$\Psi_t = \int \mathbf{B}\cdot d\mathbf{A}_t = \int_0^{2\pi}\int_0^{\psi} (\mathbf{B}\cdot\nabla\zeta) J\, d\chi\, d\psi = 2\pi\int_0^{\psi} \overline{f}_1\, d\psi \tag{7.251}$$

Again, recalling that $\psi_t = \Psi_t/2\pi$ and then differentiating with respect to ψ leads to the following expression for $\overline{f}_1$.

$$\overline{f}_1(\psi) = \frac{d\psi_t(\psi)}{d\psi} \equiv q(\psi) \tag{7.252}$$

Here, $q(\psi)$ is an alternate but general definition of the safety factor. It is easy to derive this relation once the straight field line properties of the Boozer coordinates are demonstrated. The derivation is presented in Appendix F.

The next quantities of interest are the currents flowing within a $\psi =$ contour. From the contra-variant Boozer representation of $\mathbf{J}$ one sees that the net toroidal and poloidal currents are given by

$$\begin{aligned}\mu_0 I_t &= \mu_0 \int \mathbf{J}\cdot d\mathbf{A}_t = \mu_0 \int_0^{2\pi}\int_0^{\psi} (\mathbf{J}\cdot\nabla\zeta) J\, d\chi\, d\psi = 2\pi \int_0^{\psi} \overline{h}_1 d\psi \\ \mu_0 I_p &= \mu_0 \int \mathbf{J}\cdot d\mathbf{A}_p = \mu_0 \int_0^{2\pi}\int_0^{\psi} (\mathbf{J}\cdot\nabla\chi) J\, d\zeta\, d\psi = 2\pi \int_0^{\psi} \overline{h}_2 d\psi\end{aligned} \tag{7.253}$$

Again, differentiating with respect to ψ and defining $\mathrm{i}_t = \mu_0 I_t/2\pi$ and $\mathrm{i}_p = \mu_0 I_p/2\pi$ yields

$$\begin{aligned}\overline{h}_1 &= \frac{d\,\mathrm{i}_t}{d\psi} \quad \rightarrow \quad \overline{g}_1 = \mathrm{i}_t + \mathrm{i}_{t0} \\ \overline{h}_2 &= \frac{d\,\mathrm{i}_p}{d\psi} \quad \rightarrow \quad \overline{g}_2 = \mathrm{i}_p + \mathrm{i}_{p0}\end{aligned} \tag{7.254}$$

where i_{t0}, i_{p0} are free integration constants chosen to make the magnetic field reduce to the correct limit when no plasma is present. Thus, when there is zero toroidal plasma current (i.e., $\mathrm{i}_t = 0$) then there should be zero poloidal field implying that $\mathrm{i}_{t0} = 0$. However, when there is zero poloidal plasma current (i.e., $\mathrm{i}_p = 0$) there is still a toroidal magnetic field due to the currents in the TF coil. Denoting this current by $\mu_0 I_{coil} = 2\pi \mathrm{i}_{coil}$ one sees that $\overline{g}_2 = \mathrm{i}_p + \mathrm{i}_{coil}$.

The final desired form of Boozer coordinates can now be written as

$$\begin{aligned}\mathbf{B}(\mathbf{r}) &= \nabla\psi \times \nabla(q\chi - \zeta) \\ \mathbf{B}(\mathbf{r}) &= \mathrm{i}_t \nabla\chi - \mathrm{i}_p \nabla\zeta + \tilde{k}\nabla\psi\end{aligned} \tag{7.255}$$

where hereafter i_{coil} has been absorbed into i_p; in other words $\mathrm{i}_p \rightarrow \mathrm{i}_p + \mathrm{i}_{coil}$

Properties of Boozer coordinates

There are two important and useful properties of Boozer coordinates that can be easily derived from Eq. (7.255). The first is the fact that Boozer coordinates are a special case of "straight field line" coordinates. This can be seen by using the fact that the contra-variant representation of the magnetic field has the form $\mathbf{B} = \nabla\psi \times \nabla\alpha$. One now plots the two surfaces $\psi = \psi_0 =$ constant and $\alpha = \alpha_B =$ constant as shown in Fig. 7.21. The intersection of these two surfaces defines a magnetic line; that is, since the magnetic field satisfies $\mathbf{B}\cdot\nabla\psi = \mathbf{B}\cdot\nabla\alpha = 0$ then the field lines must lie simultaneously in both surfaces which can only occur where the surfaces intersect. The conclusion is that on the flux surface $\psi = \psi_0$ the equation for the field line trajectory in χ, ζ coordinates is given by $\alpha = \alpha_B$, or

$$\zeta = q(\psi)\chi - \alpha_B \tag{7.256}$$

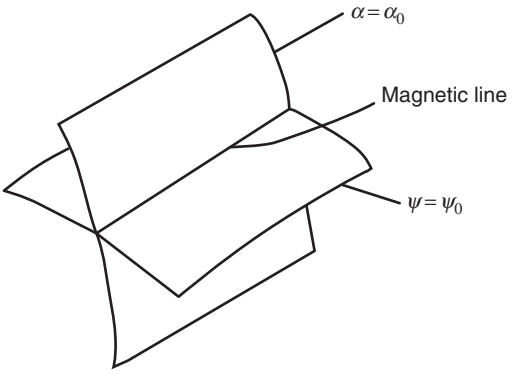

Figure 7.21 Intersection of ψ = constant, α = constant surfaces defining a magnetic line.

This is the equation of a straight line, hence, the name "straight field line coordinates."

The second useful property of Boozer coordinates is that there is a simple representation of the Jacobian. This representation is obtained by evaluating the dot product of the two forms for the magnetic field given in Eq. (7.255). The result is

$$\nabla\psi \times \nabla\chi \cdot \nabla\zeta \equiv \frac{1}{J} = \frac{B^2}{(\mathrm{i}_t - q\,\mathrm{i}_p)} \tag{7.257}$$

Observe that $J = J(\psi, B)$ a very important result for the application of Boozer coordinates to neoclassical transport.

Applications of Boozer coordinates

The required relationships have now been derived that allow application of Boozer coordinates to neoclassical transport in a stellarator. The approach is to evaluate the generalized perpendicular guiding center drift of the particles off the flux surface, demonstrate that this drift is proportional to $\mathbf{B} \times \nabla B \cdot \nabla\psi$, and then show how Boozer coordinates simplify this expression.

The analysis begins with the recognition that the guiding center drift normal to the flux surface is responsible for neoclassical transport and is comprised of three contributions: the $\mathbf{E} \times \mathbf{B}$ drift, the grad-B drift, and the curvature drift. The change in flux surface location along the guiding center trajectory satisfies the equation

$$\begin{aligned} \frac{d\psi}{dt} &= \frac{\partial\psi}{\partial t} + \mathbf{V}_D \cdot \nabla\psi = \mathbf{V}_D \cdot \nabla\psi \\ &= \left(\frac{\mathbf{E} \times \mathbf{B}}{B^2} + \frac{mv_\perp^2}{2e} \frac{\mathbf{B} \times \nabla B}{B^3} + \frac{mv_\parallel^2}{e} \frac{\mathbf{B} \times \boldsymbol{\kappa}}{B^2} \right) \cdot \nabla\psi \end{aligned} \tag{7.258}$$

Since $\mathbf{E} = -\nabla\Phi(\psi)$ then the $\mathbf{E} \times \mathbf{B}$ term automatically vanishes. The grad-B drift is already in the correct form. The curvature term is simplified by noting that

$$\begin{aligned}\boldsymbol{\kappa} = \mathbf{b} \cdot \nabla \mathbf{b} &= \frac{\mathbf{B}}{B} \cdot \nabla \frac{\mathbf{B}}{B} = \frac{1}{B^2}\mathbf{B} \cdot \nabla \mathbf{B} - \frac{\mathbf{B} \cdot \nabla B}{B^3}\mathbf{B} \\ &= \frac{1}{B^2}\nabla\left(\mu_0 p + \frac{B^2}{2}\right) - \frac{\mathbf{B} \cdot \nabla B}{B^3}\mathbf{B} \\ &= \frac{1}{B^2}\frac{dp}{d\psi}\nabla\psi + \frac{\nabla B}{B} - \frac{\mathbf{B} \cdot \nabla B}{B^3}\mathbf{B} \end{aligned} \tag{7.259}$$

The first and third terms make no contribution to $\mathbf{V}_D \cdot \nabla\psi$. Only the second term enters the analysis. After introducing the constants of the motion E, μ one sees that the perpendicular guiding center drift is given by

$$\mathbf{V}_D \cdot \nabla\psi = \frac{1}{e}(2E - \mu B)\frac{\mathbf{B} \times \nabla B \cdot \nabla\psi}{B^3} \tag{7.260}$$

The critical step is to now show how Boozer coordinates simplify Eq. (7.260). Start with a general co-variant form for the magnetic field: $\mathbf{B} = B_\psi \nabla\psi + B_\chi \nabla\chi + B_\zeta \nabla\zeta$. A short calculation shows that

$$\mathbf{V}_D \cdot \nabla\psi = \frac{1}{e}(2E - \mu B)\frac{1}{JB^3}\left(B_\chi \frac{\partial B}{\partial \zeta} - B_\zeta \frac{\partial B}{\partial \chi}\right) \tag{7.261}$$

Substituting the co-variant Boozer form of $\mathbf{B}$ leads to

$$\mathbf{V}_D \cdot \nabla\psi = \frac{(2E - \mu B)}{eB}\left(\frac{\mathrm{i}_t}{\mathrm{i}_t - q\,\mathrm{i}_p}\frac{\partial B}{\partial \zeta} + \frac{\mathrm{i}_p}{\mathrm{i}_t - q\,\mathrm{i}_p}\frac{\partial B}{\partial \chi}\right) \tag{7.262}$$

The remarkable conclusion from Eq. (7.262) is that the normal guiding center drift expressed in Boozer coordinates is only a function of the scalars ψ, B, and derivatives of B. It is not a function of the individual vector components of $\mathbf{B}$. This is not an obvious conclusion since, in general, the individual vector components of $\mathbf{B}$ (i.e., B_χ and B_ζ) appear explicitly in Eq. (7.261).

Equation (7.262) offers the possibility of generating a 2-D symmetric B from a 3-D vector $\mathbf{B}$. As an example illustrating this basic point in a simpler geometry consider the 2-D helical vector field

$$\mathbf{B}(r, \alpha) = B_\phi(r)\,\mathbf{e}_\phi + B_h(r/a)^{l-1}(\mathbf{e}_r \sin\,\alpha + \mathbf{e}_\theta \cos\,\alpha) \quad \alpha = l\theta + n\phi \tag{7.263}$$

It immediately follows that B is a 1-D function,

$$B^2(r) = B_\phi^2(r) + B_h^2\left(\frac{r}{a}\right)^{2l-2} \tag{7.264}$$

In general, it has not been possible to make an exact transition from a 3-D **B** to a 2-D B, but one can get very close, giving rise to the concepts of the quasi-isodynamic and quasi-symmetric stellarators.

From a single-particle confinement point of view, symmetry can be very important. It is well known from classical mechanics that an equilibrium system with one degree of geometric symmetry always has two constants of the motion, the energy E and a canonical angular momentum L associated with the symmetry direction. The existence of these two constants guarantees that single-particle orbits are confined. Without the geometric symmetry only the energy is a constant of the motion and single-particle orbits are in general not confined.

One can immediately see how the Boozer form of $\mathbf{V}_D \cdot \nabla\psi$ helps to design omnigenous systems. One can choose a reasonably general 3-D helical vector magnetic field $\mathbf{B}(r,\theta,\phi)$, convert to Boozer coordinates, calculate $B(\psi,\chi,\zeta)$, and evaluate the omnigenous constraint in Eq. (7.225). This process is then repeated with the aim of optimizing over the harmonic amplitudes and phases to satisfy the constraint as closely as possible. Since the constraint only involves averages over the field lines one intuitively expects that many different stellarator configurations might lead to a similar level of omnigenity. Consequently, there should still be a fair amount of freedom available to further optimize with respect to other goals such as MHD stability, reduced transport, efficient heating and current drive, or engineering simplicity.

This extra freedom can in particular be used to produce a quasi-isodynamic configuration. The corresponding constraint given in Eq. (7.225) translates to

$$\mathrm{i}_t \frac{\partial B}{\partial \zeta} + \mathrm{i}_p \frac{\partial B}{\partial \chi} = 0 \tag{7.265}$$

Keeping in mind the 2π periodicity requirements one sees that there are two ways to satisfy Eq. (7.265): (1) $\mathrm{i}_t = 0$ and $B = B(\psi, \zeta)$ or (2) $\mathrm{i}_p = 0$ and $B = B(\psi, \chi)$. The first choice corresponding to zero toroidal current is the strategy used by the Germans in their W7-X experiment. The result of trying to approach to the ideal goal of $B = B(\psi, \zeta)$ leads to a quasi-isodynamic configuration which can be equally well described as a quasi-poloidal configuration; that is, the dependence on the poloidal angle χ is minimized.

The other option where $\mathrm{i}_p = 0$ leads to a configuration which in analogy might be called quasi-toroidal since ideally there is no dependence of B on ζ. However, configurations with zero poloidal current and a large toroidal field invariably have low β which is not desirable. As is shown next there is a better way to exploit the idea of quasi-toroidal symmetry.

The last configuration of interest is the symmetric system described in Eq. (7.225). The corresponding constraint is easily evaluated by noting that the non-vanishing contribution of $\mathbf{B} \cdot \nabla B$ is given by

$$\begin{aligned} \mathbf{B} \cdot \nabla B &= (q\nabla\psi \times \nabla\chi - \nabla\psi \times \nabla\zeta) \cdot \left(\frac{\partial B}{\partial \chi} \nabla\chi + \frac{\partial B}{\partial \zeta} \nabla\zeta \right) \\ &= \frac{B^2}{\mu_0(\mathrm{i}_t - q\,\mathrm{i}_p)} \left(q \frac{\partial B}{\partial \zeta} + \frac{\partial B}{\partial \chi} \right) \end{aligned} \tag{7.266}$$

The ideal symmetric constraint reduces to

$$(\mathrm{i}_t - gq) \frac{\partial B}{\partial \zeta} + (\mathrm{i}_p - g) \frac{\partial B}{\partial \chi} = 0 \tag{7.267}$$

where $g(\psi) = G(\psi)/\mu_0$.

Several conclusions can be drawn from Eq. (7.267). First ideal poloidal symmetry, defined as $B = B(\psi, \zeta)$, is achieved by setting $g = \mathrm{i}_t/q$. In general, one does not have to set $\mathrm{i}_t = 0$ to achieve poloidal symmetry. The special choice $\mathrm{i}_t = 0$ was made by the Germans to minimize the bootstrap current in addition to achieving omnigenity. Thus, based on the definitions presented here, an ideal-isodynamic stellarator is an ideal poloidally symmetric stellarator with the additional requirement that $\mathrm{i}_t = 0$.

Similarly, ideal toroidal symmetry, defined as $B = B(\psi, \chi)$ can be realized by choosing $g = \mathrm{i}_p$. Again, it is not necessary to set $\mathrm{i}_p = 0$ in stellarators with toroidal symmetry. This is important because the presence of poloidal currents leads to configurations with higher values of β. The toroidally symmetric stellarator with $\mathrm{i}_P \neq 0$ was the approach used in the design of the canceled NCSX experiment at PPPL. The NCSX design aimed for omnigenity at reasonably high β values in the presence of substantial flows in a compact geometry.

The last geometry of interest corresponds to helical symmetry: $B = B(\psi, m\chi + n\zeta)$ where m, n are integers. This symmetry is achieved by setting

$$g = \frac{n\mathrm{i}_t + m\mathrm{i}_p}{m + nq} \tag{7.268}$$

A small helically symmetric stellarator experiment, HSX, has been built at the University of Wisconsin with $m = 2, n = 4$. The experiment does indeed observe a marked improvement in confinement when the coil currents are adjusted to approach helical symmetry.

The approximately achievable property $B \approx B(\psi, m\chi + n\zeta)$ is usually referred to in the literature as quasi-symmetry. The special cases are $m = 0$ poloidal

quasi-symmetry, $n = 0$ toroidal quasi-symmetry, and $m \neq 0$, $n \neq 0$ quasi-helical symmetry.

7.7.7 Summary of neoclassical transport in a stellarator

A major challenge facing the stellarator concept as it attempts to achieve performance comparable to a tokamak is reducing neoclassical transport losses. These losses are potentially much larger in a stellarator because of the inherent 3-D nature of the magnetic geometry. Specifically, unlike a tokamak, trapped particle orbits are in general not confined in a 3-D system and lead to large energy and particle losses.

Once this situation was recognized strategies were developed to reduce neoclassical losses in a stellarator. The basic strategy in modern stellarators is the concept of ideal-omnigenity in which all trapped particles are confined in the absence of collisions. Ideal-omnigenity involves an integral constraint that depends upon the geometric dependence of B and which must be satisfied by all particles, i.e., all E, μ. It has not been possible to exactly satisfy this constraint either theoretically or experimentally which has led to the approximate goal of quasi-omnigenity. However, since the constraint involves averaged and not local requirements on B there are many different types of stellarator configurations that can achieve a similar closeness to omnigenity.

This freedom in the design of quasi-omnigenous stellarators has led to two quite different optimizations. With the advantage of hindsight these can be put in context with the aid of the ideal stellarator constraints discussed above plus the concept of quasi-symmetry as expressed in Boozer coordinates. The key feature is that neoclassical transport depends only on B and not on the vector nature of $\mathbf{B}$ when formulated in terms of Boozer coordinates.

Optimized stellarators try to approximate some form of quasi-symmetry defined as $B(\psi, \chi, \zeta) \rightarrow B(\psi, m\chi + n\zeta)$. If a configuration could exactly satisfy the symmetry constraint it would automatically be ideally omnigenous. The case $m = 0$ corresponds to quasi-poloidal symmetry. In general, a net toroidal current i_t can flow in a quasi-poloidal stellarator. The special case in which the design attempts to make $\mathrm{i}_t = 0$ represents the quasi-isodynamic stellarator with zero bootstrap current. This is the approach used by the German's in their W7-X experiment. The W7-X design actually works harder at setting the bootstrap current to zero than achieving quasi-poloidal symmetry and the resulting optimization has led to a large aspect device. Even so, since quasi-symmetry is sufficient but not necessary for omnigenity, a considerable deviation can occur but still result in good confinement of trapped particles.

A second major design effort has been devoted to the idea of the quasi-toroidal stellarator corresponding to $n = 0$. Here, a toroidal bootstrap current is allowed which is finite but not too large. The advantages of toroidal quasi-symmetry are the possibility of large macroscopic flow velocities and machine compactness. The large flow velocities and corresponding large velocity shear are expected to reduce turbulent transport. The quasi-toroidal symmetry is expected to reduce neoclassical transport. This was the strategy used in the design of NCSX at PPPL.

7.8 Modern stellarators

There are many stellarator experiments operating or being built in the world's fusion program. The two largest flagship facilities are the Large Helical Device (LHD) in Japan and the Wendelstein 7-X (W7-X) in Germany. A brief description is now given of each of these large experiments.

7.8.1 The Large Helical Device (LHD)

The LHD is a billion dollar class experiment which achieved first plasma in 1998 and continues to successfully operate at the National Institute for Fusion Science in Toki, Japan (Motojima *et al*., 2000). Its design corresponds to one of the classic stellarator configurations known as a "heliotron." In a heliotron the main magnetic field is produced by a pair of continuous superconducting helical-toroidal coils each carrying a current in the same direction. These coils produce both a toroidal magnetic field and a predominantly $l = 2$ helical magnetic field. The coils also produce a substantial vertical field. This field is largely canceled by an additional set of superconducting toroidally symmetric vertical field coils. The current in these coils can be adjusted to leave a small net vertical field which is used to optimize performance. A schematic drawing of LHD is given in Fig. 7.22.

There is a general consensus in the world's fusion community that LHD is an engineering marvel. One main feature of the design results from the fact that at present there does *not* exist a high quality, low loss superconducting joint that could be used to connect different sections of a toroidal coil. As a consequence, the LHD coils are continuous and were actually wound in place. They have worked very successfully with high reliability although there is a belief that this type of technology will not extrapolate well into the reactor regime. The main difficulty is associated with the large cost in time and money that would be required if a fault occurred in the coil. The reactor would have to be essentially completely disassembled to make repairs. This difficulty could perhaps be overcome with the development of low loss superconducting joints which would allow multiple

Table 7.3 *Optimized parameters for LHD discharges.*

	T_e (keV)	T_i (keV)	τ_E (sec)	P_{aux} (MW)	n_e (m^{-3})
T_e maximum	**10.0**	2.0	0.06	1.2	5.0×10^{18}
T_i maximum	4.2	**13.6**	0.06	3.1	3.5×10^{18}
τ_E maximum	1.3	1.3	**0.36**	1.5	4.8×10^{18}
$p_i\tau_E$ maximum			**0.07** atm-sec		
β maximum			**0.05** at $B_\phi = 0.425T$		
n_e maximum			**1.0** $\times$ **10^{21}** m^{-3}		
τ_{pulse} maximum			**3900** sec by ECH		

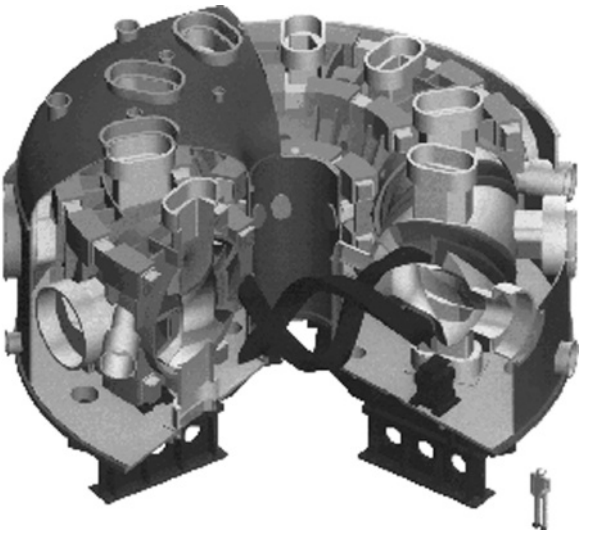

Figure 7.22 Schematic diagram of the LHD stellarator in Japan. Courtesy of Akio Komori.

section helical coils, but there is not a lot of effort, at least in the United States, devoted to achieving this high leverage technological advance. An alternate method to avoid this problem is with stand-alone modular coils as in W7-X but more on this in the next subsection.

In terms of the physics motivation behind LHD it is worth noting that at the time of its design many of the important ideas involving neoclassical transport in 3-D systems had not yet been fully developed. Thus, minimizing neoclassical transport was not a primary consideration. Instead, the design was largely based on optimizing performance with respect to certain classes of MHD instabilities.

One can now ask about the actual experimental performance of LHD. Some general trends can be noted. First, reasonably high values of β have been achieved (see Table 7.3). Furthermore, even when the β limit is exceeded, unlike a tokamak,

no major disruptions are observed. Instead there is a gradual degradation of confinement which is detrimental to the physics but is not a threat to machine integrity. This absence of disruptions is a feature of virtually all stellarators and is a major advantage of the concept. At this point it is not clear whether the confinement degradation in LHD is due to MHD instabilities or to β driven destruction of flux surfaces leading to stochastic regions of magnetic field.

With respect to transport at lower β, initial operation produced an adequate energy confinement time but not as high as comparable tokamaks. However, by reprogramming the currents in the vertical field coils to shift the plasma further inward confinement improved considerably, comparable to that in an L-mode tokamak. Presumably this optimization corresponded to a substantial increase in neoclassical confinement of trapped particles – LHD became approximately quasi-omnigenous.

The actual parameters achieved in LHD are listed in Table 7.3. The values given represent the individual optimized peak performance (as of 2006) of each critical plasma parameter; that is, the parameters are not achieved simultaneously. Each optimized parameter is given in boldface type. Observe that β values of 5% have been measured. Also, the plasma has operated over very long pulses, more than an hour, by means of electron cyclotron heating.

Overall the parameters demonstrate that stellarators can indeed achieve fusion relevant parameters. Future research and experimental upgrades will be aimed at simultaneously reaching the individual peak parameters observed in individually optimized discharges.

7.8.2 The Wendelstein 7-X (W7-X) stellarator

The W7-X stellarator is also a billion dollar class experiment currently being built at the Max Planck Institute for Plasma Physics in Greifswald, Germany (Beidler *et al*., 1990; Grieger *et al*., 1992). It is scheduled to be completed in 2014. A key feature of the engineering design is the use of modular, non-planar superconducting coils. A schematic diagram of W7-X is shown in Fig. 7.23.

The motivation for such complicated coils is associated with the scale up to fusion reactors. Should a coil failure occur it would be possible to make a repair by removing only one section of the reactor as opposed to disassembling the entire reactor as with continuously wound coils. Clearly this is an advantage. Even so there are two points worth mentioning. Repairing even one section of a modular stellarator might still involve many months of down time which is not desirable from an economic point of view. Also, experience with W7-X and the cancelled NCSX experiment has shown that it is quite difficult technologically to build modular coils – it takes more time and money than for planar, tokamak type coils.

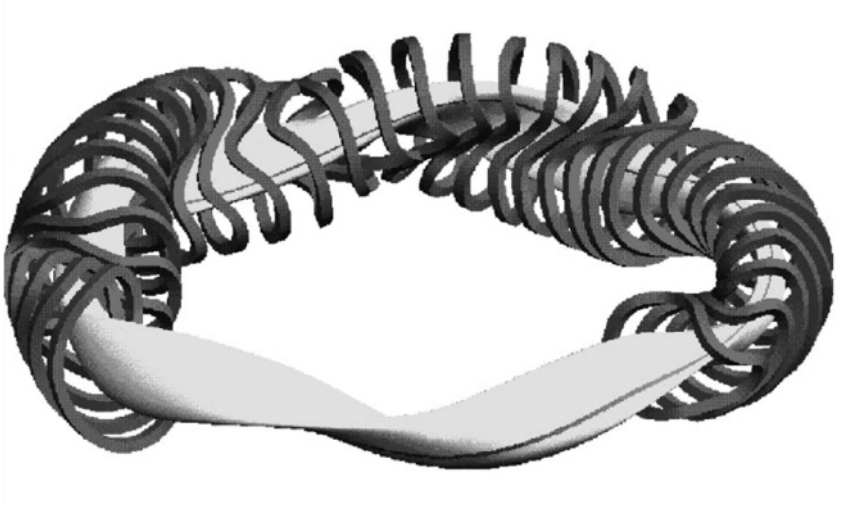

Figure 7.23 Schematic diagram of the W7-X stellarator in Germany. Courtesy of the Max Planck Institute for Plasma Physics.

Hopefully though, the lessons learned from these early modular designs will reduce the cost in future devices.

The physics motivation for W7-X has been previously discussed. Specifically, the design has paid a great deal of attention to neoclassical transport. The final design tries to create a quasi-isodynamic configuration with a minimum bootstrap current, particularly at higher values of β. The idea is that a low bootstrap current will produce robust flux surfaces even as β is increased. This in turn would help alleviate the high β destruction of flux surfaces which would lead to a degradation of confinement. It would also minimize the possibility of current-driven disruptions. The final design of W7-X has substantial $l = 2$ and $l = 0$ helical fields. The $l = 0$ harmonic corresponds to a mirror field which sometimes leads one to view W7-X as a series of linked mirrors. However, this is an oversimplification and a

Table 7.4 *Projected parameters for W7-X.*

Quantity	Value
Major radius R_0	5.5 m
Minor radius a	0.53 m
Magnetic field B_0	3 T
Pulse time τ_{pulse}	~1800 sec with beam power, ∞ with microwaves
Plasma volume V_p	30 m^3
Plasma heating P_h	14 MW
Plasma temperature T	1–6 keV
Plasma β	0.05

considerable design effort has been devoted to producing a quasi-isodynamic configuration with good MHD equilibrium and stability properties at high β.

The projected parameters for W7-X are given in Table 7.4. If W7-X can reach these parameters it, like LHD, will thereby demonstrate that the stellarator can achieve reactor grade performance.

7.9 Overall summary

Chapter 7 describes the basic MHD properties of 3-D magnetic configurations. Attention is focused solely on stellarators which at present represent the main competitor to the tokamak for a fusion reactor, at least in terms of plasma physics performance. There are many different types of configurations that are classified as stellarators. The one common feature is that they all are helical configurations bent into a torus.

In general, stellarators are more complicated and expensive to build than their axisymmetric counterpart, namely the tokamak. There are two primary motivations for investigating these more complex geometries. First, unlike a tokamak, stellarators do not require a net toroidal current to achieve MHD equilibrium. Thus they are inherently steady state devices. Second, while there are MHD β limits associated with both equilibrium and stability, stellarators so far do not observe major disruptions. These are two very important advantages which must be balanced against technology complexity.

An important stellarator concern involves particle and energy transport. Because of the 3-D geometry, stellarators in general have poorer neoclassical transport properties than tokamaks. Large theoretical/computational efforts, backed by experimental observations, have been devoted to reducing neoclassical losses in stellarators resulting in several highly innovative ideas.

The path to good neoclassical confinement is based on the idea of omnigenity. This property requires that the average drift of any plasma particle off a flux surface during one bounce period should be zero. Although it has not been possible to exactly realize this property either theoretically or experimentally there are several configurations that closely approximate this ideal but which also have a sufficient degree of remaining freedom to achieve an additional level of optimization.

One main subset of quasi-omnigenity is the idea of the quasi-isodynamic stellarator which is the basis for W7-X. This configuration is somewhat similar to a series of linked mirror machines with very careful attention paid to the plasma "elbows" connecting each mirror section. Major goals of W7-X are to minimize the bootstrap current in order to produce robust flux surfaces at high β, and to minimize the chance for current driven disruptions.

A second subset of quasi-omnigenity is the quasi-symmetric stellarator. Here, as shown by the introduction of Boozer coordinates, the drift off a given flux surface

depends only on ψ and B. Therefore, a carefully designed 3-D vector magnetic field can lead to an approximately 2-D $B = B(\psi, m\chi + n\phi)$. Classical mechanics then implies that because of the 2-D symmetry, trapped particles will be confined. An equally important feature of quasi-symmetric configurations is that they allow large macroscopic flow velocities which are believed to be a good method to suppress micro-turbulence. Two examples of quasi-symmetric stellarators are the small HSX at the University of Wisconsin and the unfortunately canceled NCSX at PPPL.

In terms of the MHD equilibrium of stellarators there are several interesting properties to note. First, equilibria are possible without a net current. A toroidal restoring force is produced by the interaction of the vacuum helical magnetic field and the helical modulation of the Pfirsch–Schluter current. Second, while current-free equilibria are possible, the amplitude of the helical magnetic field cannot be too large or else the outer flux surfaces no longer remain closed. Third, a vertical field can shift the position of a stellarator even though the configuration has no net steady state toroidal current. A force is generated only during the transient period when the vertical field is changing but then vanishes once the vertical field has reached its steady state value. It is the interaction of the transiently induced surface dipole current and the average helical field on a flux surface that produces the force that shifts the plasma from one position to another.

Overall, stellarator performance has improved considerably in recent years so that the concept remains as the main competitor to mainline tokamak in terms of achieving fusion relevant plasma physics performance.

References

Bauer, F., Betancourt, O., Garabedian, P., and Wakatani, M. (1987). *The Beta Equilibrium, Stability, and Transport Codes*. Boston, MA: Academic Press.
Beidler, C., Grieger, G., Herrnegger, F., *et al*. (1990). *Fusion Tech.* **17**, 148.
Boozer, A. H. (1982). *Phys. Fluids*, **25**, 520.
Boozer, A. H. (2004). *Rev. Modern Phys.* **76**, 1071.
Braginskii, S. I. (1965). In *Reviews of Plasma Physics*, Vol. 1, ed. M. A. Leontovich. New York: Consultants Bureau.
Canik, J. M., Anderson, D. T., Anderson, F. S. B., *et al*. (2007). *Phys. Rev. Lett.* **98**, 085002.
Freidberg, J. P. (1987). *Ideal Magnetohydrodynamics*. New York: Plenum Press.
Gori, S., Lotz, W., and Nuhrenberg, J. J. (1996). *Theory of Fusion Plasmas*. Bologna: Editrici Compositori.
Greene, J. M. and Johnson, J. L. (1961). *Phys. Fluids* **4**, 875.
Grieger, G., Lotz, W., Merkel, P. *et al*. (1992). *Phys. Fluids B*, **4**, 2081.
Helander, P. and Sigmar, D. J. (2002). *Collisional Transport in Magnetized Plasmas*. Cambridge: Cambridge University Press.
Helander, P. (2007). *Phys. Plasmas*, **14**, 104501.
Helander, P. and Nuhrenberg, J. (2009). *Plasma Phys. Controlled Fusion*, **51**, 055004.
Helander, P., Beidler, C. D., Bird, T. M., *et al*. (2012). *Plasma Phys. Controlled Fusion* **54**, 124009.

Hirshman, S. P. and Whitson, J. C. (1983). *Phys. Fluids* **26**, 3553.
Kikuchi, M., Lackner, K., and Tran, Minh Quang, eds. (2012), *Fusion Physics.* Vienna: International Atomic Energy Agency.
Landreman, M. and Catto, P. J. (2011). *Plasma Phys. Controlled Fusion*, **53**, 035106.
Landreman, M. and Catto, P. J. (2012). *Phys. Plasmas*, **19**, 056103.
Miyamoto, K. (2005). *Plasma Physics and Controlled Nuclear Fusion*. Berlin: Springer-Verlag.
Motojima, O., Akaishi, K., Chikaraishi, H., *et al*. (2000). *Nuclear Fusion* **40**, 599
Mynick, H. E. (2006). *Phys. Plasmas*, **13**, 058102.
Nuhrenberg, J. (2010). *Plasma Phys. Controlled Fusion*, **52**, 124003.
Reiman, A. and Greenside, H. S. (1986). *Comput. Phys. Commun.* **43**, 157.
Stacey, W. M. (2012). *Fusion Plasma Physics*, 2nd edn. Weinheim, Germany: Wiley-VCH.
Sugama, H., Watanabe, T. H., Nunami, M., *et al*. (2011). *Plasma Phys. Controlled Fusion*, **53**, 024004.
Zarnstorff, M. C., Berry, L. A., Brooks, A., *et al*. (2001). *Plasma Phys. Controlled Fusion*, **43**, A237.

Further reading

MHD stellarator theory

Boozer, A. H. (2004). *Rev. Modern Phys.* **76**, 1071.
Kikuchi, M., Lackner, K., and Tran, M. Q., eds. (2012). *Fusion Physics.* Vienna: International Atomic Energy Agency.
Miyamoto, K. (1978). *Nucl. Fusion* **18**, 243.
Shafranov, V. D. (1980). *Nucl. Fusion* **20**, 1075.
Shafranov, V. D. (1983). *Phys. Fluids* **26**, 357.
Solov'ev, L. S. and Shafranov, V. D. (1979). In *Reviews of Plasma Physics*, Vol V, ed. M. A. Leontovich. New York: Consultants Bureau.

MHD stellarator computation

Bauer, F., Betancourt, O., and Garabedian, P. (1980). *J. Comput. Phys.* **39**, 341.
Carraras, B. A., Cantrell, J. L., Charlton, L. A., *et al*. (1984). In *Proceedings of the International Conference on Plasma Physics and Controlled Nuclear Fusion Research*, London, UK.
Hirshman, S. P. and Whitson, J. C. (1983). *Phys. Fluids* **26**, 3553.
Mynick, H. E., Pomphrey, N., and Xanthopoulos, P. (2010). *Phys. Rev. Lett.* **105**, 095004.
Reiman, A. and Greenside, H. S. (1986). *Comput. Phys. Commun.* **43**, 157.
Sovinec, C. R., Glasser, A. H., Gianakon, T. A., *et al*. (2004). *J. Comp. Phys.* **195**, 355.
Strauss, H. R. and Monticello, D. A. (1981). *Phys. Fluids* **24**, 1148.

Problems

7.1 Generalize the formula for the total flux ψ_{tot} given by Eq. (7.90) so that it is valid for arbitrary l.

7.2 Consider a stellarator equilibrium where the applied fields consist of a toroidal field, a helical field, and a vertical field. For simplicity assume $ha \ll 1$. Show that the toroidally averaged shift of the magnetic axis for the vacuum fields is given by

$$\frac{\overline{\sigma}(0)}{a} = \left(\frac{R_0 B_V}{a B_0 \hat{\imath}_H}\right)^{1/(2l-3)}$$

for $l \geq 2$.

7.3 Prove that the expression for the helical restoring force given by Eq. (7.115) is valid for arbitrary l.

7.4 This problem involves the equilibrium β limit for a single helicity, $\beta \sim \varepsilon$ stellarator for arbitrary ℓ. Assume Solov'ev profiles for the free functions as in Section 7.6.4. Also, use the small argument expansion ($ha \ll 1$) of the Bessel functions to simplify the analysis.

(a) Show that the solution for ψ corresponding to a current-free stellarator is given by

$$\psi = \frac{a^2}{2R_0}\left[\frac{\ell \beta_t}{2\hat{\imath}_H \varepsilon}(\rho^3 - \rho)\ \cos\theta + \frac{\hat{\imath}_H}{\ell - 1}(\rho^{2\ell-2} - 1)\right]$$

where $\rho = r/a$ and $\hat{\imath}_H$ is the vacuum transform/2π at the edge of the plasma $r = a$.

(b) Calculate the MHD safety factor at the edge of the plasma. Show that there is an equilibrium limit, β_t, given by

$$\beta_t < \frac{2\hat{\imath}_H^2 \varepsilon}{\ell}$$

7.5 Derive an expression for the rotational transform for a multi-helicity stellarator described by the Greene–Johnson overlap model.

7.6 Consider a stellarator with a toroidal magnetic field $B_\varphi = B_0(R_0/R)$, a vertical field of amplitude B_V, and three helical harmonics $l = 1, 2, 3$, each with the same n. Adjust the amplitudes of the vertical field and helical harmonics so that B satisfies the following constraints as closely as possible as one moves away from the magnetic axis:

(a) $B\ (r, \theta, \varphi) \rightarrow B(r, \theta)$
(b) $B\ (r, \theta, \varphi) \rightarrow B(r, \varphi)$
(c) $B\ (r, \theta\ \varphi) \rightarrow B(r, 2\theta + \varphi)$

Is this the same as quasi-symmetry? Explain.